

2016

Structure-based drug discovery of Asu-ACR-16 agonists and allosteric modulators

Fudan Zheng
Iowa State University

Follow this and additional works at: <https://lib.dr.iastate.edu/etd>

 Part of the [Analytical Chemistry Commons](#)

Recommended Citation

Zheng, Fudan, "Structure-based drug discovery of Asu-ACR-16 agonists and allosteric modulators" (2016). *Graduate Theses and Dissertations*. 15201.
<https://lib.dr.iastate.edu/etd/15201>

This Thesis is brought to you for free and open access by the Iowa State University Capstones, Theses and Dissertations at Iowa State University Digital Repository. It has been accepted for inclusion in Graduate Theses and Dissertations by an authorized administrator of Iowa State University Digital Repository. For more information, please contact digirep@iastate.edu.

Structure-based drug discovery of *Asu*-ACR-16 agonists and allosteric modulators

by

Fudan Zheng

A thesis submitted to the graduate faculty
in partial fulfillment of the requirements for the degree of

MASTER OF SCIENCE

Major: Analytical Chemistry

Program of Study Committee:
Brett VanVeller, Major Professor
Robert S. Houk
Richard J. Martin
Alan P. Robertson

Iowa State University

Ames, Iowa

2016

Copyright © Fudan Zheng, 2016. All rights reserved.

TABLE OF CONTENTS

	Page
NOMENCLATURE.....	iv
ACKNOWLEDGEMENTS.....	v
ABSTRACT.....	vii
CHAPTER 1 GENERAL INTRODUCTION.....	1
Introduction.....	1
<i>Ascaris</i> : a soil-transmitted helminth.....	1
Anthelmintic drugs and resistance.....	3
Nicotinic acetylcholine receptors and interactions with agonists.....	5
Homology modeling and virtual screening.....	11
Electrophysiology and its technique: two-electrode voltage clamp....	13
Thesis Organization.....	16
CHAPTER 2 THE <i>ASCARIS SUUM</i> NICOTINIC RECEPTOR, ACR-16, AS A DRUG TARGET: FOUR NOVEL NEGATIVE ALLOSTERIC MODULATORS FROM VIRTUAL SCREENING.....	17
Abstract.....	18
Introduction.....	19
Methods.....	22
Results.....	30
Discussion.....	37
Acknowledgements.....	41
References.....	42
Figures.....	49
Tables.....	63
Supplementary Data.....	67

CHAPTER 3 STRUCTURE-BASED DRUG DISCOVERY:

(S)-5-ETHYNYL-ANABASINE AND OTHER NICOTINE ALKALOIDS AS

ASU-ACR-16 AGONIST.....	82
Abstract	83
Introduction	84
Materials and Methods	86
Results	91
Discussion	96
Acknowledgements	100
References	101
Figures	104
Tables	117
Supplementary Data.....	119
 CHAPTER 4 GENERAL CONCLUSION AND FUTURE OUTLOOK	 131
REFERENCE.....	134

NOMENCLATURE

STHs	soil-transmitted helminths
ach	acetylcholine
GABA	γ -aminobutyric acid
GluCl _s	glutamate-gated chloride channels
nAChRs	nicotinic acetylcholine receptors
LGICs	ligand-gated ion channels
(+)	principal face
(-)	complementary face
AChBP	acetylcholine-binding protein
TEVC	two-electrode voltage clamp
QSAR	quantitative structure-activity relation

ACKNOWLEDGMENTS

I would like to express deep gratitude to my major professor, Dr. Brett VanVeller, and my committee members, Dr. Richard Martin and Dr. Alan Robertson, for their patient guidance and enthusiastic encouragement during my graduate study. It was an exciting experience to develop and make progress in my research under their supervision. I am especially grateful to Dr. VanVeller, Dr. Martin, Dr. Robertson and Dr. Yu for their support to train me in three different labs with various skills. I would like to thank my committee member, Dr. Sam Houk, for overseeing my progress during graduate program and providing kind help. I would like to thank my previous major professor, Dr. Edward Yu, labmates Tsung-Han Chou and Sylvia Do, for providing insightful suggestions during my stay there. I would like to thank my labmates in Department of Biomedical Sciences (BMS), Dr. Saurabh Verma, Dr. Sudhanva Kashyap, Melanie Abongwa, Shivani Choudhary and Mark McHugh, for helping out when I felt down in graduate study and teaching me a lot of experimental techniques. It was full of great memories and experience working with them. I would like to thank Dr. Xiangwei Du for his great efforts in synthesizing (S)-anabasine derivatives and invaluable suggestions in research. I would like to thank funding agencies, namely Iowa State University, National Institute for Health and The Hatch Act and.

I would like to thank Department of Chemistry for supporting me throughout the graduate program by providing Teaching Assistantship (TA). It was a memorable experience to obtain confidence gradually by teaching undergraduate chemistry

courses. I would like to thank Chemistry DOGE Dr. Arthur Winter, Chemistry staff Lynette, and BMS staff, Kim, for being kind and helpful during my graduate study.

I would like to especially thank He Nan and Melanie Abongwa, who were disturbed many times by me but still always give me a hand! I would also like to thank Dr. Hsiang-Ting Lei, Dr. Jani Reddy Bolla, Nitin Kumar, Abhijith Radhakrishnan, Jared Delmar, Yen Nguyen, Huangchao Yu, Andrea Thooft, Bryan Lampkin and all the other friends for inspiration and moral support during my hard struggles in switching labs. I wish all the best to all of my friends and colleagues in Iowa State University. I am indebted to my parents, Mr. Guozhong Zheng and Miss. Lifang Zhou, and other family members, who have always inspired and encouraged me to pursue my interest. I would like to dedicate this thesis work to those I love, who made my accomplishments possible.

ABSTRACT

Ascariasis is a neglected tropical disease that is caused by the nematode parasite *Ascaris*. *Ascaris* infections have high morbidity, cause debilitating conditions and affect at least one-quarter of world's population. With no effective vaccine available, the prophylaxis and treatment of ascariasis rely on a limited supply of anthelmintic drugs. The massive use of anthelmintics led to the selection of resistant parasites, which has incurred anthelmintic resistance in many parasite species. It is therefore important to identify new lead compounds for anthelmintic drugs or to enhance the potency of existing anthelmintics. To address this issue, I chose a recently characterized ligand-gated ion channel, ACR-16 on *Ascaris suum*, as my drug target and attempted to discover new therapeutic compounds targeting at *Asu*-ACR-16 receptor. I used two approaches of structure-based drug discovery that are arranged into individual chapters in my thesis. In Chapter 2, the receptor-based drug design was applied to perform virtual screening of a library of ligands into the potential binding sites of receptor structure. The hit candidates were then pharmacologically characterized on *Asu*-ACR-16 expressed in *Xenopus laevis* oocytes using two-electrode voltage clamp. In Chapter 3, the ligand-based drug design was applied to optimize the structure of nicotine, a known nAChR agonist, to identify more potent and efficacious *Asu*-ACR-16 agonists. In conclusion, we reported four novel allosteric modulators from virtual screening and several (S)-anabasine derivatives as highly potent *Asu*-ACR-16 agonists.

CHAPTER I

GENERAL INTRODUCTION

1. Introduction

1.1 *Ascaris*: a soil-transmitted helminth

Parasites are organisms that live on (ectoparasites) or in (endoparasites) the host organism and harm the host. Endoparasites, including all parasitic worms, are parasites that inhabit in different organs and tissues of the host. Helminths, meaning parasitic worms, comprise three main groups: the *nemathelminths* (roundworms), the *trematodes* (flukes) and the *cestodes* (tapeworms). Intestinal helminths, namely roundworms (*Ascaris*), whipworms (*Trichuris trichiura*) and hookworms (*Anclostoma duodenale* and *Necator americanus*), are transmitted through contaminated soil, and thus called soil-transmitted helminths (STHs).

As a most widespread STH, *Ascaris* infects approximately 1.4 billion people worldwide and is most common in school-aged children (Keiser *et al.*, 2010; Wani *et al.*, 2010; Dold *et al.*, 2011). *Ascaris* transmits its eggs via the feces of infected persons. Eggs are deposited and become mature on soil if the feces are used as fertilizer. People are infected with *Ascaris* when they ingest eggs, which then grow into adult worms in human intestine. Adult worms feed on nutrients at the expense of the host, and can cause intestinal obstruction, malnutrition and iron-deficiency anemia (Brooker *et al.*, 2004). *Ascariasis* occurs mainly in areas with warm and moist climates where sanitation and hygiene are poor, including sub-Saharan Africa,

the Central and South Americas, China, India and south-east Asia (Savioli *et al.*, 2004).

Ascaris lumbricoides is a human roundworm that infects more than one billion people (de Silva *et al.*, 2003a). *Ascaris suum*, a roundworm that is very similar to the human parasite, *A. lumbricoides*, infects pigs with high prevalence rates. *A. suum* infection reduces porcine feed to gain ratios and causes liver condemnation, which incur severe economic losses (Stewart *et al.*, 1988).

The life cycle of *A. suum*, starts from eggs that are ingested by the host pig (Fig. 1). The one-celled stage eggs are later develops into the infective stages (L2) larvae, which are then released from the small intestine of the host during hatching. The L2 juveniles after hatching penetrate the intestinal mucosa and enter into the portal circulation of the liver within 24 h. The L2 moults into L3 juvenile in liver and later enters into the systemic circulation. The larvae traverse from the blood stream into the lungs via pulmonary arteries, 4 to 6 days after infection. The larvae penetrate the lung tissue to reach pulmonary capillaries and later into alveoli of the lung, 2 weeks after infection. The larvae ascend the bronchial tree to reach the throat and are swallowed during coughing. The L3 larvae are re-ingested and arrive in the small intestine to complete their growth from L3 to L4 and adults. It takes about 2-3 months for this cycle to complete from ingestion of eggs to the adult worms. The adult worms can reproduce and live 1-2 years in the intestine. Female worms reproduce about 200,000 eggs per day, which are then passed in the host feces. The contaminated feces are source of infection to other hosts (Dold *et al.*, 2011).

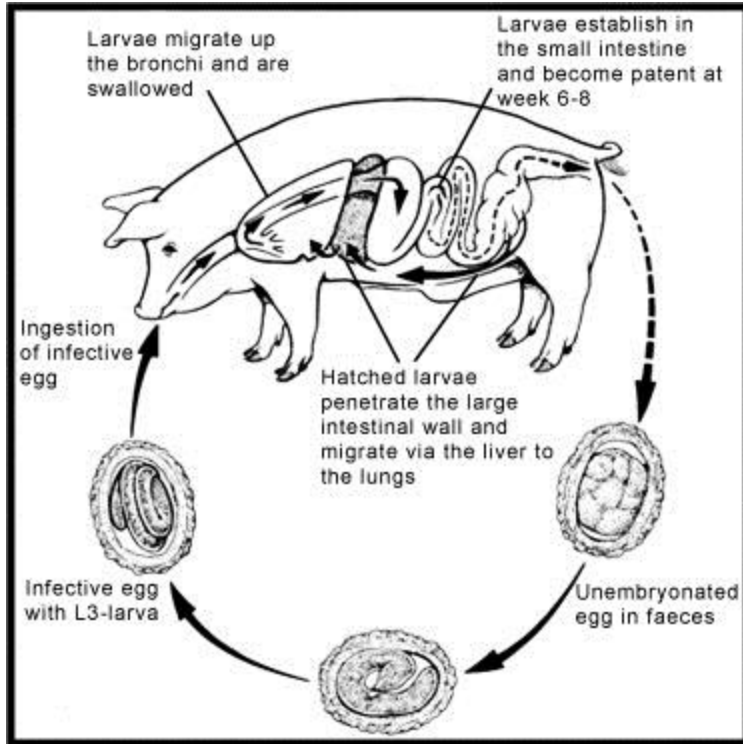


Fig 1. the life cycle of *A. suum* in the pig (Dold *et al.*, 2011).

1.2 Anthelmintic drugs and resistance

No vaccines are currently effective against nematode helminthiasis (Hewitson *et al.*, 2014). The prophylaxis and treatment of these infections mainly rely on chemotherapy. The drugs that are used to control helminthiasis are called “anthelmintics”. Regrettably, there are few classes of anthelmintic drugs, classified based on similar chemical structure and mode of action.

Some classic anthelmintic drugs act rapidly and selectively on neuromuscular transmission of nematodes. The neurotransmitters, such as acetylcholine (ach), γ -aminobutyric acid (GABA) and glutamate, are released at the neuromuscular

junctions and activate the post synaptic receptors on the somatic muscle (nicotinic acetylcholine receptors (nAChRs) or GABA-gated chloride channels) and pharynx (nAChRs or glutamate-gated chloride channels (GluCl)). Nicotinic agonists, namely levamisole, butamisole, pyrantel, morantel, bephenium, thenium and methyridine, are cholinomimetics that act selectively as agonists at synaptic and extra-synaptic nAChRs on nematode muscle cells, produce contraction and spastic paralysis (Martin, 1997). Paraherqumide is a competitive antagonist of levamisole-sensitive nAChRs in nematode body wall and induces flaccid paralysis (Robertson *et al.*, 2002). Piperazine is a GABA receptor agonist on nematode muscles that increases the opening of the muscle membrane Cl⁻ channels, hyperpolarizes the membrane potential and causes flaccid paralysis (Martin, 1982). The avermectins, such as ivermectin, abamectin and milbemycin, are a group of broad-spectrum macrocyclic lactone antibiotic anthelmintics to control nematode parasites in human and livestock. The avemectins increase the opening of GluCl and produce paralysis of pharyngeal pumping (Campbell *et al.*, 1984).

Other classic anthelmintics inhibit biochemical pathways. The benzimidazoles, such as albendazole and mebendazole, bind selectively to β -tubulin of nematodes and inhibit microtubule formation (Lacey, 1990).

Several modern anthelmintic drugs are recently reported. Emodepside is a cyclooctadepsipeptide that potentiates the SLO-1 Ca²⁺-dependent K⁺ channels on nematode body muscle (Kulke *et al.*, 2014). Tribendimidine is a selective agonist of bephenium-sensitive nAChRs and produces muscle depolarization and contraction (Robertson *et al.*, 2015).

Unfortunately, the wide and intensive use of limited number of anthelmintics has selected the nematodes that can survive the treatment in the worm population. These nematodes are genetically and physiologically resistant to the anthelmintic drugs and remain their resistant genotypes and phenotypes to next generation (Prichard, 1994). Anthelmintic resistance has been reported in many animals (Kaplan, 2004; Wolstenholme *et al.*, 2004) and raised the concerns for the development of resistance in humans (Taman *et al.*, 2014). Resistance to nicotinic agonists is associated with changes in structures of target nAChRs in nematodes (Lewis *et al.*, 1980). Ivermectin resistance may be caused by alteration of P-glycoproteins which transport ivermectin (Xu *et al.*, 1998). Benzimidazole resistance is attributed to alterations in their high-affinity binding to parasite β -tubulin (Lubega *et al.*, 1990). Resistance has reduced the efficacy of many currently used anthelmintics and restricted available treatments for helminthiasis. Therefore, it is crucial to identify new drug target sites on nematode or develop new therapeutic drugs that selectively target nematode receptors to counter the development of anthelmintic resistance (Shalaby, 2013).

1.3 Nicotinic acetylcholine receptors and interactions with agonists

Ach was first identified as a neurotransmitter in vertebrates in 1920s. Ach was isolated from *Ascaris* and was found to produce muscle contractions on *Ascaris* in 1950s (Mellanby, 1955). The activity of choline acetyltransferase was later studied in the excitatory motor neuron of *Ascaris*, which confirmed ach was the excitatory neurotransmitter (Johnson *et al.*, 1985). Ach elicited depolarization and increased muscle cell conductance of *Ascaris* (Coloquhoun *et al.*, 1991).

There are two main classes of acetylcholine receptors in vertebrates, nicotinic and muscarinic. Nicotinic AChRs are ligand-gated ion channels (LGICs) that are activated by nicotine, whereas muscarinic AChRs are G-protein coupled receptors (GRCRs) that are activated by muscarine. nAChRs present in both neuronal cells and non-neuronal cells, and mediate synaptic transmission at the neuromuscular junction of vertebrates (Changeux *et al.*, 1998).

nAChRs are non-selective cation channels that belong to the Cys-loop LGIC superfamily, which also includes cation channel: 5-hydroxytryptamine type 3 receptors (5-HT₃Rs), two anion channels: GABA and glycine receptors. The common feature of this superfamily is a cys-loop formed by disulphide bonds between two cysteines separated by 13 conserved amino acids in the N-terminal domain (Lester *et al.*, 2004). nAChRs comprise five subunits arranged around a central ion-conducting pore that is permeable to Na⁺, K⁺ and sometimes Ca²⁺ depending on the receptor subtypes. Each subunit starts from extracellular N terminal, followed by an extracellular immunoglobulin fold (about ten β strands), four transmembrane spanning domains (M1, M2, M3, M4), a cytoplasmic domain between M3 and M4, ended with extracellular C terminal. M2 helix lines the channel pore. Subunits are classified into α -subunit and non- α subunit, depending on the appearance of vicinal cysteines on the extracellular domain. The pentameric nAChRs are made of two or more α -subunits, and three or less non- α subunits (Fig. 2). The *Asu-ACR-16*, the drug target I am working on in this thesis, is made up of five α -subunits and thus is a homomeric pentamer which is sensitive to nicotine.

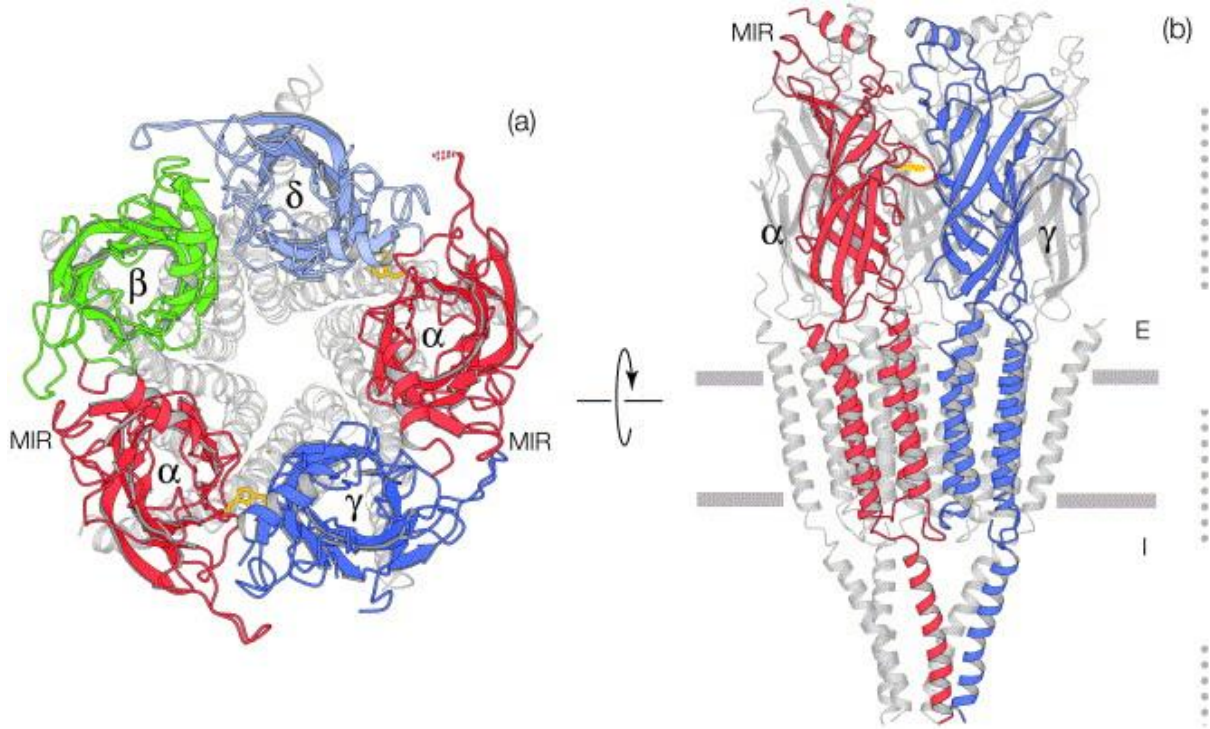


Fig 2. *Torpedo* nAChR at 4 Å resolution (PDB ID: 2BG9), as viewed from the synaptic cleft (A) and parallel with the membrane plane (B). The orthosteric ligand-binding site is highlighted in (A) and the front two subunits are highlighted in (B) (α , red; β , green; γ , blue; δ , light blue). In (B), horizontal bars, the membrane; E, extracellular; I, intracellular. (Unwin, 2005a)

The vicinal cysteines in loop C are important for agonists and competitive antagonists binding to open the channel. The orthosteric ligand-binding site for agonists and competitive antagonists to bind in is at the interface of two adjacent subunits, which is formed by the loops A, B & C from the principal face (+) of α -subunit and by the loops D, E & F from the complementary face (-) of non- α subunit or α -subunit (Wu *et al.*, 2015). The allosteric ligand-binding site for allosteric

modulators or non-competitive ligands to bind in can be predicted from the crystal structure of *Caenorhabditis elegans* GluCl_s in complex with its allosteric modulator (ivermectin) (Hibbs *et al.*, 2011). The allosteric site is thus at the interface region between M2(+), M3(+), M1(-) and M2(-) in the transmembrane domain of nAChRs (Fig. 3).

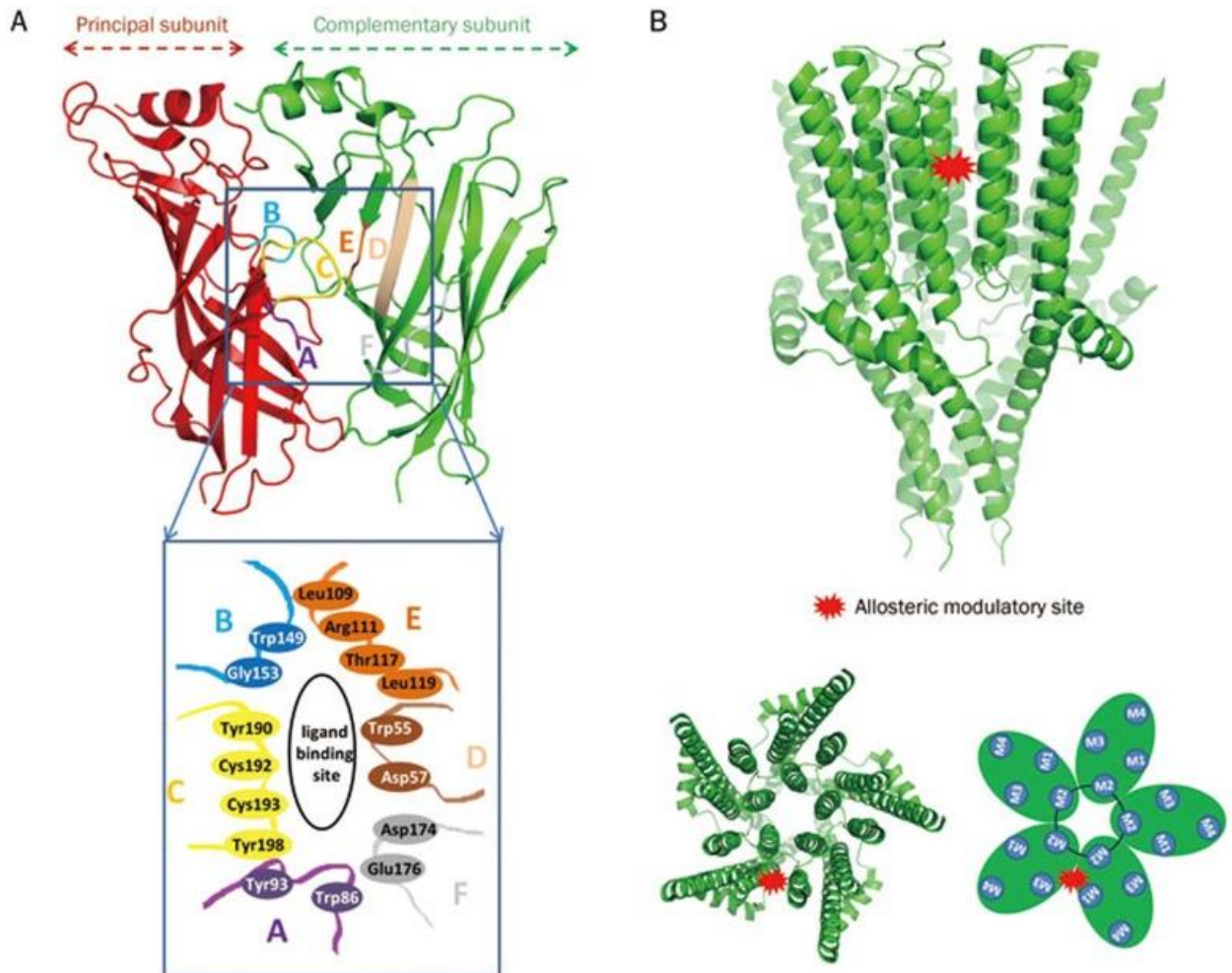


Fig 3. Orthosteric ligand-binding and allosteric ligand-binding sites of Cys-loop receptors. (A) Closed-up view of the orthosteric ligand-binding site of $\alpha_4\beta_2$ nAChR showing the amino acid residues in the loops that participate in its formation. Loops A, B and C are provided by the principal subunit and loops D, E and F by the

complementary subunit. (B) The X-ray structure of the transmembrane domain of the 5-HT₃ receptor, a nAChR homolog protein. Each subunit of the transmembrane domain contributes four helices (M1-4), which approach one another at the intracellular membrane surface, creating a tapered central pore. View of the side of the transmembrane domain showing a potential binding site for allosteric modulators (marked by a red asterisk). The intersubunit allosteric modulatory site is modeled based on the crystal structure of ivermectin bound GluCl. The site is located in the transmembrane domain between the four transmembrane segments (M1-4). (Wu *et al.*, 2015)

Nicotinic agonists target at nAChRs, and typically contain a protonatable amine (eg. nicotine and epibatidine) or quaternary ammonium (eg. ach) that makes cation- π interaction with five highly conserved aromatic residues from the principal subunit (Xiu *et al.*, 2009). Another feature of nicotinic agonists is a hydrogen bond acceptor (eg. pyridine N of nicotine and carbonyl O of ach), which is about 4-6 Å away from the cationic nitrogen, that make water-mediated hydrogen bonds with the carboxyl and amide backbones of two residues from the complementary subunit (Fig. 4) (Blum *et al.*, 2010). All the nicotinic full agonists of *Asu-ACR-16* share these characteristics (Fig. 5).

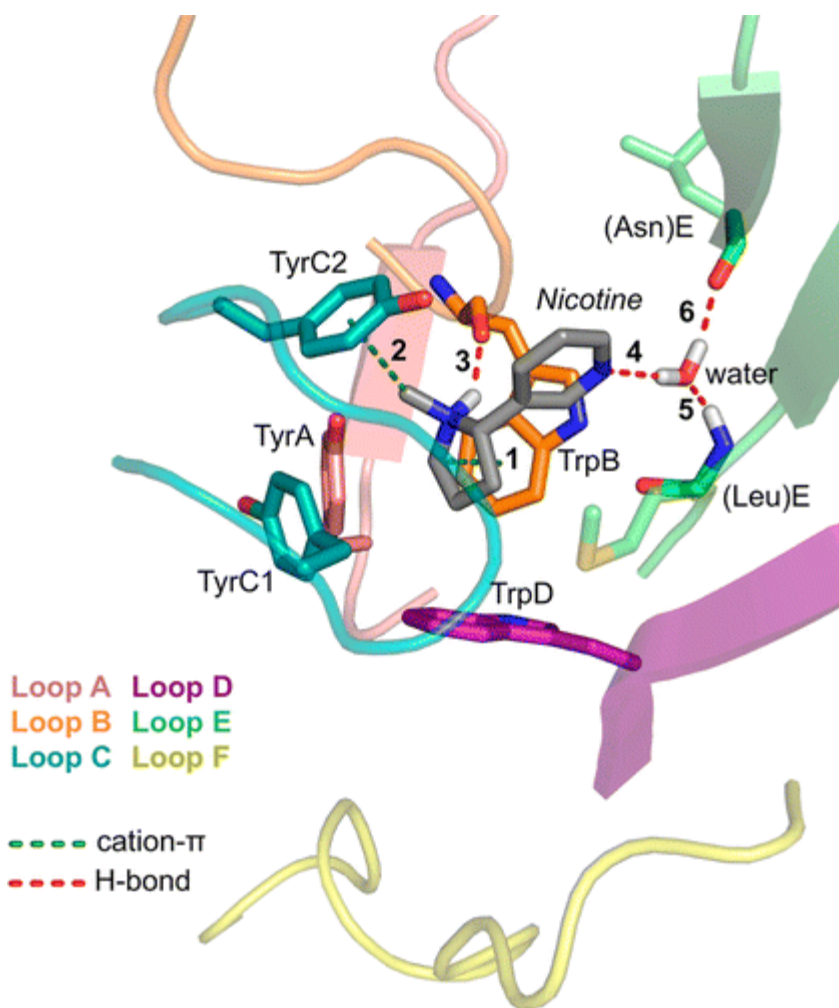


Fig 4. Nicotinic agonist binding interactions suggested by acetylcholine-binding protein (AChBP) and key binding site residues. Shown is a structure of AChBP in complex with nicotine (PDB ID: 1UW6). Explicit hydrogens are displayed for hydrogen bonding groups. Asn (loop E) and Leu (loop E) are conserved in all nAChRs but are replaced by Leu and Met respectively in the AChBP structure shown. (Van Arnam *et al.*, 2014)

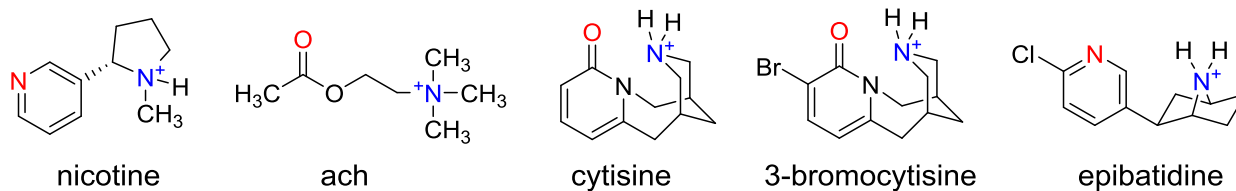


Fig 5. Nicotinic agonists that are full agonists of *Asu*-ACR-16. Cationic nitrogen (blue) and hydrogen bond acceptor (red) correspond to the nicotinic pharmacophore.

1.4 Homology modeling and virtual screening

Though the three-dimensional structure of *Asu*-ACR-16 has not been determined to date, last decade has witnessed discoveries of several pentameric LGICs structures that are homologous proteins of *Asu*-ACR-16. The X-ray structures of invertebrate acetylcholine-binding proteins (AChBPs) in complex with different ligands were reported since 2001 (Brejc *et al.*, 2001). AChBPs share 20-25% sequence identity with the nAChR extracellular domain and thus serve atomic model of the nAChR extracellular domain for studying the ligand-receptor interactions. The first full-length structure was the *Torpedo marmorata* nAChR by cryo-electron microscopy (cryo-EM) published in 2005 (Unwin, 2005a). Two prokaryotic LGICs, which are cation ion channels and show high sequence similarity to the nAChRs, were determined three years later (Hilf *et al.*, 2008; Hilf *et al.*, 2009). The crystal structure of a eukaryotic LGIC, *C. elegans* GluCl was determined in 2011, which revealed the transmembrane allosteric ligand-binding site for the first time (Hibbs *et al.*, 2011). Two mammalian LGICs, the human GABA_Aβ3 receptor and the mouse 5-HT_{3A} receptor were determined in 2014, which gave insight into the signaling mechanisms (Hassaine *et al.*, 2014; Miller *et al.*, 2014).

These nAChRs homologs sharing high sequence identities ($\geq 30\%$) with our target receptor, *Asu-ACR-16* can be used as structural templates to predict *Asu-ACR-16* structure using homology modeling (Cavasotto *et al.*, 2009). The basic assumption of homology modeling is that homologous proteins remain evolutionarily conserved sequence and three-dimensional structure as well (Kaczanowski *et al.*, 2009). The homologous proteins similar in sequences usually imply significant structural similarity (Marti-Renom *et al.*, 2000). Thus, we can replace the amino acids on the homologous structure with those on the target protein, followed by optimization of the model geometry to predict the target protein structure.

With the structural model of *Asu-ACR-16* receptor and ligand library, potential binding ligands can be found through *in silico* screening, based on the binding affinities calculated from the ligand-receptor interactions (Rester, 2008). AutoDock is one of the most popular docking programs to perform virtual screening (Morris *et al.*, 2009b). One successive application of AutoDock is the discovery of novel binding modes of HIV integrase inhibitor by J. Andrew McCammon. This helped the pharmaceutical company Merck to design new drug targeting HIV integrase, which led to the first clinically-approved HIV integrase inhibitor (raltegravir).

1.5 Electrophysiology and its technique: two-electrode voltage clamp

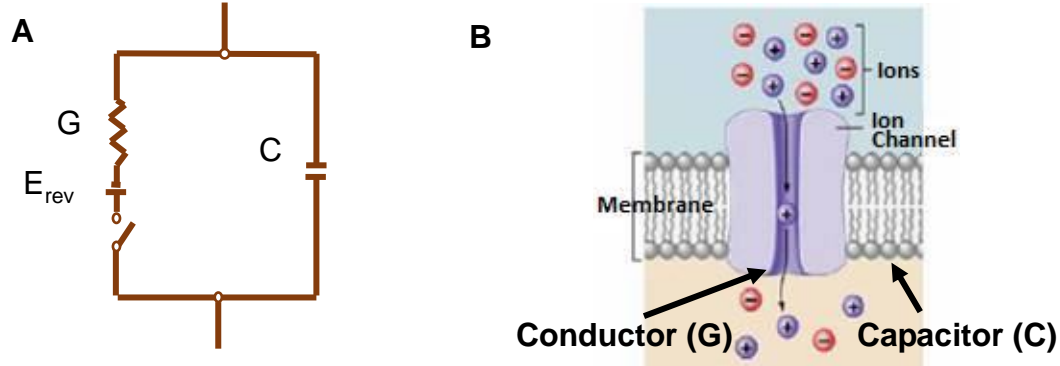


Fig 6. Equivalent circuit (A) representing a membrane ion channel (B). G: conductor, E_{rev} : reversal potential, C: capacitor.

Ion channel is a pore-forming membrane protein where ions fast transport through by passing down their electrochemical potential gradient (Hille, 2001). For a selective channel that is permeable to one type of ion (i), the electrochemical potential difference between the interior and exterior of cell is:

$$\Delta \mu_i = \mu_i^{in} - \mu_i^{out} = RT \ln \frac{c_i^{in}}{c_i^{out}} + z_i F (V^{in} - V^{out}) .$$

Where μ_i^{in} and μ_i^{out} are the electrochemical potentials of ion i inside and outside the cell, R is the gas constant ($8.314 \text{ V C K}^{-1} \text{ mol}^{-1}$), T is the absolute temperature, c_i^{in} and c_i^{out} are the concentrations of ion i inside and outside the cell, z_i is the charge of ion i , F is Faraday's constant ($9.648 70 \times 10^4 \text{ C mol}^{-1}$). The Nernst or equilibrium potential is $E_i = -\frac{RT}{z_i F} \ln \frac{c_i^{in}}{c_i^{out}}$, whereas the membrane potential is $V_m = V^{in} - V^{out}$. The

reversal potential is the voltage at which the current changes its direction, in other words, there is no net flow of ion i . This happens when the electrical potential gradient (V_m) balances off the concentration gradient, which makes the reversal potential equals the Nernst potential E_i (Sherman-Gold *et al.*, 1993).

Conductor is the place where current flow through. In electrophysiology, several ion channels in membrane that open simultaneously behave similar to the parallel conductors ($G_{total} = \sum G_i$) (Fig. 6). More accurate representation of an ion channel is a conductor in series with two additional circuit elements: 1) a switch that represents the channel gating, which will be in the conducting position when the gate is open, and 2) a battery that represents the reversal potential of the channel (E_i). The ion channels (conductors) contribute to the ionic current: $I_{ionic} = N \times G_i \times (V_m - E_i)$, where N is the number of channels, each conductance of which is G_i .

The thinness of membrane makes it a good capacitor, which has the ability to store charge (ΔQ) when a voltage occurs across the two boundaries (ΔV_m). The membrane capacitors contribute to the capacitive current: $I_c = \frac{\Delta Q}{t} = \frac{C_m \Delta V_m}{t}$, where C_m is the membrane capacitance.

Hence, the total membrane current is $I_m = I_{ionic} + I_c$. The membrane current (I_m) can be used to study the bioelectrical properties of ion channels (I_{ionic}), if we offset the interference of capacitive current (I_c) by keeping the membrane potential constant.

A OOCYTE TWO-ELECTRODE VOLTAGE CLAMP

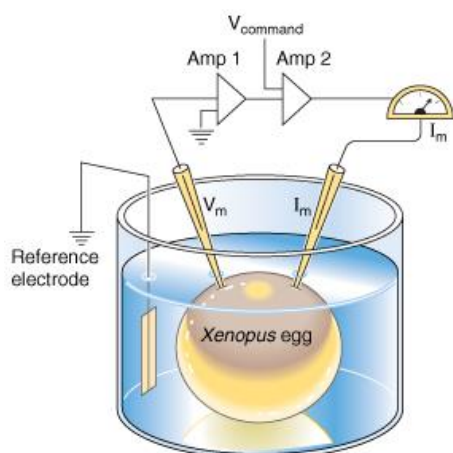


Fig 7. Simplified electrical scheme of two-electrode voltage clamp.

The two-electrode voltage clamp (TEVC) is an electrophysiological technique which was first introduced by Kenneth Cole and George Marmont in 1940s and later became a technique for measuring ion flow through cell membrane channels (I_m) and understanding the physiological and pharmacological properties of ion channels in various living systems. Two intracellular microelectrodes are used in TEVC: a voltage sensing electrode (V_m) and a current injecting electrode (I_m). The general principle of TEVC is to clamp the membrane voltage at a desired value ($V_{command}$), meanwhile measure the transmembrane current (I_m) required in maintaining the voltage (Fig. 7) (Finkel *et al.*, 1985). *Xenopus laevis* oocytes are widely used expression systems for cloned ion channels. The expressed ion channels then can be characterized as potential target for drug treatment by using TEVC or whole-cell patch clamp. TEVC recording of *Xenopus* oocytes provides information of current-voltage relationships, kinetics and response of ion channels to

different drugs under different physiological conditions (Robertson *et al.*, 2008). In this thesis, I used TEVC to characterize and validate the pharmacological activities of ligands selected from virtual screening toward the drug target, *Asu-ACR-16*.

2. Thesis Organization

Chapter 1 gives the general background introduction of the need to identify new lead compounds as anthelmintic drugs to counter the increasing anthelmintic resistance globally. The structural and functional information of the drug target, *Asu-ACR-16* are described in detailed. The general principals of computational biology and electrophysiology used in this thesis are also discussed.

Chapter 2 is a manuscript published in *International Journal for Parasitology: Drugs and Drug Resistance* in 2016. Four novel allosteric modulators of *Asu-ACR-16* were identified from virtual screening based on the structural models of drug target. The electrophysiological studies were performed to validate the pharmacological activities of these modulators.

Chapter 3 is a manuscript in preparation for a peer-review journal. Nicotine is a potent agonist of nAChRs. I investigated several nicotine derivatives as *Asu-ACR-16* agonists using electrophysiological techniques. With the help of synthetic chemistry, the nicotinic pharmacophore was optimized to enhance the potency and efficacy of *Asu-ACR-16* agonists.

Chapter 4 presents the general conclusion and future studies in this area.

CHAPTER 2**THE ASCARIS SUUM NICOTINIC RECEPTOR, ACR-16, AS A DRUG TARGET:
FOUR NOVEL NEGATIVE ALLOSTERIC MODULATORS FROM VIRTUAL
SCREENING**

A manuscript published in *International Journal for Parasitology: Drugs and Drug Resistance* **6**(1): 60-73.

Fudan Zheng¹, Alan P. Robertson², Melanie Abongwa², Edward W. Yu^{1, 3}, Richard J. Martin^{2*}

¹ *Department of Chemistry, College of Liberal Arts and Sciences, Iowa State University, Ames, Iowa 50011, USA*

² *Department of Biomedical Sciences, College of Veterinary Medicine, Iowa State University, Ames, Iowa 50011, USA*

³ *Department of Physics and Astronomy, College of Liberal Arts and Sciences, Iowa State University, Ames, Iowa 50011, USA*

Abstract

Soil-transmitted helminths infections in humans and livestock cause significant debility, reduced productivity and economic losses globally. There are a limited number of effective anthelmintic drugs available for treating helminths infections, and their frequent use has led to the development of resistance in many parasite species. There is an urgent need for novel therapeutic drugs for treating these parasites. We have chosen the ACR-16 nicotinic acetylcholine receptor of *Ascaris suum* (*Asu*-ACR-16), as a drug target and have developed three-dimensional models of this transmembrane protein receptor to facilitate the search for new bioactive compounds. Using the human $\alpha 7$ nAChR chimeras and *Torpedo marmorata* nAChR for homology modeling, we defined orthosteric and allosteric binding sites on *Asu*-ACR-16 receptor for virtual screening. We identified four ligands that bind to sites on *Asu*-ACR-16 and tested their activity using electrophysiological recording from *Asu*-ACR-16 receptors expressed in *Xenopus* oocytes. The four ligands were acetylcholine inhibitors (SB-277011-A, IC_{50} , $3.12 \pm 1.29 \mu\text{M}$; (+)-butaclamol Cl, IC_{50} , $9.85 \pm 2.37 \mu\text{M}$; fmoc-1, IC_{50} , $10.00 \pm 1.38 \mu\text{M}$; fmoc-2, IC_{50} , $16.67 \pm 1.95 \mu\text{M}$) that behaved like negative allosteric modulators. Our work illustrates a structure-based *in silico* screening method for seeking anthelmintic hits, which can then be tested electrophysiologically for further characterization.

Keywords

Asu-ACR-16; Structure-based drug discovery; Homology modeling; Orthosteric site; Allosteric modulator; *Xenopus* expression

Abbreviations

ECD, extracellular domain; TID, transmembrane and intracellular domain; (+), principal subunit; (-), complementary subunit; NAM, negative allosteric modulator; nAChR, nicotinic acetylcholine receptor; AChBP, acetylcholine-binding protein

1. Introduction

Soil-transmitted gastrointestinal nematodes, namely roundworms, whipworms and hookworms, infect approximately two billion people worldwide and pose a significant health challenge to humans and animals (de Silva *et al.*, 2003b; Bethony *et al.*, 2006). The infections with the soil-transmitted helminths can cause malnutrition, iron-deficiency anemia and impaired cognitive performance (Crompton, 2000; Hotez *et al.*, 2007). Currently, there are no effective vaccines available (Hewitson *et al.*, 2014), and sanitation is not adequate in many countries. The World Health Organization (WHO) recommends four anthelmintics for treatment and prophylaxis of soil-transmitted nematode infections: albendazole, mebendazole, levamisole and pyrantel (Keiser *et al.*, 2008). The repeated use of a limited number of anthelmintic drugs has led to an increase in drug resistance in animals and there are similar concerns for humans. It is therefore important to identify novel therapeutic compounds that selectively target receptors of parasitic nematodes so that we maintain effective therapeutics.

The nicotinic acetylcholine receptors (nAChRs) are pentameric ligand-gated ion channels that mediate synaptic transmission at neuromuscular junctions of vertebrates and invertebrates (Changeux *et al.*, 1998). The neurotransmitter, acetylcholine, activates nAChRs by binding to orthosteric binding sites on the extracellular domain of the receptor and triggers the opening of the channel pore in the transmembrane domain. The opening of the nicotinic receptors leads to an influx of sodium and calcium depending on the receptor subtypes, as well as an output of potassium ions, followed by membrane depolarization and muscle contraction.

Nicotinic anthelmintics are selective agonists of nematode muscle nAChRs which cause spastic paralysis of the parasites (Martin *et al.*, 2010). There are three different pharmacological subtypes of nAChRs present on muscle of *Ascaris suum*. The anthelmintics, levamisole and pyrantel are selective agonists of L-subtypes of nAChRs in *A. suum* (Martin *et al.*, 2012). Bephenium selectively activates B-subtypes of nAChRs. Nicotine and oxantel selectively activate N-subtypes of nAChRs in *A. suum* (Qian *et al.*, 2006). The anthelmintic monepantel activates nAChRs which are composed of DEG-3-like subunits (*Haemonchus contortus* MPTL-1, *Caenorhabditis elegans* ACR-20 and *H. contortus* ACR-23 subunits; (Rufener *et al.*, 2010; Buxton *et al.*, 2014). We have selected the N-subtype of nAChR that is composed of ACR-16 subunits (Ballivet *et al.*, 1996; Polli *et al.*, 2015) for a drug target, because it is pharmacologically different to the other nicotinic receptor subtypes (Raymond *et al.*, 2000), for further study. *Asu*-ACR-16 transcript has been found in the *A. suum* muscle and may be involved in locomotion.

The ACR-16 nicotinic acetylcholine receptor of *A. suum* (*Asu*-ACR-16) is a homomeric receptor made up of five identical α subunits. Homomeric nAChRs have five identical orthosteric binding sites where agonists and competitive antagonists bind at the interface of two adjacent subunits. The orthosteric site is in the extracellular domain and is formed by the loops A, B & C of the principal subunit and by the loops D, E & F on the complementary subunit (Galzi *et al.*, 1991; Arias, 2000b). In addition, three allosteric binding sites close to the orthosteric binding sites in the extracellular domain have been observed in the $\alpha 7$ nAChR-AChBP chimera (Spurny *et al.*, 2015). In the transmembrane domain, an intrasubunit allosteric binding site was found in *Rattus norvegicus* $\alpha 7$ nAChR (Young *et al.*, 2008), while an intersubunit allosteric binding site has been found in *C. elegans* glutamate-gated chloride channel (GluCl) (Young *et al.*, 2008; Hibbs *et al.*, 2011; Spurny *et al.*, 2015). These well-studied binding sites in nAChRs or other Cys-loop receptors provided our framework for characterizing putative orthosteric and allosteric sites in *Asu*-ACR-16.

Because of the lack of a crystal structure for *Asu*-ACR-16, we used homology modeling to predict the protein structure, based on the observations that proteins with similar sequences usually have similar structures (Cavasotto *et al.*, 2009). In this study, we used homology modeling to predict the three-dimensional structure of *Asu*-ACR-16, based on the observed experimental structures of the human $\alpha 7$ nAChR chimeras and the *Torpedo marmorata* nAChR as templates. Virtual screening was performed for the ACR-16 orthosteric binding sites, using the predicted structure to identify the potential candidates of agonists and competitive antagonists. Allosteric binding sites were also used to examine the binding

properties of virtual screening hits. Subsequently, we tested the pharmacological profiles of virtual screening hits on *Asu*-ACR-16 receptors expressed in *Xenopus laevis* oocytes, using a two-electrode voltage clamp to test the activity of the hits on the receptors.

2. Materials and methods

2.1 Identification of template structures

We selected the extracellular domain of *Asu*-ACR-16 (ECD-*Asu*-ACR-16) because it forms a homologomer that allows homology modeling. In addition, many of the agonists that activate *Asu*-ACR-16, acetylcholine, nicotine, cytosine, epibatidine (Abongwa et al., under review), are also known to bind to the orthosteric binding sites of extracellular domain of *Lymnaea stagnalis* AChBP or *Aplysia californica* AChBP (Celie et al., 2004; Li et al., 2011b; Rucktooa et al., 2012; Olsen et al., 2014a). In addition to the orthosteric binding site, three separate allosteric binding sites in the extracellular domain of $\alpha 7$ nAChR are now recognized (Bertrand et al., 2008; Pan et al., 2012; Spurny et al., 2015), increasing the possibility of identifying allosteric modulators.

The amino acid sequence of *Asu*-ACR-16 (Fig. 1) was obtained from the UniProtKB/SwissProt database with the accession number **F1KYJ9** (Wang et al., 2011). Structural templates were identified by using BLASTP on NCBI network service (Altschul et al., 1997) and PSI-BLAST on the ProtMod server (Rychlewski et al., 2000) by searching in the Protein Data Bank (Berman et al., 2000). Three crystal structures of human $\alpha 7$ nAChR chimeras with different co-crystal ligands in

orthosteric binding site were used: epibatidine bound (PDB code: 3SQ6; (Li *et al.*, 2011b), no ligand (PDB code: 3SQ9; (Li *et al.*, 2011b), and α -bungarotoxin bound (PDB code: 4HQP; (Huang *et al.*, 2013). These structures were selected as the templates for three different bound-forms of the ECD-*Asu*-ACR-16. The three models were: the agonist-bound form ECD-*Asu*-ACR-16; the apo form ECD-*Asu*-ACR-16 and; the antagonist-bound form ECD-*Asu*-ACR-16 (Fig. 2A).

We modeled the transmembrane and intracellular domains of *Asu*-ACR-16 (TID-*Asu*-ACR-16, Fig. 2B) because of the presence of an intrasubunit allosteric binding site that is found in $\alpha 7$ nAChR and an intersubunit allosteric binding site that is demonstrated in a Cys-loop receptor, GluCl crystal structure in complex with ivermectin (Bertrand *et al.*, 2008; Young *et al.*, 2008; Hibbs *et al.*, 2011). Ivermectin is a known allosteric modulator of $\alpha 7$ nAChRs (Krause *et al.*, 1998). The *T. marmorata* nAChR (PDB code: 2BG9 chain A; (Unwin, 2005b) is the only pentameric nAChR structure with the transmembrane domains and partial intracellular domains determined. Therefore, the transmembrane and intracellular domains of *T. marmorata* nAChR (TID-*Tma*-nAChR) were selected as the template for our TID-*Asu*-ACR-16 model.

The sequence of the ECD-*Asu*-ACR-16 and the human $\alpha 7$ nAChR chimera (SwissProt ID: P36544; (Peng *et al.*, 1994) were aligned using CLUSTALW multiple alignment (Thompson *et al.*, 1994). The sequence of the TID-*Asu*-ACR-16 and TID-*Tma*-nAChR (SwissProt ID: P02711; (Devillers-Thiery *et al.*, 1983; Devillers-Thiery *et al.*, 1984) were aligned using CLUSTALW.

2.2 Homology modeling of *Asu*-ACR-16

We used Modeller (Eswar *et al.*, 2007) to build a three-dimensional model of ECD-*Asu*-ACR-16 and used JACKAL (http://wiki.c2b2.columbia.edu/honiglab_public/index.php/Software:Jackal) to build the model of TID-*Asu*-ACR-16 for each of the five subunits. These five subunits were then assembled to generate the pentamer using COOT software (Emsley *et al.*, 2004). The model geometry was first refined manually, and then optimized by PHENIX software (Adams *et al.*, 2010). Each of the TID-*Asu*-ACR-16 subunits were then merged into the ECD-*Asu*-ACR-16 model by using COOT to edit and alter the C α coordinates of residues around the outer membrane regions. The final optimized pentameric model was then visualized using the program PyMol (The PyMOL Molecular Graphics System, Version 1.7.4, Schrödinger, and LLC., Fig. 2C & S1).

2.3 Structure-based virtual screening

Smiles strings of ligands were downloaded from the lead-like subset of commercially available compounds in the ZINC Database (Irwin *et al.*, 2012) and were converted initially to PDB formats using the PHENIX-eLBOW program (Moriarty *et al.*, 2009). The ligand and receptor input files were then prepared in PDBQT format for AutoDock Vina by using the AutoDock Tools package (Morris *et al.*, 2009a). For initial screening, a docking area was defined visually around the orthosteric binding site of ECD-*Asu*-ACR-16 (Fig. 2D S2A & S2B) by a grid box of 40 Å × 40 Å × 40 Å using 0.375 Å grid point spacing in AutoGrid. The conformations of ligands in the binding sites of the receptor were searched with GALS (Genetic

Algorithm with Local Search; (Morris *et al.*, 1998). The binding free energies between the ligands and receptor were calculated by the combination of the knowledge-based and empirical scoring function in AutoDock Vina (Trott *et al.*, 2010). The best nine binding modes of ligand based on the binding affinities towards the three bound-forms of ECD-Asu-ACR-16 models were implemented by AutoDock 20 runs for each ligand. Each docked ligand was then ranked by its highest binding affinity to the orthosteric binding site of the apo, agonist-bound, or antagonist-bound model. From the 60,000 screened molecules, we selected the top 9 ligands (0.015%) with the highest predicted affinities that had appropriate binding modes within the ligand-binding pockets for further study. We rejected those compounds without a cationic nitrogen in their structure and that were known to be: acutely toxic, or carcinogenic, or respiratory depressants, caused dermatitis or conjunctivitis or to be significant environmental hazards as recorded on the compound Safety Data Sheets available from Sigma Aldrich (<http://www.sigmaaldrich.com/safety-center.html>).

The four virtual screen hits (Table 1) out of the top 9 selected ligands (44%) were then specifically docked into five allosteric binding pockets: the agonist sub-pocket (Fig. S2C & S2D); the vestibule pocket (Fig. S2E & S2F) and; the top pocket (Fig. S2G & S2H); the intersubunit and; the intrasubunit transmembrane sites (Fig. 2E S2I S2J). The docking area was defined visually around each allosteric binding pockets of Asu-ACR-16 by a grid box of 40 Å × 40 Å × 40 Å using 0.375 Å grid point spacing in AutoGrid. The docking was performed by AutoDock Vina (Fig. 3).

2.4 *In vitro* synthesis of cRNA and microinjection into *Xenopus laevis* oocytes

We used TRIzol (Invitrogen™) to extract the total RNA samples from a 1 cm muscle flap and dissected the whole pharynx of *A. suum*. The first-strand of cDNA was synthesized with oligo RACER primer, Random Hexamer and superscript III reverse transcriptase (Invitrogen, Carlsbad, CA, USA) from total RNA in the muscle and pharynx by reverse transcription polymerase chain reaction (RT-PCR). Full-length *Asu-acr-16* cDNA was amplified with the forward primer TTGATGTAGTGGCGTCGTGT, ATCACGCATTACGGTTGATG and the reverse primer GCATTGATGTTCCCTCACCT, ATTAGCGTCCCAAGTGGTTG (Boulin *et al.*, 2011). The XhoI and ApaI restriction enzymes were used to digest the amplified product, which was then cloned into pTB207 expression vector (Boulin *et al.*, 2008) and linearized by NheI. We used the mMessage mMachine T7 kit (Ambion) to *in vitro* transcribe the linearized cDNA to cRNA, which was then precipitated with lithium chloride, re-suspended in RNase-free water, aliquoted and stored at -80 °C.

The ancillary protein RIC-3 is required for the expression of ACR-16 in *Xenopus* oocytes (Halevi *et al.*, 2003). A 50 nL cRNA mixture was prepared with 25 ng *Asu-acr-16* cRNA, 5 ng *Asu-ric-3* cRNA (SwissProt ID: F1L1D9; (Wang *et al.*, 2011) dissolved in RNase-free water. The nanoject II microinjector (Drummond Scientific, PA, USA) was used to inject the cRNA mixture into the animal pole of the de-folliculated *X. laevis* oocyte (Ecocyte Bioscience, Austin, TX, USA). The injected oocytes were separated into 96-well culture plates and incubated in the incubation solution (pH 7.5), which is composed of 100 mM NaCl, 2 mM KCl, 1.8 mM CaCl₂·2H₂O, 1 mM MgCl₂·6H₂O, 5 mM HEPES, 2.5 mM Na pyruvate, 100 U/mL

penicillin, 100 µg/mL streptomycin and changed daily. The injected oocytes were stored at 19 °C for 4-8 days to allow the receptor to be expressed.

2.5 Two-electrode voltage-clamp oocyte recording

We used two-electrode voltage-clamp electrophysiology to record the inward current generated by the activated *Asu*-ACR-16 receptors expressed in *X. laevis* oocytes. 100 µM BAPTA-AM (final concentration) was added into the oocyte incubation solution 4 h prior to recording, to prevent the current produced by the endogenous calcium-activated chloride channels during recording. An Axoclamp 2B amplifier (Molecular Devices, CA, USA) was used for recording and oocytes were held at -60 mV. A PC computer with software Clampex 9.2 (Molecular Devices, CA, USA) was used to acquire the recording data. The microelectrodes used to measure current in oocytes were pulled on a Flaming/Brown horizontal electrode puller (Model P-97, Sutter Instruments), filled with 3 M KCl and had resistances of 20-30 MΩ. The microelectrode tips were broken back carefully with Kimwipes (Wilmington, NC, USA) to reduce the resistance to 2-5 MΩ. The recording solution was: 100 mM NaCl, 2.5 mM KCl, 1 mM CaCl₂·2H₂O and 5 mM HEPES, pH 7.3 (Buxton *et al.*, 2014). Oocytes were placed into a tiny groove of the narrow oocyte recording chamber. The Digidata 1322A (Molecular Devices, CA, USA) was used to control the switches that controlled the perfusion of the chamber at a speed of 4-6 ml/min.

100 µM acetylcholine was applied initially for 10 s as a control to check the viability of the oocytes and *Asu*-ACR-16 expression for all the recordings. Recording

solution was then used to wash out the drug from the oocytes for 2-3 min before next application of drug perfusion.

2.6 Drugs

Table 1 lists the compounds used, their chemical properties and structures. Fmoc-4-(naphthalen-2-yl)-piperidine-4-carboxylic acid (fmoc-2), SB-277011-A hydrochloride hydrate (SB-277011-A), fmoc-4-(naphthalen-1-yl)-piperidine-4-carboxylic acid (fmoc-1) and (+)-butaclamol hydrochloride ((+)-butaclamol Cl), acetylcholine chloride (ach), methyllycaconitine citrate salt (mla) were purchased from Sigma-Aldrich (St Louis, MO, USA). Levamisole hydrochloride (levamisole) was purchased from MP Biomedicals (Santa Ana, CA, USA). With the exception of ach and mla which were dissolved in the recording solution, the rest of chemicals were dissolved in dimethyl sulfoxide (DMSO) to make stock solutions. Stock solutions of 100 mM were prepared, except for SB-277011-A where a stock solution of 10 mM was prepared due to the solubility; stock solutions were frozen until required. Working solutions were then prepared by dilution on the day of the experiment.

2.7 Pharmacological characterization of molecules selected by virtual screening

To characterize the four hits (Table 1) selected by our virtual screening, each drug was applied for 10 s to the oocytes expressing *Asu*-ACR-16 to test if the drugs were agonists. They were then tested as antagonists against ach.

To characterize the antagonistic properties of the four hits, the following protocol was used: a) 10 s of 100 μ M ach alone; b) then 10 s of 100 μ M ach + hit

and then; c) 10 s of 100 μM ach alone. This test procedure was repeated with increasing concentrations of the four hits (Fig. 4A-4D), to determine the inhibitory dose-response relationships and IC_{50} by fitting Hill equations to the inhibitory dose-response curves using GraphPad Prism 5.0 (Graphpad Software Inc., CA, USA). As a further study of the antagonism, each of the four hits was applied before and during 10 s test applications of increasing concentrations of ach (Fig. S4).

2.8 Data analysis

The data from electrophysiological recordings were analyzed using Clampfit 9.2 (Molecular Devices, CA, USA) and GraphPad Prism 5.0 (Graphpad Software Inc., CA, USA). In all recordings, the peak currents in response to applied drugs were measured, which were later normalized to the control 100 μM ach response, and expressed as mean \pm S.E.M. The mean % inhibition of currents elicited by 100 μM ach \pm S.E.M. was used to determine the inhibition percentage, which was quantified using the following equation:

$$\text{Inhibition (\%)} = \left(1 - \frac{I_{ant}}{\frac{I_{ant control}}{I_{max control}} \times I_{max}} \right) \times 100\%$$

where $I_{max control}$ was the peak current of the control 30 s application of 100 μM ach, I_{max} was the peak current of the 100 μM ach that preceded the 10 s co-application of ach and antagonist. I_{ant} was the minimal current during the co-application of 100 μM ach and antagonist. $I_{ant control}$ was the current at the same point from the beginning of the 30 s application as I_{ant} during the control 30 s application of 100 μM ach (Fig. 4E). Concentration-response relationships or concentration-inhibition (%)

relationships were analyzed by fitting data points into the Hill equation, with at least four replicates of each experiment set.

2.9 Drug treatment of *C. elegans*

The wild-type *C. elegans* strain N2 were obtained from the *Caenorhabditis* Genetics Center (University of Minnesota, MN, USA). We grew *C. elegans* at 20 °C on nematode growth media (NGM, 3 g/l NaCl, 17 g/l agar, 2.5 g/l peptone, 1 mM CaCl₂, 5 mg/l cholesterol, 1 mM MgSO₄, 25 mM KPO₄ buffer) agar plates, seeded with *Escherichia coli* OP50 lawn under standard conditions (Brenner, 1974). Ten larvae at L4 stage with active thrashing movement (defined as “normal”) were transferred from NGM plates into M9 buffer (3 g/l KH₂PO₄, 6 g/l Na₂HPO₄, 5 g/l NaCl, 1 mM MgSO₄) in 24-wall plates for each treatment. We counted the number of worms with normal motility in M9 buffer with diluted drugs from the stock solutions ($\leq 1\%$ DMSO) at 0, 5, 10, 15 and 20 min. Five replicates were applied for each treatment. Motility between negative control (1% DMSO, final concentration) and drug treated worms were compared at each time point using student *t*-test.

3. Results

3.1 Sequence alignment of *Asu*-ACR-16 and template homologue proteins

The full-length protein sequence of *Asu*-ACR-16 (504 residues) was retrieved from the SwissProt database, of which the ECD-*Asu*-ACR-16 accounts for 234 residues. The first 25 residues of *Asu*-ACR-16 were excluded from alignment with the full length human nAChR $\alpha 7$ chimera (204 residues) because of the shorter length of the template protein sequence. The human $\alpha 7$ nAChR chimera shows 37.6%

sequence identity and 72.9% sequence similarity with the ECD-*Asu*-ACR-16, based on the alignment generated by CLUSTALW (Fig. 1A, job ID: 65782ad6ad6d). The TID-*Tma*-nAChR subunit A shows 22.0% sequence identity and 45.4% sequence similarity with TID-*Asu*-ACR-16, aligned by CLUSTALW (Fig. 1B, job ID: 644888f4f30e). The residues involved in the putative orthosteric and the allosteric binding sites are highlighted in amino acids sequence of *Asu*-ACR-16.

3.2 Models of the *Asu*-ACR-16 pentamer

The model of the antagonist-bound form of the ECD-*Asu*-ACR-16 subunit starts from an N-terminal α helix followed by seven β strands that comprise an immunoglobulin fold. Loop A (Val114 – Ala122), loop B (Lys169 – Lys179), loop C (Phe213 – Pro220) from the principal subunit, and loop D (Ala78 – Ala83), loop E (Ile143 – Pro144), loop F (Gly185 – Met204) from the complementary subunit are involved in forming the orthosteric binding site. A disulphide bond between Cys152 and Cys166 forms the characteristic component of Cys-loop receptors. The C-terminal continues into the transmembrane domain (Fig. S1A).

The transmembrane domains of the *Asu*-ACR-16 model are made of four α -helices (M1, M2, M3 and M4). M1 links to the $\beta 7$ sheet of the extracellular domain and extends down into the membrane and is followed by the M2 and the M3 helices as the membrane-spanning portions. The MA cytoplasmic loop (helix) connects between M3 and M4. The region between M3 and MA is not modeled due to the poorly defined intracellular domain of the template structure. The C-terminal follows the M4 helix and faces toward the extracellular surface (Fig. S1B).

The pentameric model of *Asu*-ACR-16 has a five-fold symmetric around the channel pore. The average pairwise Root Mean Square Deviation (RMSD) fit of the C α coordinates of the antagonist-bound ECD-*Asu*-ACR-16 pentameric model and human α 7 nAChR chimera pentamer (PDB code: 4HQP) was 0.9 Å, which indicates a strong structural conservation between the model and the template structures (Fig. S1C). The C α -RMSD between the TID-*Asu*-ACR-16 pentamer and the TID-*Tma*-AChR pentamer was 1.5 Å, which shows the TID fit is still good but not as good as the ECD fit. The membrane-spanning domains are arranged symmetrically. The M2 helix lines the channel pore, while M1, M3 and M4 do not contribute to the channel pore and are arranged peripherally (Fig. S1D).

Since no binding sites data of *Asu*-ACR-16 is available to date, we used the published orthosteric binding site and allosteric binding sites in nAChRs or other Cys-loop receptors to predict the putative binding sites in *Asu*-ACR-16 (Galzi *et al.*, 1991; Arias, 2000b; Young *et al.*, 2008; Hibbs *et al.*, 2011; Spurny *et al.*, 2015). The orthosteric binding site is at the interface between the principal site and the complementary site in two adjacent subunits of the ECD-*Asu*-ACR-16 pentamer (Fig. 2 S2A & S2B). The principal subunit (+) has vicinal cysteines (Cys216, Cys217) that makes up of the loop C of the binding site. The complementary subunit (-) does not use vicinal cysteines as part of the binding pocket and the residues are more variable when nAChRs are compared. The agonist sub-pocket, which we argue is a less significant allosteric binding site in ECD-*Asu*-ACR-16, is located right below the orthosteric binding site in the extracellular domain (Fig. 2 S2C & S2D). The vestibule pocket (Fig. S2E & S2F) and the top pocket (Fig. S2G & S2H) were not high affinity

binding sites for the ligands and are not discussed further in this manuscript. The intersubunit allosteric binding sites in TID-*Asu*-ACR-16 are at the interface region between M2(+), M3(+), M1(-) and M2(-) (Fig. 2 S2I & S2J). The intrasubunit allosteric binding sites are at the center of the four transmembrane helices (M1, M2, M3 and M4) in each of the five subunits.

3.3 Binding properties of virtual screening hits

We carried out virtual screening of the ZINC ligand-database by using the three different bound forms of the ECD-*Asu*-ACR-16 models. Four molecules were selected as hits based on their high binding affinities and appropriate binding modes within the ligand-binding sites. The 9-fluorenylmethoxycarbonyl group (FMOC) was observed in twelve out of top forty hits ranked by binding affinities and exists in the two out of four hits, which suggests that FMOC could be necessary for the ligand recognition by the receptor. The FMOC group has a low predicted bioavailability due to the biphenyl scaffold, which limits aqueous solubility and may affect distribution to the *A. suum* parasite. Table 1 lists the physicochemical characteristics of four hits. They have relatively high molecular weights and are more hydrophobic compared to known *Asu*-ACR-16 agonists. However, they do follow the Lipinski's rule of five, which suggests that these molecules may be orally active (Lipinski *et al.*, 2001; Lipinski, 2004).

The atomic structure predicts the partition-coefficients (XlogP) of the four hits to be between 4.27 and 6.04 (Table 1). The XlogPs suggest that the four hits are 10,000-1,000,000 times more concentrated in the lipophilic phase of the lipid bilayer

than the aqueous phase of the extracellular domain (Cheng *et al.*, 2007). The four hydrophobic hits are, therefore, more likely to bind into the transmembrane allosteric binding pockets rather than to the extracellular ligand binding sites. The four hits which bind in the transmembrane allosteric binding pockets are therefore predicted to be allosteric modulators of the *Asu*-ACR-16 receptor that alter the activity of the agonists or competitive antagonists that bind to orthosteric binding site. SB-277011-A is known to be a potent and selective dopamine D₃ receptor antagonist with high oral availability (Stemp *et al.*, 2000). (+)-butaclamol Cl is a non-selective dopamine receptor antagonist and a potent antipsychotic agent (Chrzanowski *et al.*, 1985). No paper reporting on the activities of fmoc-2 and fmoc-1 has been published to date.

The four hits (Table 1) were tested for docking into the orthosteric binding sites of the three forms of ECD-*Asu*-ACR-16 models and the five allosteric binding pockets in the antagonist-bound form of full-length *Asu*-ACR-16 models. All four hits bound to the orthosteric binding sites of three ECD-*Asu*-ACR-16 models, but only bound to the three allosteric binding sites out of five: intersubunit and intrasubunit transmembrane pockets and agonist sub-pocket (Fig. 3) with high binding affinities.

In the intersubunit transmembrane site of TID-*Asu*-ACR-16 model, M243 (M1, (-)), L247 (M1, (-)) make hydrophobic interactions with naphthalene of fmoc-2. T312 (M3, (+)), S284 (M2, (+)) form hydrogen bond with carboxylic acids of fmoc-2. F279 (M2, (-)), I282 (M2, (-)) make hydrophobic contacts with fluorene of fmoc-2. F279 (M2, (-)), P244 (M1, (-)) make hydrophobic interactions with tetrahydroisoquinoline of SB-277011-A. N240 (M1, (-)) forms a hydrogen bond with carboxamide of SB-277011-A. P288 (M2, (+)) has hydrophobic interaction with quinoline of SB-277011-

A. L247 (M1, (-)), F279 (M2, (-)) make hydrophobic contacts with dibenzocycloheptene of (+)-butaclamol Cl.

Ach, the natural agonist of *Asu*-ACR-16 was docked into the ligand binding sites of three forms of *Asu*-ACR-16 models for comparison. As expected, ach bound to the orthosteric binding site of the agonist-bound *Asu*-ACR-16 with an affinity (-4.3 kcal/mol), which was higher than the affinities at the other binding sites. The binding pose of ach docked in the orthosteric binding site of the agonist-bound *Asu*-ACR-16 model was in agreement with the binding pose of ach in the *L. stagnalis* AChBP cocrystal structure (PDB code: 3WIP; (Olsen *et al.*, 2014b). The quaternary ammonium of ach faces to the basal side of the binding cavity and makes cation- π interaction with five aromatic residues from the *Asu*-ACR-16 ((+): Y89, W143, Y185, Y192; (-): W53), while the carbonyl oxygen of ach faces toward the apical side of the binding cavity. The binding affinities of the selected four compounds were higher than -8.0 kcal/mol in the three different bound forms of *Asu*-ACR-16, while the binding affinities of ach were lower than -4.5 kcal/mol in three states of *Asu*-ACR-16 (Table 2).

3.4 Pharmacological properties of virtual screening hits

We tested the effects of the putative allosteric modulators on *Asu*-ACR-16 receptors expressed in *Xenopus* oocyte using two-electrode voltage clamp to observe the currents that flow through *Asu*-ACR-16 receptors. Representative traces showing the inhibitory dose-response relationships are shown in Fig. 4. Their IC_{50} (Fig. 5A & 5B) and maximum inhibition (Fig. S3) were determined as described in

the methods (Table 3). The most potent antagonist among them was SB-277011-A, which had an IC_{50} of $3.12 \pm 1.29 \mu\text{M}$ and maximum inhibition effect of $96.07 \pm 10.66\%$ ($n = 4$).

The ach concentration-response plots in the presence of $3 \mu\text{M}$ of each putative allosteric modulator (Fig. S4 & 5C), show the reduced maximum current responses with little shift in EC_{50} of ach (Fig. 5D 5E & Table 4), and that the hits were non-competitive antagonists and negative allosteric modulators.

At $10 \mu\text{M}$, SB-277011-A, showed evidence of a mixed competitive and non-competitive antagonism (Fig. S5), characterized by a reduced maximum current response and a right-shift in the EC_{50} of ach (Fig. 5D & 5E). Thus, $10 \mu\text{M}$ SB-277011-A appears to act at more than one binding site which may include the orthosteric binding sites and additional allosteric binding sites.

3.5 SB-277011-A reversibly inhibits locomotion in *C. elegans*

We tested the effects of each allosteric modulator on the locomotion of *C. elegans* L4 larvae. The number of normal worms with thrashing-like movement dropped by 60% in 5 min after exposed to $30 \mu\text{M}$ SB-277011-A ($p < 0.01$, $n = 5$, t -test). Paralysis-like movement was observed in the rest of the worms. The number of worms with normal motility recovered to 50% ($p < 0.05$, $n = 5$, t -test) in 10 min, 85% in 15 min ($p > 0.05$, $n = 5$, t -test) and returned to near negative control values after 20 min (Fig. S6). The recovery may relate to the desensitization properties of the ACR-16 receptor. The reversible inhibition of motility in worms was also observed in $100 \mu\text{M}$ (+)-butaclamol Cl, but no significant difference between the

number of normal treated worms and negative control was observed at any time point. No visual effects of 100 μ M fmoc-2 or 100 μ M fmoc-1 were found on the locomotion of worms.

4. Discussion

4.1 *Asu*-ACR-16 models

We have built up three-dimensional models of full-length structures of *Asu*-ACR-16 at the atomic level for the first time. We used homology modeling based on X-ray crystal structures of human α 7 nAChR chimeras and the electron microscopic structure of the *T. marmorata* nAChR as templates for different domains. The quality of our homology models are dependent on the sequence identity of the templates (human α 7 nAChR chimeras and *T. marmorata* nAChR) and the target sequence (*Asu*-ACR-16) and the resolutions of template structures (Hillisch *et al.*, 2004; Cavasotto *et al.*, 2009). Our three ECD-*Asu*-ACR-16 models are likely to be reliable for virtual screening because they have high sequence identities (37.6% identity and 72.9% similarity) with high resolution ($< 4\text{\AA}$) templates. More errors might be expected in the TID-*Asu*-ACR-16 model, because of the missing loop between M3 and MA in the template structure which reduces sequence identity with the target protein. The missing loop does not include an allosteric binding site. So we can assume that the TID-*Tma*-nAChR structure is similar to the TID-*Asu*-ACR-16 structure (Bertrand *et al.*, 2008). The overall secondary structures of our models are also consistent with published nAChRs structures (Finer-Moore *et al.*, 1984; Miyazawa *et al.*, 2003; Unwin, 2005b).

We developed the apo, the agonist-bound and the antagonist-bound models of the ECD-Asu-ACR-16 on the assumption that these three states of the Asu-ACR-16 receptor most closely represent the receptor conformations in the presence and absence of agonists or antagonists. To produce a realistic dynamic model would require more extensive work (Cavasotto *et al.*, 2007; Spyrakis *et al.*, 2011) and is beyond the scope of this study.

4.2 Virtual screening

Our structure-based virtual screening approach identified four novel and potent negative allosteric modulators of Asu-ACR-16, which were validated by our electrophysiological studies. The putative ligands were initially selected based on the virtual screening using the orthosteric binding site of the receptor. It was possible that these ligands could have been agonists or competitive antagonists that bind within the orthosteric binding site. In contrast, the pharmacological characterization of the four virtual screening hits shows that they behave as negative allosteric modulators and bind to allosteric sites. This outcome may be due to the hydrophobic properties of the four compounds that impedes their interactions with the orthosteric site in the extracellular domain of the receptor. The high lipid solubility of these compounds increases their concentration in the membrane lipid phase, in the region of the transmembrane allosteric sites.

The binding affinities calculated in the scoring function of AutoDock Vina software usually increase with the number of non-hydrogen atoms, which may be due to the neglect of desolvation in the scoring function (Kuntz *et al.*, 1999; Shoichet

et al., 1999; Park *et al.*, 2006). This leads to a bias of virtual screening methods towards big molecules which are more hydrophobic, concentrated in the lipid bilayer, and less likely to interact with the binding sites in the extracellular domains (Hopkins *et al.*, 2004). It is also pointed out that the simplified force fields used to estimate the binding free energies are unable to evaluate the conformational entropies and other contributions to the free energies (Cosconati *et al.*, 2010). Thus, the success rate of identifying bioactive hits (44%) would be enhanced if we are able to include these additional parameters into a scoring function for virtual screening. Another approach, which we did not follow here, to enhance the success rate of identifying bio-active hits, is to use the known agonists or antagonists as scaffolds. This would facilitate the identification of low molecular-weight and more hydrophilic agonists or antagonists, and allow further study of the quantitative structure-activity relationships (Sun, 2008).

4.3 Four negative allosteric modulators of *Asu-ACR-16*

We evaluated the potency of inhibition for the four negative allosteric modulators in our electrophysiology studies on *Xenopus* oocytes: SB-277011-A (IC_{50} $3.12 \pm 1.29 \mu\text{M}$) < (+)-butaclamol Cl (IC_{50} $9.85 \pm 2.37 \mu\text{M}$) \approx fmoc-1 (IC_{50} $10.00 \pm 1.38 \mu\text{M}$) < fmoc-2 (IC_{50} $16.67 \pm 1.95 \mu\text{M}$). This rank of inhibition agrees with the level of effects of the four modulators in the motility of *C. elegans*. The most potent modulator SB-277011-A was shown to decrease the motility of *C. elegans* larvae for a duration of about ten minutes, yet less effective on adult *C. elegans*. Desensitization of the ACR-16 or other nAChRs in *C. elegans* body muscle may be a reason for the reduced effects of SB-277011-A on worms (Hernando *et al.*, 2012).

Treating the *acr-16*-null mutant of *C. elegans* with SB-277011-A can help us to investigate the mode of action of SB-277011-A on *C. elegans* as genetic models to understand SB-277011-A action on the parasitic nematode *A. suum* (Ward, 2015).

4.4 Allosteric binding sites may offer a better opportunity for drugs that can discriminate between the parasite *Asu*-ACR-16 and mammalian host $\alpha 7$

nAChR

Asu-ACR-16 shows 42.5% sequence identity and 71.2% sequence similarity with the human $\alpha 7$ nAChR (SwissProt ID: P36544) based on the alignment generated by CLUSTALW (Fig. S7, CLUSTALW job ID: cfed4f821eaf). The residues constituting the orthosteric binding site (pink and orange arrows in Fig. S7) are highly conserved between *Asu*-ACR-16 and human $\alpha 7$ nAChR, which shows 66.7% identity and 100% similarity (Fig. S8). In contrast, the residues of the four allosteric binding sites have much greater differences (variance) between the nematode parasite and the equivalent sites on the $\alpha 7$ receptor (identities: 62.5%, 45.5%, 66.7%, 62.5% and 40.0% and; similarities: 87.5%, 81.8%, 83.3, 93.8% and 100%). The sequence divergence in the allosteric binding sites between *Asu*-ACR-16 and host human $\alpha 7$ nAChR indicates that drugs targeted at these sites may be more selective than drugs targeted at orthosteric binding sites. Virtual screening specifically targeting the allosteric binding sites is predicted to offer a better opportunity for development of drugs with much greater receptor subtype selectivity (Nussinov *et al.*, 2013; Iturriaga-Vasquez *et al.*, 2015).

4.4 Conclusion

We have developed a structure-based *in silico* screening approach to search for the bioactive hits that target at a parasitic nematode receptor. This approach allowed us to identify four negative allosteric modulators that were validated using our electrophysiological studies. These four compounds may be useful leads for anthelmintic drug discovery. We point out however, that we have not yet made the structural models for the host human $\alpha 7$ nAChR or other receptors, which would help to distinguish compounds that are active only on the nematode receptors, thereby reducing potential toxicity. It would also be desirable to perform virtual screening for toxicity on a range of host receptors, some structures of which have already been determined and others need to be modeled.

Acknowledgements

We would like to thank Tsung-Han Chou for the help and advice in modeling and docking. The research funding was by The Hatch Act, State of Iowa, and by NIH grants R01 AI047194 (to RJM) and AI114629 (to EWY) of the National Institute of Allergy and Infectious Diseases. The funding agencies had no role in the design, execution or publication of this study. The content is solely the responsibility of the authors and does not necessarily represent the official views of the National Institute of Allergy and Infectious Diseases.

References

Abongwa, M., Buxton, S.K., Courtot, E., Charvet, C., Neveu, C., McCoy, C.J., Verma, S., Robertson, A.P., Martin, R.J., 2015. Pharmacological profile of Asu-ACR-16, a new homomeric nAChR widely distributed in *Ascaris* tissues. (Under review).

Adams, P.D., Afonine, P.V., Bunkoczi, G., Chen, V.B., Davis, I.W., Echols, N., Headd, J.J., Hung, L.W., Kapral, G.J., Grosse-Kunstleve, R.W., McCoy, A.J., Moriarty, N.W., Oeffner, R., Read, R.J., Richardson, D.C., Richardson, J.S., Terwilliger, T.C., Zwart, P.H., 2010.

PHENIX: a comprehensive Python-based system for macromolecular structure solution. *Acta crystallographica. Section D, Biological crystallography* 66, 213-221.

Altschul, S.F., Madden, T.L., Schaffer, A.A., Zhang, J., Zhang, Z., Miller, W., Lipman, D.J., 1997. Gapped BLAST and PSI-BLAST: a new generation of protein database search programs. *Nucleic acids research* 25, 3389-3402.

Arias, H.R., 2000. Localization of agonist and competitive antagonist binding sites on nicotinic acetylcholine receptors. *Neurochemistry International* 36, 595-645.

Ballivet, M., Alliod, C., Bertrand, S., Bertrand, D., 1996. Nicotinic acetylcholine receptors in the nematode *Caenorhabditis elegans*. *Journal of molecular biology* 258, 261-269.

Berman, H.M., Westbrook, J., Feng, Z., Gilliland, G., Bhat, T.N., Weissig, H., Shindyalov, I.N., Bourne, P.E., 2000. The Protein Data Bank. *Nucleic acids research* 28, 235-242.

Bertrand, D., Bertrand, S., Cassar, S., Gubbins, E., Li, J., Gopalakrishnan, M., 2008. Positive allosteric modulation of the alpha7 nicotinic acetylcholine receptor: ligand interactions with distinct binding sites and evidence for a prominent role of the M2-M3 segment. *Molecular pharmacology* 74, 1407-1416.

Bethony, J., Brooker, S., Albonico, M., Geiger, S.M., Loukas, A., Diemert, D., Hotez, P.J., 2006. Soil-transmitted helminth infections: ascariasis, trichuriasis, and hookworm. *The Lancet* 367, 1521-1532.

Boulin, T., Fauvin, A., Charvet, C.L., Cortet, J., Cabaret, J., Bessereau, J.L., Neveu, C., 2011. Functional reconstitution of *Haemonchus contortus* acetylcholine receptors in *Xenopus* oocytes provides mechanistic insights into levamisole resistance. *British journal of pharmacology* 164, 1421-1432.

Boulin, T., Gielen, M., Richmond, J.E., Williams, D.C., Paoletti, P., Bessereau, J.L., 2008. Eight genes are required for functional reconstitution of the *Caenorhabditis*

C. elegans levamisole-sensitive acetylcholine receptor. Proceedings of the National Academy of Sciences of the United States of America 105, 18590-18595.

Brenner, S., 1974. The genetics of *Caenorhabditis elegans*. Genetics 77, 71-94.

Buxton, S.K., Charvet, C.L., Neveu, C., Cabaret, J., Cortet, J., Peineau, N., Abongwa, M., Courtot, E., Robertson, A.P., Martin, R.J., 2014. Investigation of acetylcholine receptor diversity in a nematode parasite leads to characterization of tribendimidine- and derquantel-sensitive nAChRs. PLoS pathogens 10, e1003870.

Canutescu, A.A., Shelenkov, A.A., Dunbrack, R.L., Jr., 2003. A graph-theory algorithm for rapid protein side-chain prediction. Protein science : a publication of the Protein Society 12, 2001-2014.

Cavasotto, C.N., Orry, A.J., 2007. Ligand docking and structure-based virtual screening in drug discovery. Current topics in medicinal chemistry 7, 1006-1014.

Cavasotto, C.N., Phatak, S.S., 2009. Homology modeling in drug discovery: current trends and applications. Drug discovery today 14, 676-683.

Celie, P.H., van Rossum-Fikkert, S.E., van Dijk, W.J., Brejc, K., Smit, A.B., Sixma, T.K., 2004. Nicotine and carbamylcholine binding to nicotinic acetylcholine receptors as studied in AChBP crystal structures. Neuron 41, 907-914.

Changeux, J.-P., Edelstein, S.J., 1998. Allosteric receptors after 30 years. Neuron 21, 959-980.

Cheng, T., Zhao, Y., Li, X., Lin, F., Xu, Y., Zhang, X., Li, Y., Wang, R., Lai, L., 2007. Computation of octanol-water partition coefficients by guiding an additive model with knowledge. Journal of chemical information and modeling 47, 2140-2148.

Chrzanowski, F.A., McGrogan, B.A., Maryanoff, B.E., 1985. The pKa of butaclamol and the mode of butaclamol binding to central dopamine receptors. Journal of Medicinal Chemistry 28, 399-400.

Cosconati, S., Forli, S., Perryman, A.L., Harris, R., Goodsell, D.S., Olson, A.J., 2010. Virtual Screening with AutoDock: Theory and Practice. Expert opinion on drug discovery 5, 597-607.

Crompton, D.W., 2000. The public health importance of hookworm disease. Parasitology 121 Suppl, S39-50.

de Silva, N.R., Brooker, S., Hotez, P.J., Montresor, A., Engels, D., Savioli, L., 2003. Soil-transmitted helminth infections: updating the global picture. Trends in Parasitology 19, 547-551.

Devillers-Thiery, A., Giraudat, J., Bentaboulet, M., Changeux, J.P., 1983. Complete mRNA coding sequence of the acetylcholine binding alpha-subunit of *Torpedo marmorata* acetylcholine receptor: a model for the transmembrane organization of the polypeptide chain. *Proceedings of the National Academy of Sciences of the United States of America* 80, 2067-2071.

Devillers-Thiery, A., Giraudat, J., Bentaboulet, M., Klarsfeld, A., Changeux, J.P., 1984. Molecular genetics of *Torpedo marmorata* acetylcholine receptor. *Advances in experimental medicine and biology* 181, 17-29.

Emsley, P., Cowtan, K., 2004. Coot: model-building tools for molecular graphics. *Acta crystallographica. Section D, Biological crystallography* 60, 2126-2132.

Eswar, N., Webb, B., Marti-Renom, M.A., Madhusudhan, M.S., Eramian, D., Shen, M.Y., Pieper, U., Sali, A., 2007. Comparative protein structure modeling using MODELLER. *Current protocols in protein science / editorial board, John E. Coligan ... [et al.] Chapter 2, Unit 2.9.*

Finer-Moore, J., Stroud, R.M., 1984. Amphipathic analysis and possible formation of the ion channel in an acetylcholine receptor. *Proceedings of the National Academy of Sciences of the United States of America* 81, 155-159.

Galzi, J.-L., Bertrand, D., Devillers-Thiéry, A., Revah, F., Bertrand, S., Changeux, J.-P., 1991. Functional significance of aromatic amino acids from three peptide loops of the $\alpha 7$ neuronal nicotinic receptor site investigated by site-directed mutagenesis. *FEBS Letters* 294, 198-202.

Halevi, S., Yassin, L., Eshel, M., Sala, F., Sala, S., Criado, M., Treinin, M., 2003. Conservation within the RIC-3 gene family. Effectors of mammalian nicotinic acetylcholine receptor expression. *The Journal of biological chemistry* 278, 34411-34417.

Hernando, G., Berge, I., Rayes, D., Bouzat, C., 2012. Contribution of subunits to *Caenorhabditis elegans* levamisole-sensitive nicotinic receptor function. *Molecular pharmacology* 82, 550-560.

Hewitson, J.P., Maizels, R.M., 2014. Vaccination against helminth parasite infections. *Expert review of vaccines* 13, 473-487.

Hibbs, R.E., Gouaux, E., 2011. Principles of activation and permeation in an anion-selective Cys-loop receptor. *Nature* 474, 54-60.

Hillisch, A., Pineda, L.F., Hilgenfeld, R., 2004. Utility of homology models in the drug discovery process. *Drug discovery today* 9, 659-669.

Hopkins, A.L., Groom, C.R., Alex, A., 2004. Ligand efficiency: a useful metric for lead selection. *Drug discovery today* 9, 430-431.

Hotez, P.J., Molyneux, D.H., Fenwick, A., Kumaresan, J., Sachs, S.E., Sachs, J.D., Savioli, L., 2007. Control of neglected tropical diseases. *New England Journal of Medicine* 357, 1018-1027.

Huang, S., Li, S.-X., Bren, N., Cheng, K., Gomoto, R., Chen, L., Sine, S.M., 2013. Complex between α -bungarotoxin and an $\alpha 7$ nicotinic receptor ligand-binding domain chimera. *The Biochemical journal* 454, 303-310.

Irwin, J.J., Sterling, T., Mysinger, M.M., Bolstad, E.S., Coleman, R.G., 2012. ZINC: a free tool to discover chemistry for biology. *Journal of chemical information and modeling* 52, 1757-1768.

Iturriaga-Vasquez, P., Alzate-Morales, J., Bermudez, I., Varas, R., Reyes-Parada, M., 2015. Multiple binding sites in the nicotinic acetylcholine receptors: An opportunity for polypharmacology. *Pharmacological research* 101, 9-17.

James, C.E., Hudson, A.L., Davey, M.W., 2009. Drug resistance mechanisms in helminths: is it survival of the fittest? *Trends Parasitol* 25, 328-335.

Kaplan, R.M., 2004. Drug resistance in nematodes of veterinary importance: a status report. *Trends in parasitology* 20, 477-481.

Keiser, J., Utzinger, J., 2008. Efficacy of current drugs against soil-transmitted helminth infections: systematic review and meta-analysis. *Jama* 299, 1937-1948.

Kuntz, I.D., Chen, K., Sharp, K.A., Kollman, P.A., 1999. The maximal affinity of ligands. *Proceedings of the National Academy of Sciences of the United States of America* 96, 9997-10002.

Li, S.X., Huang, S., Bren, N., Noridomi, K., Dellisanti, C.D., Sine, S.M., Chen, L., 2011. Ligand-binding domain of an $\alpha 7$ -nicotinic receptor chimera and its complex with agonist. *Nature neuroscience* 14, 1253-1259.

Lipinski, C.A., 2004. Lead- and drug-like compounds: the rule-of-five revolution. *Drug Discovery Today: Technologies* 1, 337-341.

Lipinski, C.A., Lombardo, F., Dominy, B.W., Feeney, P.J., 2001. Experimental and computational approaches to estimate solubility and permeability in drug discovery and development settings. *Advanced drug delivery reviews* 46, 3-26.

Martin, R., Robertson, A., 2010. Control of Nematode Parasites with Agents Acting on Neuro-Musculature Systems: Lessons for Neuropeptide Ligand Discovery, in:

Geary, T., Maule, A. (Eds.), *Neuropeptide Systems as Targets for Parasite and Pest Control*. Springer US, pp. 138-154.

Martin, R.J., Robertson, A.P., Buxton, S.K., Beech, R.N., Charvet, C.L., Neveu, C., 2012. Levamisole receptors: a second awakening. *Trends Parasitol* 28, 289-296.

Miyazawa, A., Fujiyoshi, Y., Unwin, N., 2003. Structure and gating mechanism of the acetylcholine receptor pore. *Nature* 423, 949-955.

Mongan, N.P., Baylis, H.A., Adcock, C., Smith, G.R., Sansom, M.S., Sattelle, D.B., 1998. An extensive and diverse gene family of nicotinic acetylcholine receptor alpha subunits in *Caenorhabditis elegans*. *Receptors & channels* 6, 213-228.

Moriarty, N.W., Grosse-Kunstleve, R.W., Adams, P.D., 2009. electronic Ligand Builder and Optimization Workbench (eLBOW): a tool for ligand coordinate and restraint generation. *Acta crystallographica. Section D, Biological crystallography* 65, 1074-1080.

Morris, G.M., Goodsell, D.S., Halliday, R.S., Huey, R., Hart, W.E., Belew, R.K., Olson, A.J., 1998. Automated docking using a Lamarckian genetic algorithm and an empirical binding free energy function. *Journal of Computational Chemistry* 19, 1639-1662.

Morris, G.M., Huey, R., Lindstrom, W., Sanner, M.F., Belew, R.K., Goodsell, D.S., Olson, A.J., 2009. AutoDock4 and AutoDockTools4: Automated Docking with Selective Receptor Flexibility. *Journal of computational chemistry* 30, 2785-2791.

Nussinov, R., Tsai, C.J., 2013. Allostery in disease and in drug discovery. *Cell* 153, 293-305.

Olsen, J.A., Balle, T., Gajhede, M., Ahring, P.K., Kastrop, J.S., 2014a. Molecular recognition of the neurotransmitter acetylcholine by an acetylcholine binding protein reveals determinants of binding to nicotinic acetylcholine receptors. *PLoS one* 9, e91232.

Olsen, J.A., Balle, T., Gajhede, M., Ahring, P.K., Kastrop, J.S., 2014b. Molecular Recognition of the Neurotransmitter Acetylcholine by an Acetylcholine Binding Protein Reveals Determinants of Binding to Nicotinic Acetylcholine Receptors. *PLoS one* 9.

Pan, J., Chen, Q., Willenbring, D., Mowrey, D., Kong, X.P., Cohen, A., Divito, C.B., Xu, Y., Tang, P., 2012. Structure of the pentameric ligand-gated ion channel GLIC bound with anesthetic ketamine. *Structure* 20, 1463-1469.

Park, H., Lee, J., Lee, S., 2006. Critical assessment of the automated AutoDock as a new docking tool for virtual screening. *Proteins* 65, 549-554.

Peng, X., Katz, M., Gerzanich, V., Anand, R., Lindstrom, J., 1994. Human alpha 7 acetylcholine receptor: cloning of the alpha 7 subunit from the SH-SY5Y cell line and determination of pharmacological properties of native receptors and functional alpha 7 homomers expressed in *Xenopus oocytes*. *Molecular pharmacology* 45, 546-554.

Polli, J.R., Dobbins, D.L., Kobet, R.A., Farwell, M.A., Zhang, B., Lee, M.H., Pan, X., 2015. Drug-dependent behaviors and nicotinic acetylcholine receptor expressions in *Caenorhabditis elegans* following chronic nicotine exposure. *Neurotoxicology* 47, 27-36.

Qian, H., Martin, R.J., Robertson, A.P., 2006. Pharmacology of N-, L-, and B-subtypes of nematode nAChR resolved at the single-channel level in *Ascaris suum*. *FASEB journal : official publication of the Federation of American Societies for Experimental Biology* 20, 2606-2608.

Raymond, V., Mongan, N.P., Sattelle, D.B., 2000. Anthelmintic actions on homomer-forming nicotinic acetylcholine receptor subunits: chicken $\alpha 7$ and ACR-16 from the nematode *Caenorhabditis elegans*. *Neuroscience* 101, 785-791.

Rucktooa, P., Haseler, C.A., van Elk, R., Smit, A.B., Gallagher, T., Sixma, T.K., 2012. Structural characterization of binding mode of smoking cessation drugs to nicotinic acetylcholine receptors through study of ligand complexes with acetylcholine-binding protein. *The Journal of biological chemistry* 287, 23283-23293.

Rufener, L., Baur, R., Kaminsky, R., Maser, P., Sigel, E., 2010. Monepantel allosterically activates DEG-3/DES-2 channels of the gastrointestinal nematode *Haemonchus contortus*. *Molecular pharmacology* 78, 895-902.

Rychlewski, L., Jaroszewski, L., Li, W., Godzik, A., 2000. Comparison of sequence profiles. Strategies for structural predictions using sequence information. *Protein science : a publication of the Protein Society* 9, 232-241.

Shoichet, B.K., Leach, A.R., Kuntz, I.D., 1999. Ligand solvation in molecular docking. *Proteins* 34, 4-16.

Spurny, R., Debaveye, S., Farinha, A., Veys, K., Vos, A.M., Gossas, T., Atack, J., Bertrand, S., Bertrand, D., Danielson, U.H., Tresadern, G., Ulens, C., 2015. Molecular blueprint of allosteric binding sites in a homologue of the agonist-binding domain of the alpha7 nicotinic acetylcholine receptor. *Proceedings of the National Academy of Sciences of the United States of America* 112, E2543-2552.

Spyrakis, F., BidonChanal, A., Barril, X., Luque, F.J., 2011. Protein flexibility and ligand recognition: challenges for molecular modeling. *Current topics in medicinal chemistry* 11, 192-210.

Stemp, G., Ashmeade, T., Branch, C.L., Hadley, M.S., Hunter, A.J., Johnson, C.N., Nash, D.J., Thewlis, K.M., Vong, A.K.K., Austin, N.E., Jeffrey, P., Avenell, K.Y., Boyfield, I., Hagan, J.J., Middlemiss, D.N., Reavill, C., Riley, G.J., Routledge, C., Wood, M., 2000. Design and Synthesis of trans-N-[4-[2-(6-Cyano-1,2,3,4-tetrahydroisoquinolin-2-yl)ethyl]cyclohexyl]-4-quinolinecarboxamide (SB-277011): A Potent and Selective Dopamine D3 Receptor Antagonist with High Oral Bioavailability and CNS Penetration in the Rat. *Journal of Medicinal Chemistry* 43, 1878-1885.

Sun, H., 2008. Pharmacophore-based virtual screening. *Current medicinal chemistry* 15, 1018-1024.

Thompson, J.D., Higgins, D.G., Gibson, T.J., 1994. CLUSTAL W: improving the sensitivity of progressive multiple sequence alignment through sequence weighting, position-specific gap penalties and weight matrix choice. *Nucleic acids research* 22, 4673-4680.

Trott, O., Olson, A.J., 2010. AutoDock Vina: improving the speed and accuracy of docking with a new scoring function, efficient optimization, and multithreading. *J Comput Chem* 31, 455-461.

Unwin, N., 2005. Refined structure of the nicotinic acetylcholine receptor at 4Å resolution. *Journal of molecular biology* 346, 967-989.

Wang, J., Czech, B., Crunk, A., Wallace, A., Mitreva, M., Hannon, G.J., Davis, R.E., 2011. Deep small RNA sequencing from the nematode *Ascaris* reveals conservation, functional diversification, and novel developmental profiles. *Genome research* 21, 1462-1477.

Ward, J.D., 2015. Rendering the Intractable More Tractable: Tools from *Caenorhabditis elegans* Ripe for Import into Parasitic Nematodes. *Genetics* 201, 1279-1294.

Williamson, S.M., Robertson, A.P., Brown, L., Williams, T., Woods, D.J., Martin, R.J., Sattelle, D.B., Wolstenholme, A.J., 2009. The nicotinic acetylcholine receptors of the parasitic nematode *Ascaris suum*: formation of two distinct drug targets by varying the relative expression levels of two subunits. *PLoS pathogens* 5, e1000517.

Yang, J., Yan, R., Roy, A., Xu, D., Poisson, J., Zhang, Y., 2015. The I-TASSER Suite: protein structure and function prediction. *Nat Meth* 12, 7-8.

Young, G.T., Zwart, R., Walker, A.S., Sher, E., Millar, N.S., 2008. Potentiation of $\alpha 7$ nicotinic acetylcholine receptors via an allosteric transmembrane site. *Proceedings of the National Academy of Sciences of the United States of America* 105, 14686-14691.

Figure 1. (A) Sequence and numbering of the ECD-*Asu*-ACR-16 and its alignment with the template, human α_7 nAChR chimera subunit. Completely conserved residues (red background) and partially conserved residues (yellow background) are indicated. Secondary structures are shown schematically above the sequences. α_1 represents α helix. β_{1-7} represent β strand. η_1 represents 3_{10} helix. The Cysteine loop and loop A - F are labeled by dark green bars. Residues in the orthosteric binding site are indicated by arrows (principal subunit, pink; complementary subunit, orange). Residues in three allosteric binding pockets are highlighted by arrows (principal subunit of agonist sub-pocket, turquoise; complementary subunit of agonist sub-pocket, green; principal subunit of vestibule pocket, dark green; complementary subunit of vestibule pocket, gold; principal subunit of top pocket, purple).

(B) Sequence and numbering of the TID-*Asu*-ACR-16 and its alignment with the template TID-*Tma*-AChR subunit A. Completely conserved residues (red background) and partially conserved residues (yellow background) are indicated. Four transmembrane α helices (M1, M2, M3 and M4) are shown schematically above the sequences. Residues in the allosteric binding pocket are indicated by arrows (principal subunit, pink; complementary subunit, orange).

Figure 2

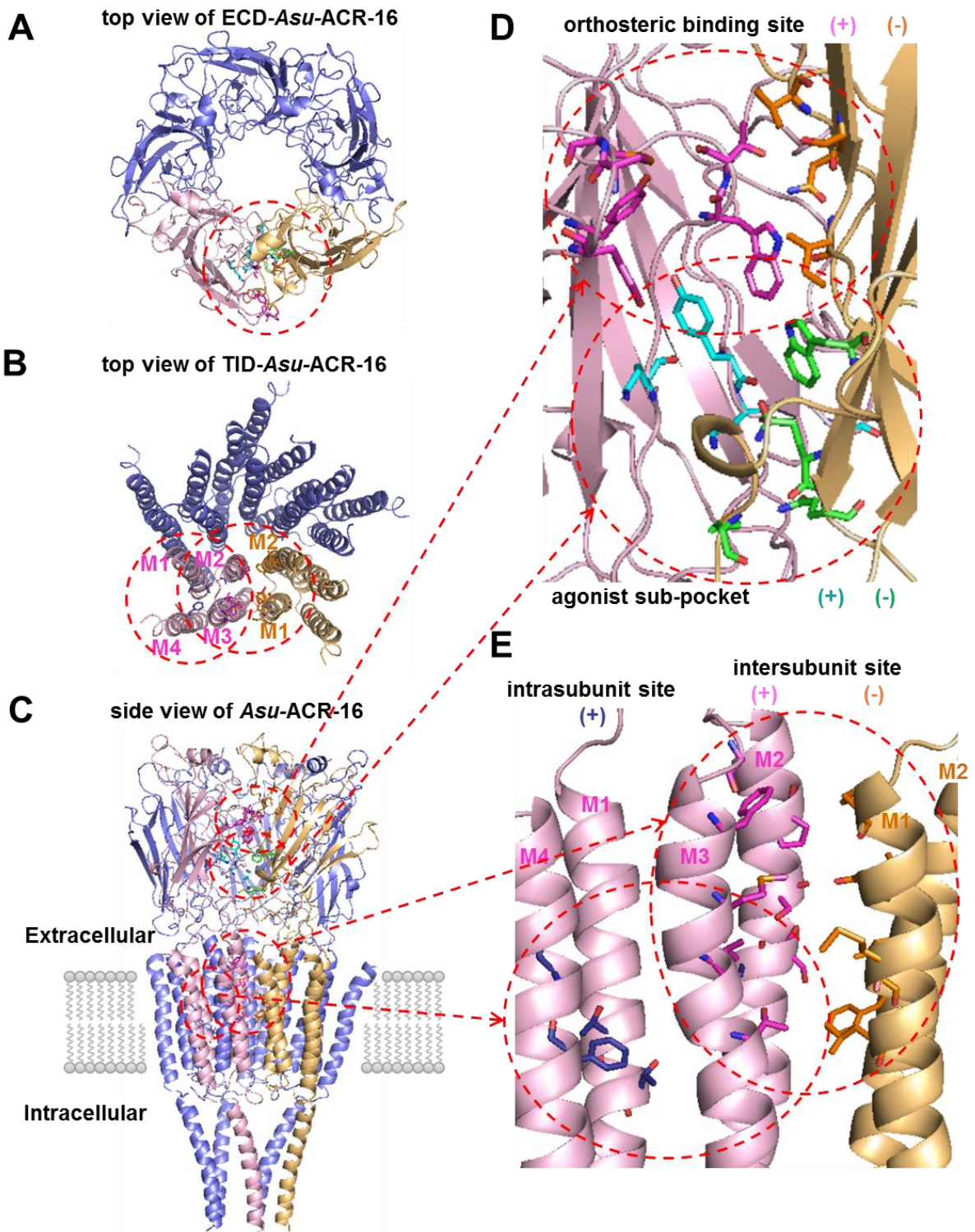


Figure 2. (A) Ribbon diagram of the antagonist-bound model of ECD-*Asu*-ACR-16 viewed from the synaptic cleft, showing the location of the orthosteric binding site and agonist sub-pocket. For clarity, only the front two subunits are highlighted (principal subunit, light pink; complementary subunit, yellow). The residues that contribute to the orthosteric binding site (principal side, pink; complementary side, orange) and the agonist sub-pocket (principal side, turquoise; complementary side, green) are represented by sticks and highlighted inside the red dotted circle.

(B) Ribbon diagram of the antagonist-bound model of TID-*Asu*-ACR-16 viewed above the membrane, showing the location of two transmembrane allosteric binding sites. For clarity, only the front two subunits are highlighted (principal subunit, light pink; complementary subunit, yellow). The residues that contribute to the intersubunit site (principal side, pink; complementary side, orange) and intrasubunit site (principal side, purpleblue) are represented by sticks and highlighted inside the red dotted circle.

(C) Ribbon diagram of the antagonist-bound model of full-length *Asu*-ACR-16 viewed parallel to the membrane plane, showing the location of the orthosteric binding site and the agonist sub-pocket in the extracellular domain, the intersubunit and intrasubunit binding sites in the transmembrane domain. For clarity, only the front two subunits are highlighted (principal subunit, light pink; complementary subunit, yellow). The residues that contribute to the ligand binding sites are represented by sticks (orthosteric site: (+), pink; (-), orange; agonist sub-pocket: (+), turquoise; (-), green; intersubunit transmembrane site: (+), pink; (-), orange;

intrasubunit transmembrane site: purpleblue) and highlighted inside the red dotted circle.

(D) Detailed view of the orthosteric binding site and agonist sub-pocket in the antagonist-bound model of ECD-Asu-ACR-16. The principal subunit is colored light pink, whereas the complementary subunit is colored yellow. The residues that contribute to the orthosteric binding site (principal side, pink; complementary side, orange) and the agonist sub-pocket (principal side, turquoise; complementary side, green) are represented by sticks and highlighted inside the red dotted circle. Carbon is in either turquoise or green. Nitrogen is in blue. Oxygen is in red.

(E) Detailed view of the transmembrane allosteric binding sites in the antagonist-bound model of TID-Asu-ACR-16. The principal subunit is colored light pink, whereas the complementary subunit is colored yellow. The residues that contribute to intersubunit site (principal side, pink; complementary side, orange) and intrasubunit site (principal side, purpleblue) are represented by sticks and highlighted inside the red dotted circle. Carbon is in either pink or orange or purpleblue. Nitrogen is in blue. Oxygen is in red. Sulfur is in yellow.

Figure 3

fmoc-2

SB-277011-A

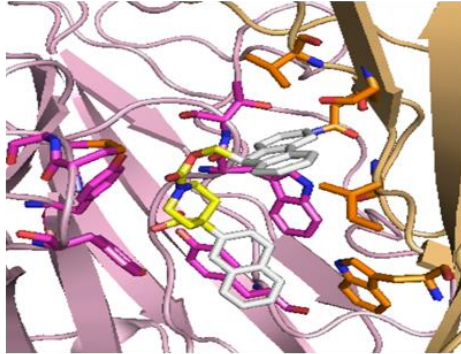
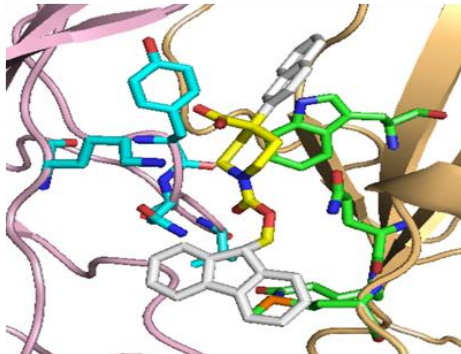
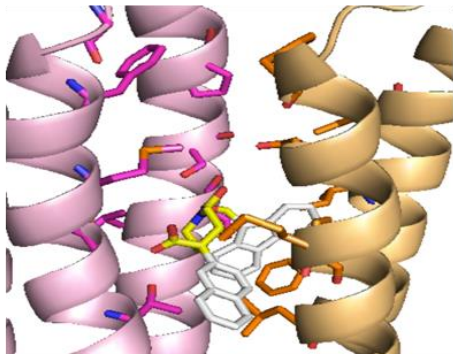
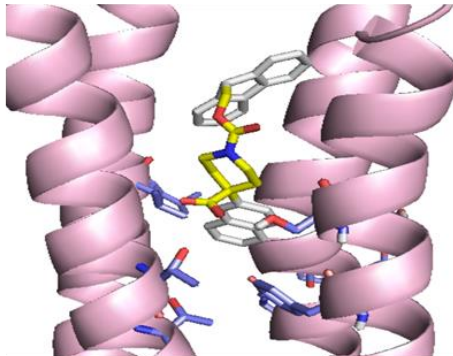
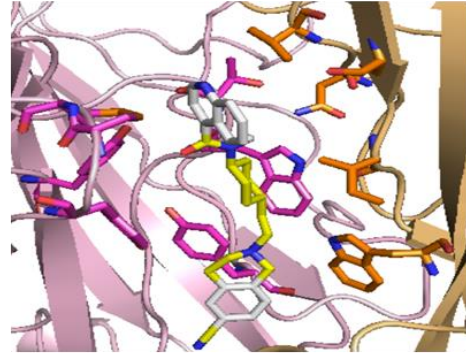
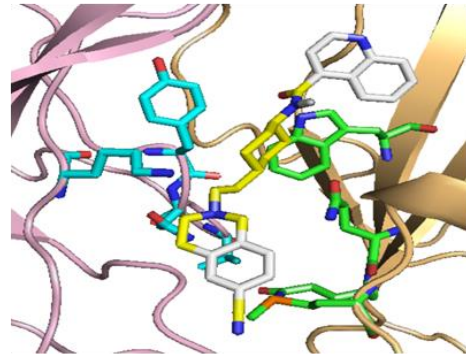
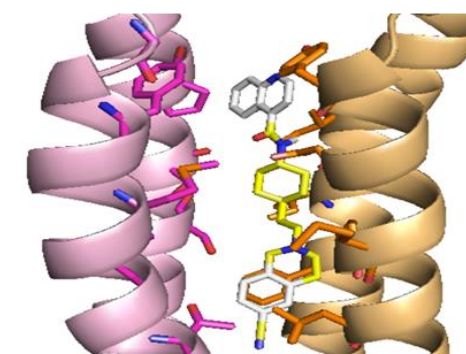
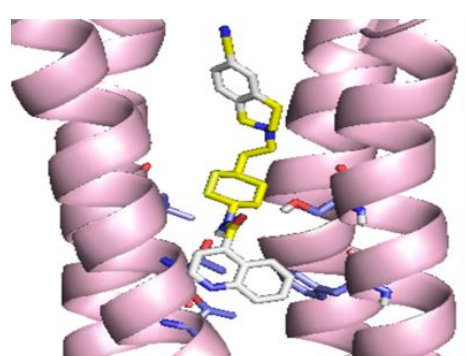
A orthosteric binding site**B** agonist sub-pocket**C** intersubunit transmembrane site**D** intrasubunit transmembrane site**E** orthosteric binding site**F** agonist sub-pocket**G** intersubunit transmembrane site**H** intrasubunit transmembrane site

Figure 3

fmoc-1

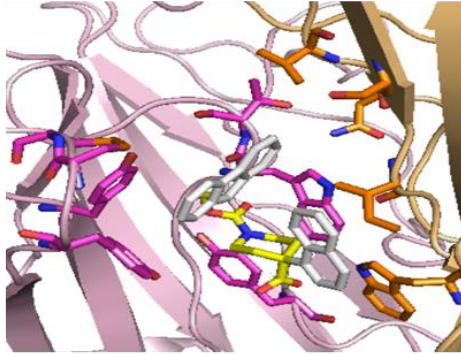
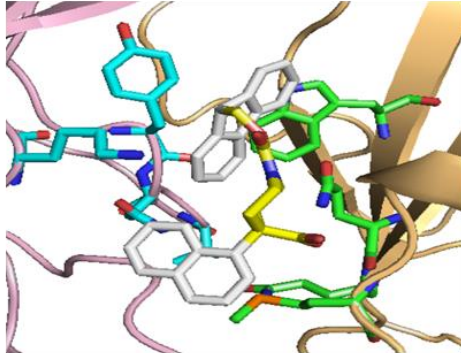
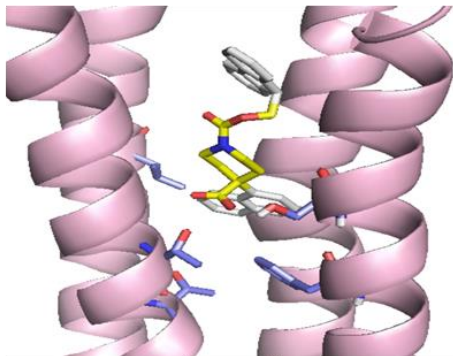
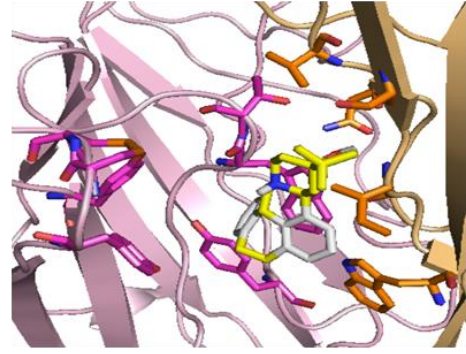
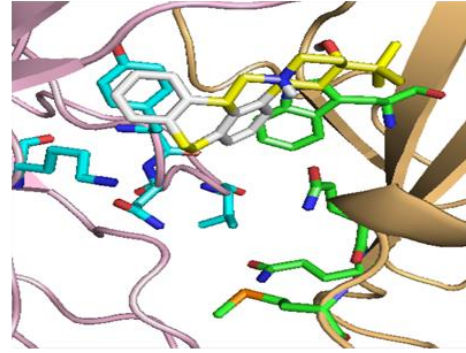
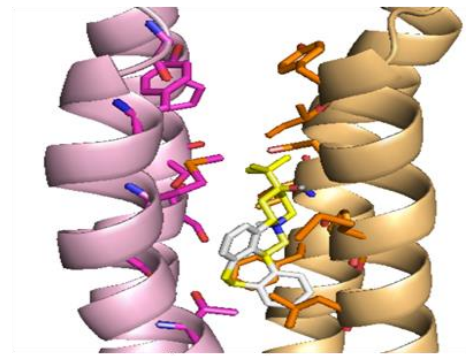
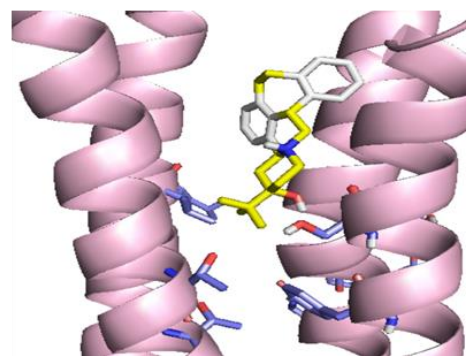
I orthosteric binding site**J** agonist sub-pocket**K** intrasubunit transmembrane site**(+)-butaclamol Cl****L** orthosteric binding site**M** agonist sub-pocket**N** intersubunit transmembrane site**O** intrasubunit transmembrane site

Figure 3. Binding modes of four virtual screening hits in the orthosteric binding site, the agonist sub-pocket, the intersubunit and intrasubunit transmembrane allosteric binding pockets of the antagonist-bound model of *Asu*-ACR-16: (A), (B), (C), (D) fomc-2; (E), (F), (G), (H) SB-277011-A; (I), (J), (K) fomc-1; (L), (M), (N), (O) (+)-butaclamol Cl. Hits docked into the binding pockets are represented by sticks (carbon in yellow; ring in white; nitrogen in blue; oxygen in red).

(A), (E), (I) and (L) show the four hits bound in the orthosteric binding site of the antagonist-bound model of ECD-*Asu*-ACR-16. The front two subunits are highlighted (principal subunit, light pink; complementary subunit, yellow). The residues in the orthosteric binding site are labeled (principal side, pink; complementary side, orange) to show the location of the orthosteric binding site.

(B), (F), (J) and (M) show the four hits bound in the agonist sub-pocket of the antagonist-bound model of ECD-*Asu*-ACR-16. The front two subunits are highlighted. The residues in the agonist sub-pocket are labeled (principal side, turquoise; complementary side, green) to show the location of the agonist sub-pocket.

(C), (G) and (N) show the four hits bound in the intersubunit transmembrane site of the antagonist-bound model of TID-*Asu*-ACR-16. The front two subunits are highlighted. The residues in the intersubunit transmembrane site are labeled (principal side, pink; complementary side, orange) to show the location of the intersubunit transmembrane binding site.

(D), (H), (K) and (O) show the four hits bound in the intrasubunit transmembrane site of the antagonist-bound model of TID-*Asu*-ACR-16. The residues in the intrasubunit

transmembrane site are labeled (purple/blue) to show the location of the intersubunit
transmembrane binding site.

Figure 4

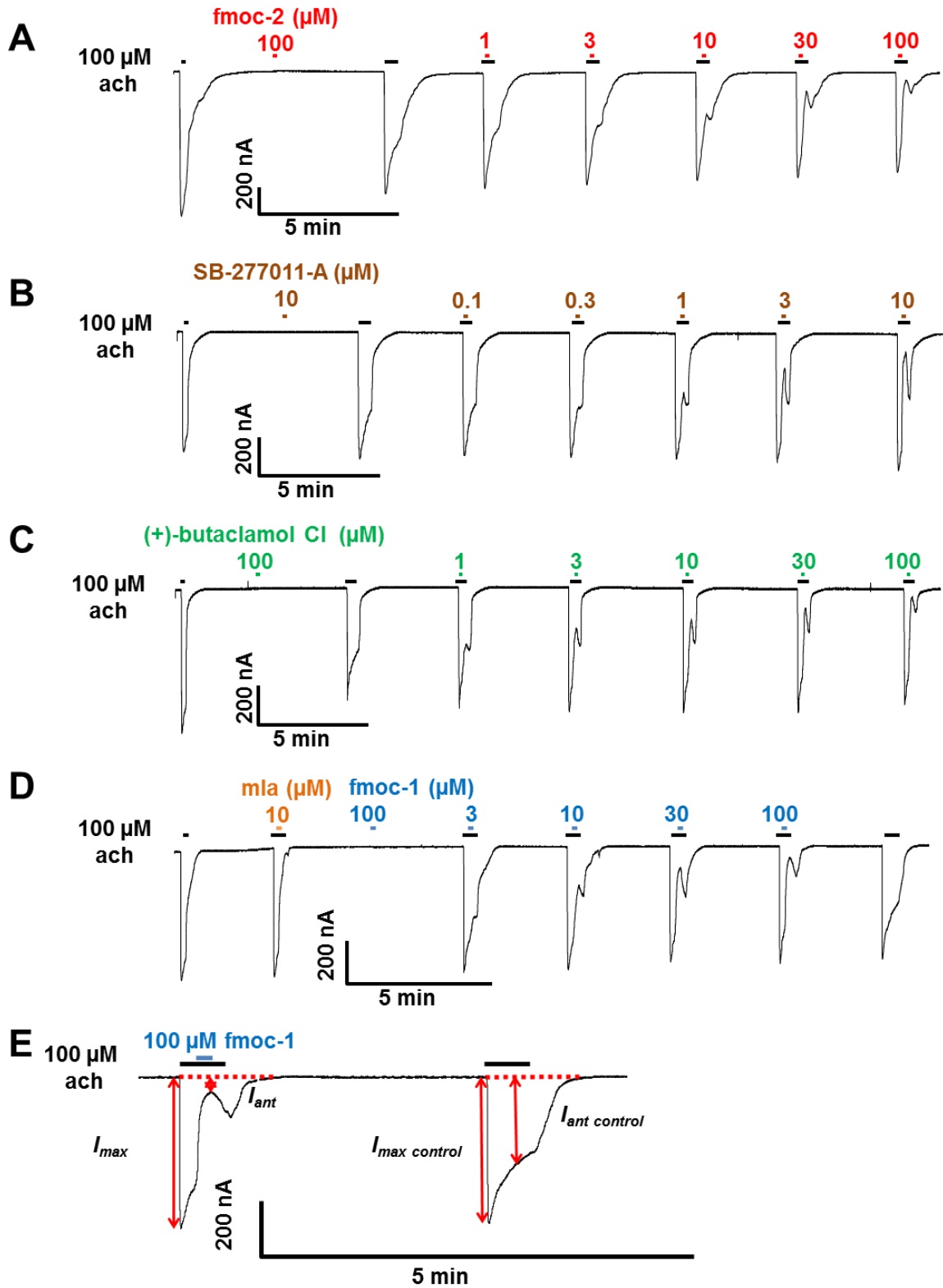


Figure 4. Effects of four virtual screening hits on *Asu*-ACR-16 mediated ach responses. Sample traces for: (A) fmoc-2, (B) SB-277011, (C) (+)-butaclamol Cl, (D) fmoc-1 concentration-inhibition relationships on *Asu*-ACR-16. Mla in (D), which stands for methyllycaconitine citrate salt, was used as an antagonist control of *Asu*-ACR-16. All four hits did not induce the current response by themselves, while produced the concentration-depended inhibition of ach current response. (E) is the magnified figure of part of (D) as an example to show the four parameters needed to measure the inhibition percentage. $I_{max\ control}$ was the peak current of the control 30 seconds application of 100 μ M ach. I_{max} was the peak current of the 100 μ M ach that preceded the 10 second co-application of ach and antagonist. I_{ant} was the minimal current during the co-application of 100 μ M ach and antagonist. $I_{ant\ control}$ was the current at the same point from the beginning of the 30 second application as I_{ant} during the control 30 seconds application of 100 μ M ach.

Figure 5

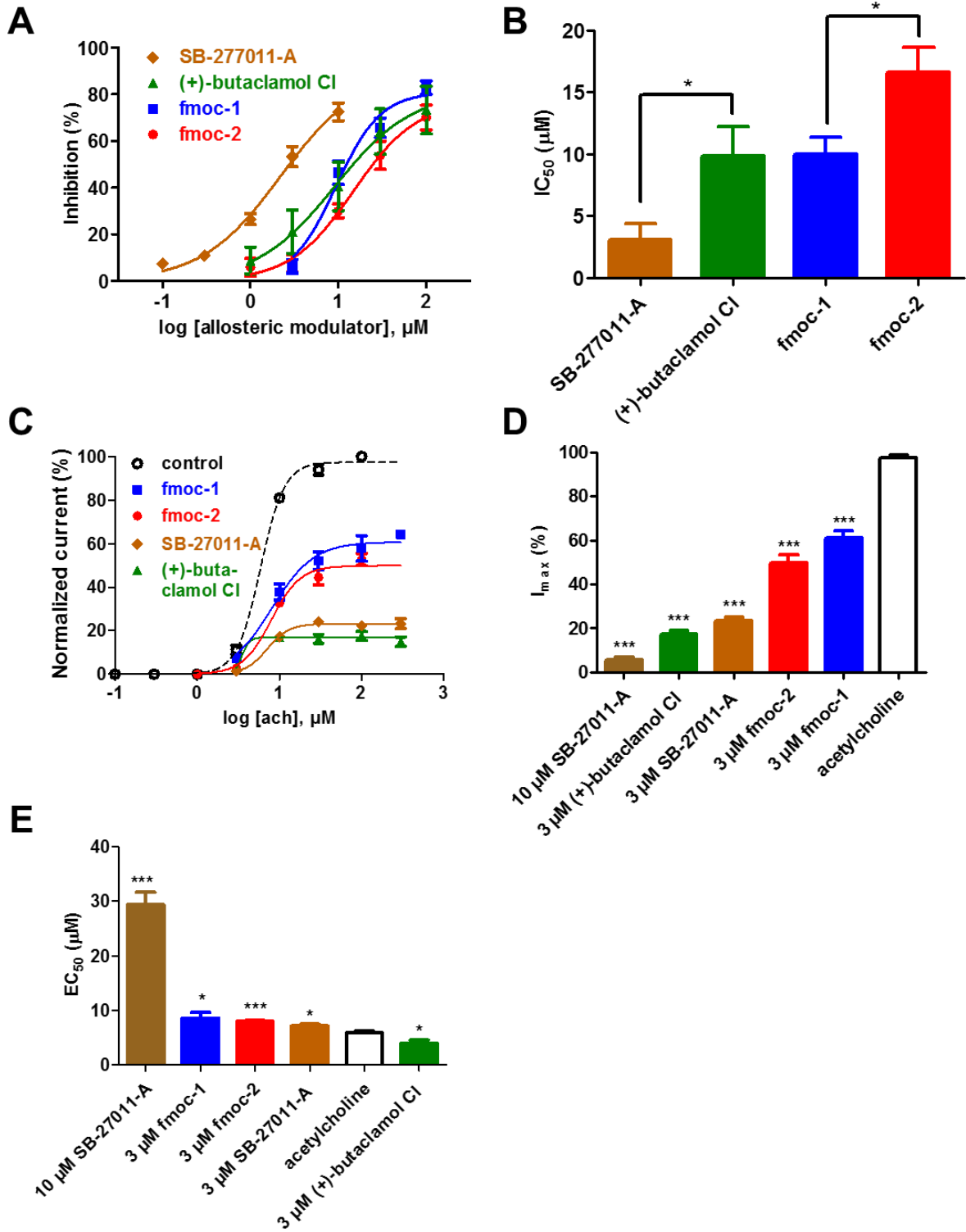


Figure 5. (A) Effects of four virtual screening hits on *Asu*-ACR-16 mediated ach responses. Fmoc-2, fmoc-1, (+)-butaclamol Cl and SB-277011-A concentration-inhibition curves for *Asu*-ACR-16. Results were expressed as mean % inhibition of currents elicited by 100 μ M ach \pm S.E.M.

(B) Bar chart representing the IC_{50} (mean \pm S.E.M, μ M) of each plots in (A). The rank order series of inhibition based on IC_{50} for four hits is: SB-277011-A ($3.12 \pm 1.29 \mu$ M, $n = 4$) < (+)-butaclamol Cl ($9.85 \pm 2.37 \mu$ M, $n = 4$) \approx fmoc-1 ($10.00 \pm 1.38 \mu$ M, $n = 4$) < fmoc-2 ($16.67 \pm 1.95 \mu$ M, $n = 4$). * represents $p < 0.05$ (unpaired t -test).

(C) Ach concentration-response plots for *Asu*-ACR-16 in the absence of hits as a control (ach) and in the continual presence of four hits identified in (A). Ach concentration-response curves for *Asu*-ACR-16 in the presence of 3 μ M of four hits: fmoc-1, fmoc-2, SB-27011-A and (+)-butaclamol Cl.

(D) Bar chart (mean \pm S.E.M, %) representing the reduced maximum current response of ach concentration-response curves in (C). The series of reduced maximum response of each hits compared to that of ach by unpaired t -test is: 10 μ M SB-27011-A ($5.51 \pm 1.38\%$, $n = 4$), 3 μ M (+)-butaclamol Cl ($17.22 \pm 1.94\%$, $n = 4$), 3 μ M SB-27011-A ($23.25 \pm 1.80\%$, $n = 5$), 3 μ M fmoc-2 ($49.92 \pm 3.27\%$, $n = 4$), 3 μ M fmoc-1 ($61.25 \pm 3.08\%$, $n = 4$) and ach ($97.45 \pm 1.19\%$, $n = 4$). * represents $p < 0.05$, ** represents $p < 0.01$, *** represents $p < 0.001$. All four hits significantly inhibited the maximum current response induced by ach.

(E) Bar chart (mean \pm S.E.M, μ M) displaying the EC_{50} of ach concentration-response curves in (C). The series of variable EC_{50} of each hits compared to that of ach by unpaired t -test is: 10 μ M SB-27011-A ($29.40 \pm 2.27 \mu$ M, $n = 4$), 3 μ M fmoc-1 ($8.62 \pm$

1.04 μM , $n = 4$), 3 μM fmoc-2 ($8.01 \pm 0.18 \mu\text{M}$, $n = 4$), 3 μM SB-27011-A ($7.17 \pm 0.33 \mu\text{M}$, $n = 5$), ach ($5.92 \pm 0.29 \mu\text{M}$, $n = 4$) and 3 μM (+)-butaclamol Cl ($3.94 \pm 0.66 \mu\text{M}$, $n = 4$). The EC_{50} of all four hits obviously shift away from the control when applied.

Tables

Table 1. Physicochemical properties and chemical structures of four virtual screen hits. The four hits are: fmoc-4-(naphthalen-2-yl)-piperidine-4-carboxylic acid (fmoc-2), SB-277011-A hydrochloride hydrate (SB-277011-A), fmoc-4-(naphthalen-1-yl)-piperidine-4-carboxylic acid (fmoc-1), (+)-butaclamol hydrochloride ((+)-butaclamol Cl). The molecular mass (Mol. Mass), number of hydrogen bond donors, number of hydrogen bond acceptors, number of rotatable bonds and partition coefficient (xlogP) are listed for each hits.

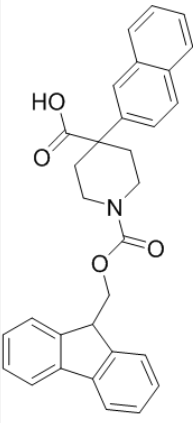
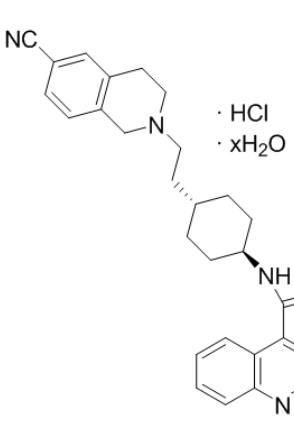
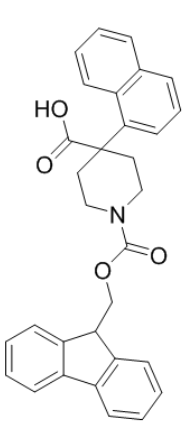
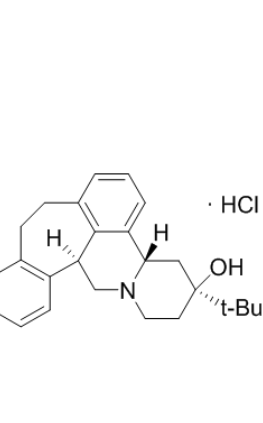
ZINC ID	44122512	26574567	44122502	02008410
Hits	fmoc-2	SB-277011-A	fmoc-1	(+)-butaclamol Cl
Structure				
Mol. Mass	478	475	478	363
H-bond donors	0	1	0	2
H-bond acceptors	5	5	5	2
Rotatable bonds	5	5	5	1
XlogP	6.04	4.27	6.02	4.96

Table 2. Binding affinities (kcal/mol) of the four hits and ach in the orthosteric binding sites of the three different bound models of ECD-*Asu*-ACR-16 and three allosteric binding sites of the antagonist-bound model of full-length *Asu*-ACR-16.

Hits	Binding affinities (kcal/mol)					
	Apo	Agonist-bound	Antagonist-bound		Transmembrane site	
	Orthosteric binding site	Orthosteric binding site	Orthosteric binding site	Agonist sub-pocket	Inter-subunit	Intra-subunit
fmoc-2	-10.4	-13.0	-10.2	-8.5	-11.4	-10.8
SB-277011-A	-9.8	-12.3	-9.2	-9.5	-10.8	-9.7
fmoc-1	-10.6	-12.3	-10.3	-8.9	NA	-11.0
(+)-butaclamol Cl	-9.5	-11.8	-8.2	-9.2	-10.8	-9.0
ach	-4.2	-4.3	-3.9	-4.0	-3.7	NA

Table 3. Pharmacological profiles of the inhibitory effects of four hits on *Asu*-ACR-16 mediated ach responses. Results (mean \pm S.E.M.) were expressed as IC_{50} (μ M), hill slope (n_H), maximum inhibition (%) and the number of repeats (N) of each experiment.

Hits	IC_{50} (μ M)	n_H	Inhibition _{max} (%)	N
fmoc-2	16.67 \pm 1.95	1.22 \pm 0.17	80.34 \pm 10.32	4
SB-277011-A	3.12 \pm 1.29	0.99 \pm 0.11	96.07 \pm 10.66	4
fmoc-1	10.00 \pm 1.38	1.97 \pm 0.37	82.49 \pm 4.74	4
(+)-butaclamol CI	9.85 \pm 2.37	1.34 \pm 0.29	79.53 \pm 12.41	4

Table 4. Pharmacological profiles of EC_{50} shifts and maximum current reductions of *Asu*-ACR-16 mediated ach responses in the presence and absence of four hits. Results (mean \pm S.E.M.) were expressed as EC_{50} (μ M), hill slope (n_H) and maximum response (%) and the number of repeats (N) of each experiment.

Hits	IC_{50} (μ M)	n_H	Inhibition _{max} (%)	N
fmoc-2	16.67 \pm 1.95	1.22 \pm 0.17	80.34 \pm 10.32	4
SB-277011-A	3.12 \pm 1.29	0.99 \pm 0.11	96.07 \pm 10.66	4
fmoc-1	10.00 \pm 1.38	1.97 \pm 0.37	82.49 \pm 4.74	4
(+)-butaclamol CI	9.85 \pm 2.37	1.34 \pm 0.29	79.53 \pm 12.41	4

Supplementary Data

The following is the supplementary data related to this article:

Figure S1

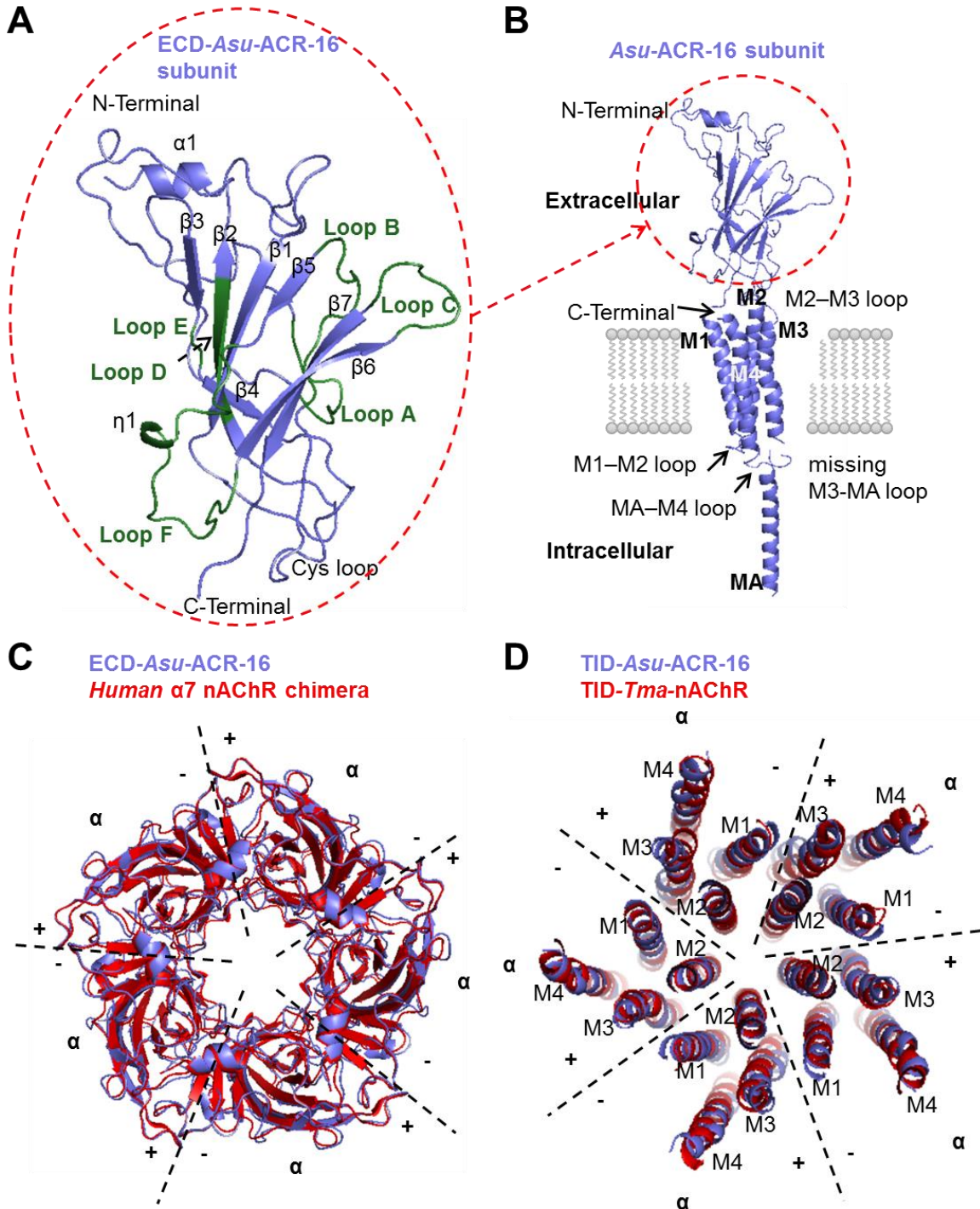


Figure S1. (A) Ribbon representation of the ECD-*Asu*-ACR-16 monomer. Secondary elements are indicated. Loop A, B, C in the principal subunit and loop D, E, F in the complementary subunit which mainly contribute to the orthosteric binding site are labeled by dark green. In the complete structure, the C-terminal would enter the membrane at the bottom and link to M1 helix in the transmembrane domain.

(B) Ribbon representation of the full-length *Asu*-ACR-16 monomer, as viewed parallel to the membrane plane. Four α helices (M1, M2, M3 and M4) that contribute to transmembrane domain and one MA helix that makes up the intracellular domain are indicated. The functionally important M1-M2, M2-M3 and MA-M4 loops are labeled.

(C) Superposition of antagonist-bound model of ECD-*Asu*-ACR-16 pentamer (purple blue) and template human $\alpha 7$ nAChR chimera (red; PDB code: 4HQP, ligands removed for clarity) viewed from the synaptic cleft. Five homomeric α -subunits are labeled. The interfaces between two vicinal α -subunits are marked by dotted lines. Five orthosteric binding sites are at each interface between the principal side (+) and the complementary side (-) from two vicinal subunits.

(D) Superposition of TID-*Asu*-ACR-16 pentamer (purple blue) and template TID-*Tma*-AChR (red; PDB code: 2BG9) viewed above the membrane. Five homomeric α -subunits are labeled. The interfaces between two vicinal α -subunits are marked by dotted lines. Five allosteric binding sites are at each interface among the M2, M3 in the principal side (+) and the M1 in the complementary side (-) from two vicinal subunits.

Figure S2

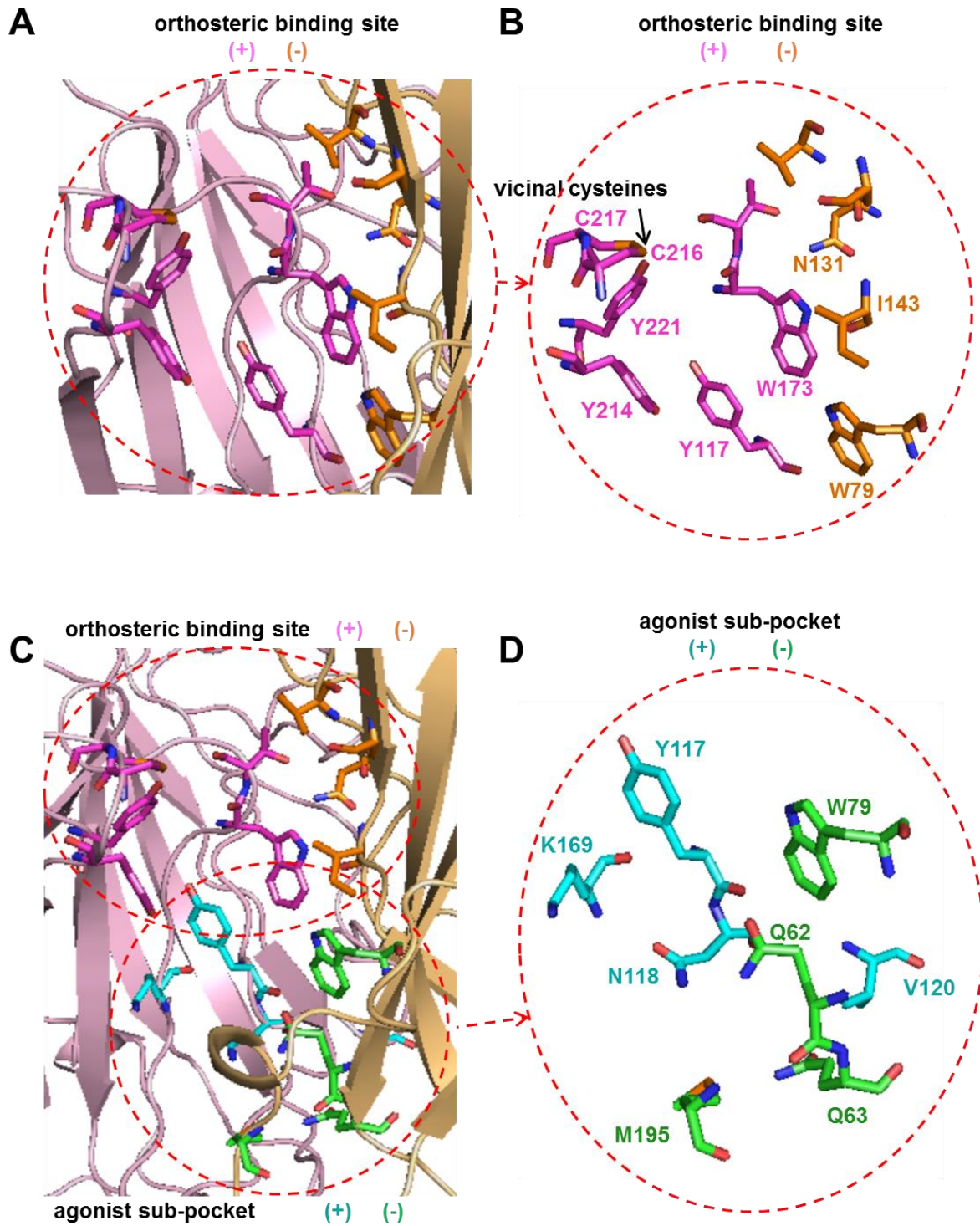


Figure S2

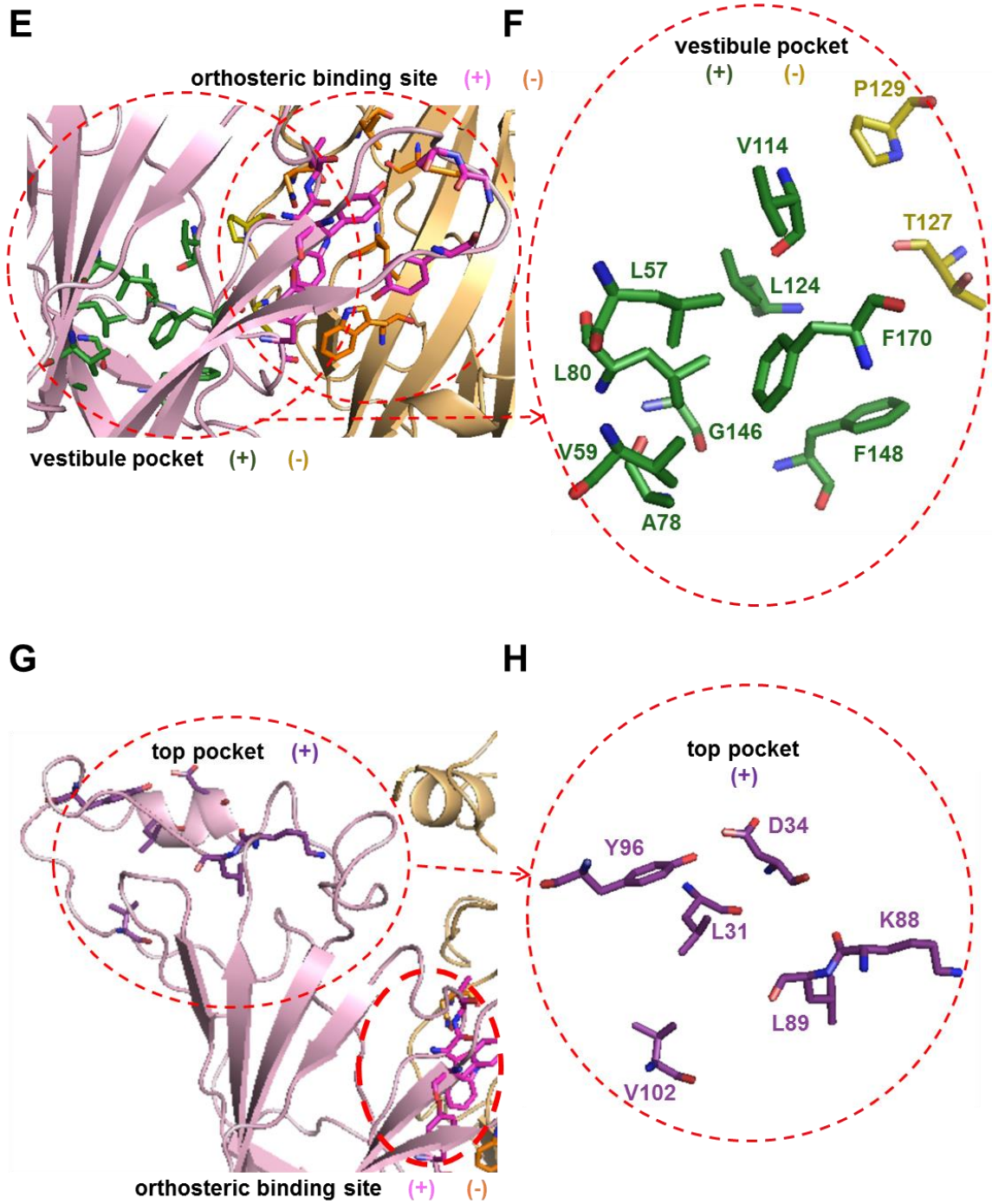


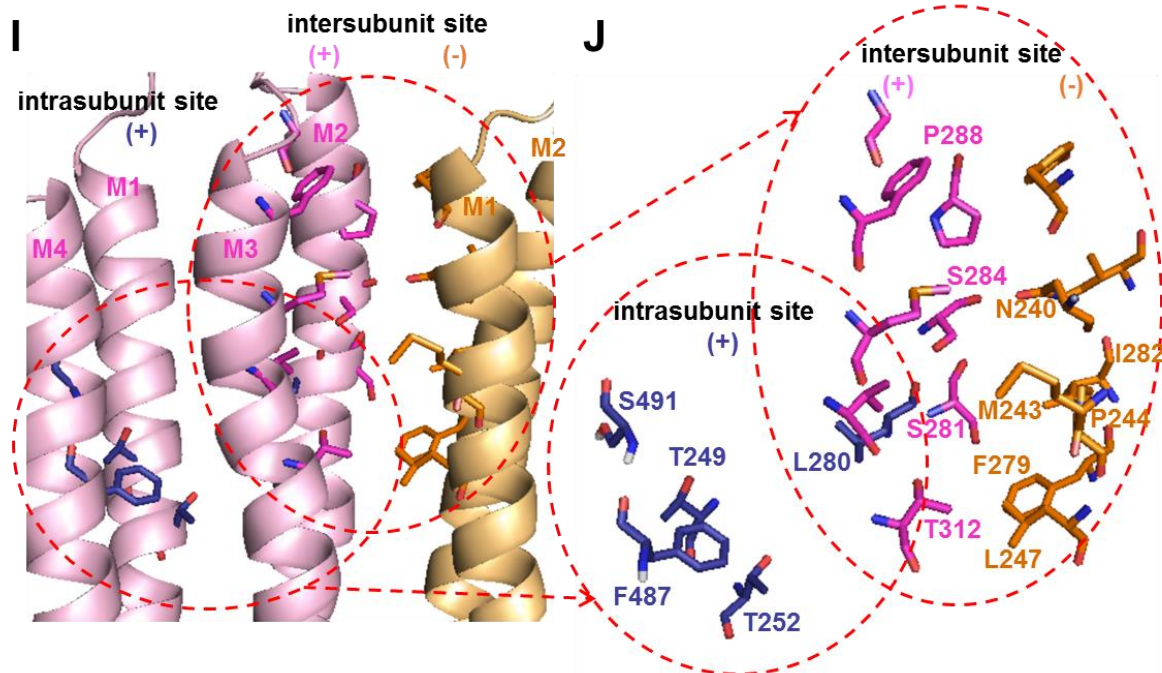
Figure S2

Figure S2. (A) Detailed view of the orthosteric binding site in the antagonist-bound model of ECD-Asu-ACR-16. Principal subunit is colored light pink, whereas the complementary subunit is colored yellow. The residues that contribute to the orthosteric binding site are represented by sticks (principal side (+), pink; complementary side (-), orange) and highlighted inside the red dotted circle. Carbon is in either pink or orange. Nitrogen is in blue. Oxygen is in red. Sulfur is in yellow.

(B) Detailed view of the residues involving in the orthosteric binding site in the antagonist-bound model of ECD-Asu-ACR-16. Functionally important amino acids which interact with the ligands bound in this region are labeled.

(C) Detailed view of the agonist sub-pocket relative to the location of the orthosteric binding site in the antagonist-bound model of ECD-Asu-ACR-16. Principal subunit is colored light pink, whereas the complementary subunit is colored yellow. The residues that contribute to the agonist sub-pocket are represented by sticks

(principal side (+), turquoise; complementary side (-), green) and highlighted inside the red dotted circle at the bottom. Carbon is in either turquoise or green. Nitrogen is in blue. Oxygen is in red.

(D) Detailed view of the residues involving in the agonist sub-pocket in the antagonist-bound model of ECD-*Asu*-ACR-16. Functionally important amino acids which interact with the allosteric modulators bound in this region are labeled.

(E) Detailed view of the vestibule pocket relative to the location of the orthosteric binding site in the antagonist-bound model of ECD-*Asu*-ACR-16. Principal subunit is colored light pink, whereas the complementary subunit is colored yellow. The residues that contribute to the vestibule pocket are represented by sticks (principal side (+), dark green; complementary side (-), gold) and highlighted inside the red dotted circle on the left. Carbon is in either dark green or gold. Nitrogen is in blue. Oxygen is in red.

(F) Detailed view of the residues involving in the vestibule pocket in the antagonist-bound model of ECD-*Asu*-ACR-16. Functionally important amino acids which interact with the allosteric modulators bound in this region are labeled.

(G) Detailed view of the top pocket relative to the location of the orthosteric binding site in the antagonist-bound model of ECD-*Asu*-ACR-16. Principal subunit is colored light pink, whereas the complementary subunit is colored yellow. The residues that contribute to the vestibule pocket are represented by sticks (principal side (+), purple) and highlighted inside the red dotted circle at the top. Carbon is in purple. Nitrogen is in blue. Oxygen is in red.

(H) Detailed view of the residues involving in the top pocket in the antagonist-bound model of ECD-*Asu*-ACR-16. Functionally important amino acids which interact with the allosteric modulators bound in this region are labeled.

(I) Detailed view of the two transmembrane allosteric binding sites in the antagonist-bound model of TID-*Asu*-ACR-16. Principal subunit is colored light pink, whereas the complementary subunit is colored yellow. The residues that contribute to the intersubunit site (principal side, pink; complementary side, orange) and intrasubunit site (principal side, purpleblue) are represented by sticks and highlighted inside the red dotted circle. Carbon is in either pink or orange or purpleblue. Nitrogen is in blue. Oxygen is in red. Sulfur is in yellow.

(J) Detailed view of the residues involving in the two transmembrane allosteric binding sites in the antagonist-bound model of TID-*Asu*-ACR-16. Functionally important amino acids which interact with the allosteric modulators bound in this region are labeled.

Figure S3

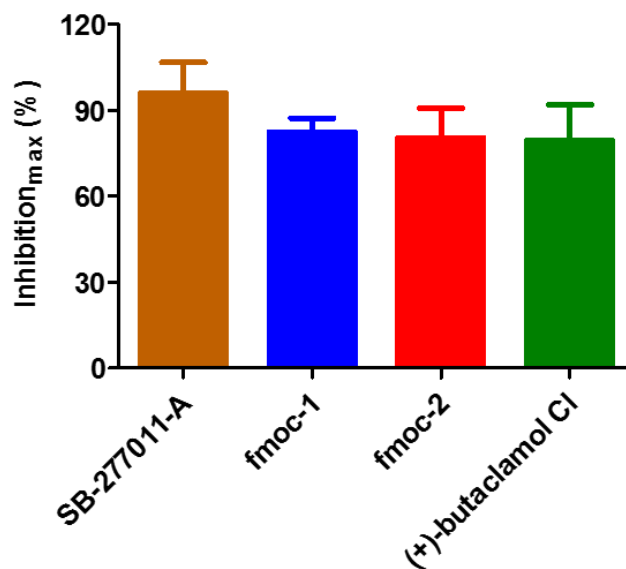


Figure S3. Bar chart showing effects of the four hits on *Asu*-ACR-16. Results are expressed as maximum inhibition (mean \pm S.E.M, %) of each plots in (Fig. 5A). The rank order series of inhibition based on maximum inhibition percentage for four hits is: SB-277011-A ($96.07 \pm 10.66\%$, $n = 4$) \approx fmoc-1 ($82.49 \pm 4.74\%$, $n = 4$) \approx fmoc-2 ($80.34 \pm 10.32\%$, $n = 4$) \approx (+)-butaclamol Cl ($79.53 \pm 12.41\%$, $n = 4$) using unpaired *t*-test.

Figure S4

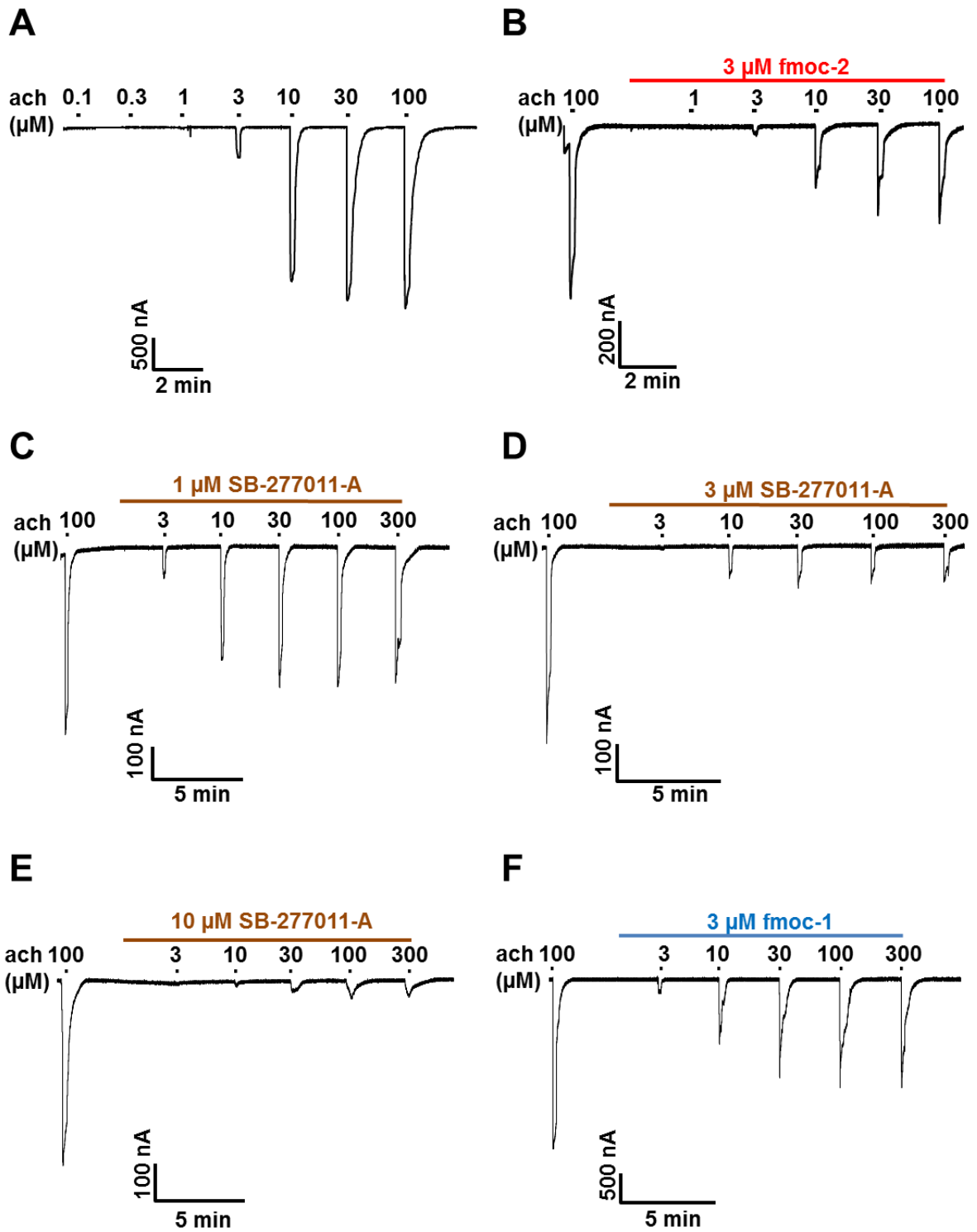


Figure S4

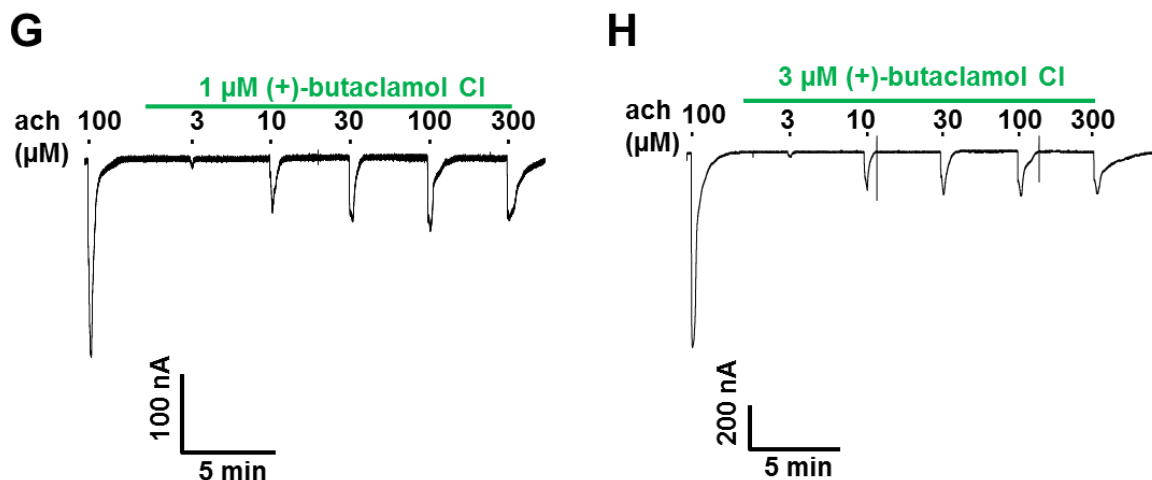


Figure S4. Sample traces showing the effects of four hits on the acetylcholine concentration-response relationships for *Asu-ACR-16*. Sample trace of acetylcholine concentration-response relationships in the absence of hits is depicted in (A) as a control. 3 μM of each of four hits are applied: (B) fmoc-2, (D) SB-277011, (F) fmoc-1, (H) (+)-butaclamol Cl, to compare the EC_{50} shifts and the maximum response reduction for four hits. 1 μM SB-277011-A (C), 1 μM (+)-butaclamol Cl (G) and 10 μM SB-277011-A (E) were tested to study the concentration effects on the mode of inhibition.

Figure S5

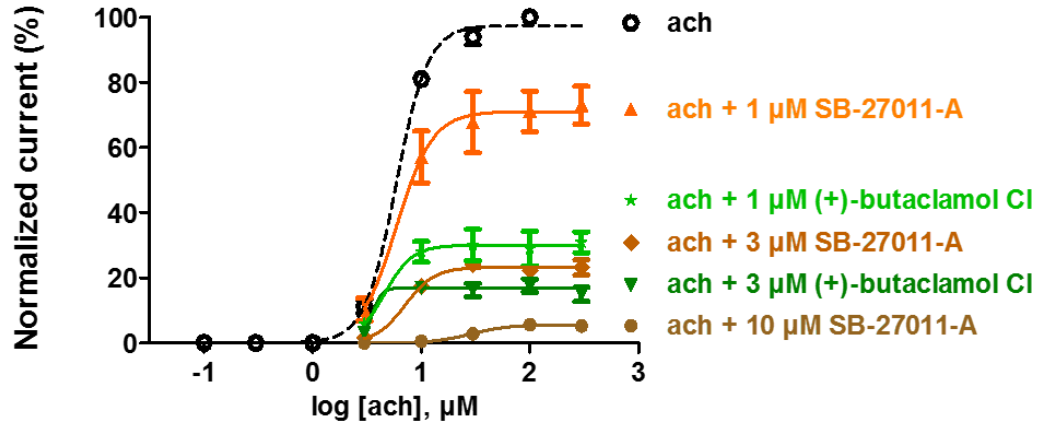


Figure S5. Ach concentration-response curves for *Asu*-ACR-16 in the absence of hits as a control (ach) and in the continual presence of 1 μ M, 3 μ M, 10 μ M SB-277011-A, 1 μ M, 3 μ M (+)-butaclamol Cl.

Figure S6

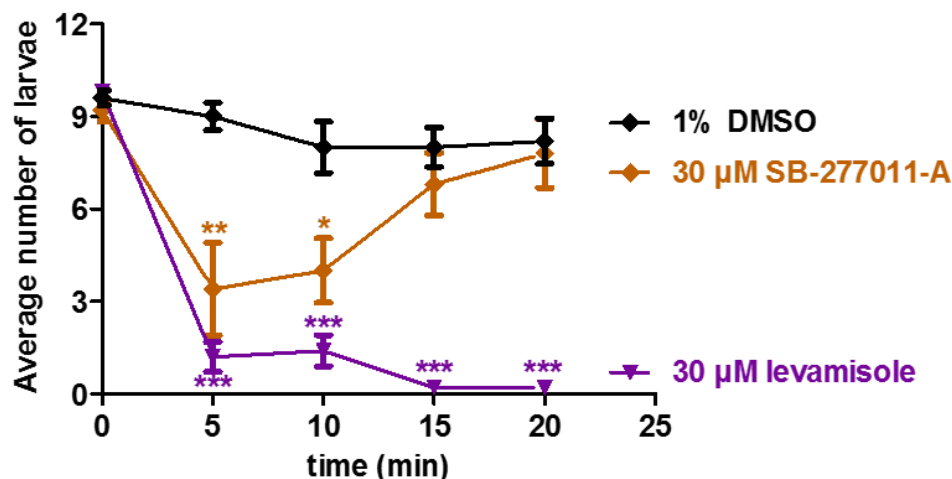
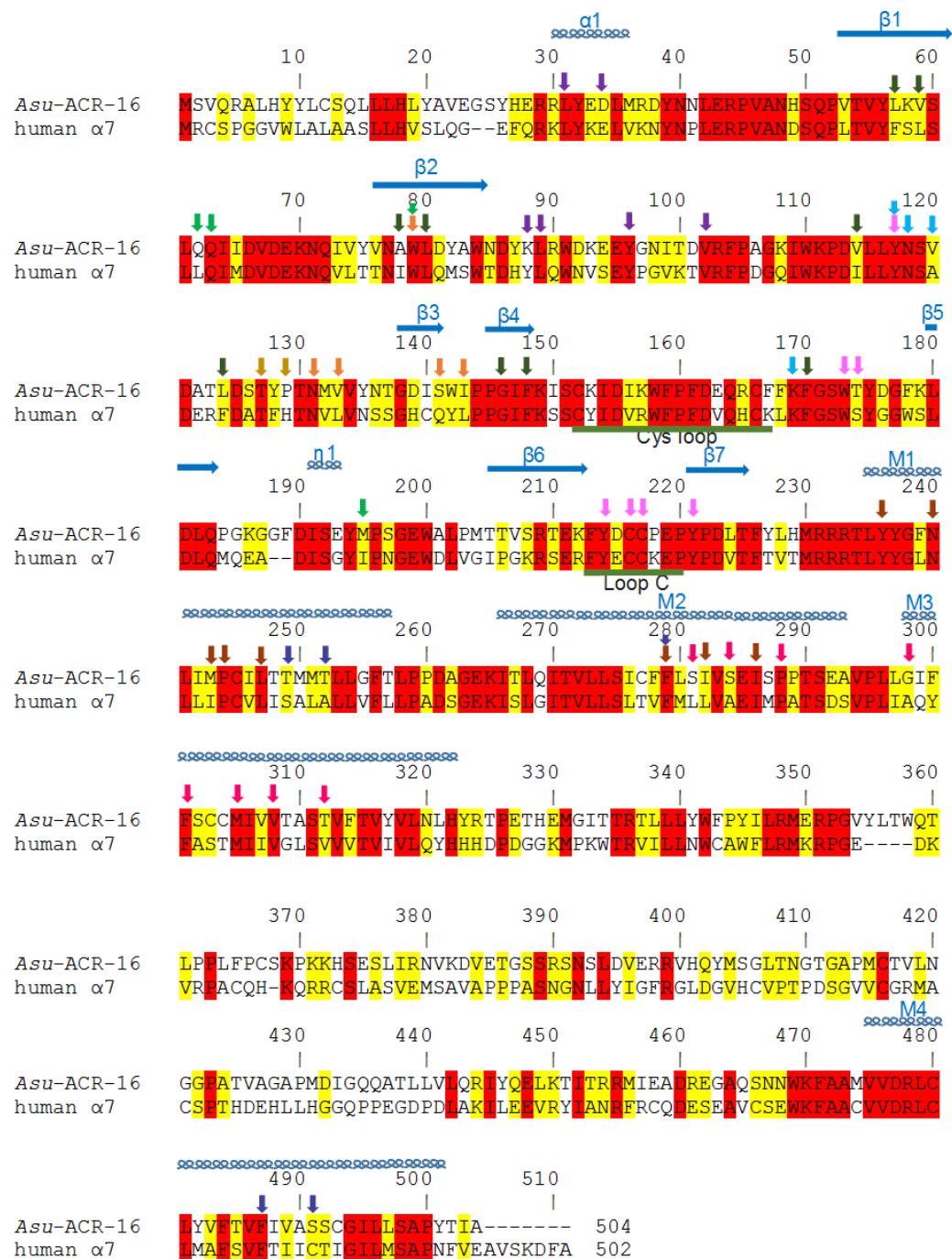


Figure S6. Plot of average number of L4 *C. elegans* larvae with normal motility (A) vs. time (min) in the absence of drug (1% DMSO, control), presence of 30 μM SB-277011-A and 30 μM levamisole. Ten worms were used for each treatment, which was replicated by five times. Comparisons of locomotion were made between control and treated worms at each time point. * $p < 0.05$, ** $p < 0.01$, *** $p < 0.001$. The recovery of normal motility was observed only in the larvae treated with 30 μM SB-277011-A within 20 minutes, but not in the larvae treated with 30 μM levamisole within 24 hours.

Figure S7



Orthosteric binding site	(+)	(-)
Agonist sub-pocket	(+)	(-)
Vestibule pocket	(+)	(-)
Top pocket	(+)	
Transmembrane intersubunit site	(+)	(-)
Transmembrane intrasubunit site	(+)	

Figure S7. Sequence and numbering of the full-length *Asu*-ACR-16 and its alignment with the human $\alpha 7$ nAChR subunit. Completely conserved residues (red background) and partially conserved residues (yellow background) are indicated. Secondary structures are shown schematically above the sequences. α_1 represents α helix. β_{1-7} represent β strand. η_1 represents 3_{10} helix. The Cysteine loop labeled by green bars. Four transmembrane α helices (M1, M2, M3 and M4) are labeled by blue coils. Residues in the orthosteric binding site are indicated by arrows (principal subunit, pink; complementary subunit, orange). Residues in four allosteric binding sites are highlighted by arrows (principal subunit of agonist sub-pocket, turquoise; complementary subunit of agonist sub-pocket, green; principal subunit of vestibule pocket, dark green; complementary subunit of vestibule pocket, gold; principal subunit of top pocket, purple; principal subunit of intersubunit transmembrane site: bright pink; complementary subunit of intersubunit site: brown; principal subunit of intrasubunit site: purpleblue).

Figure S8

		Identity		Similarity	
Orthosteric binding site	(+)	6/7		7/7	
	(-)	2/5		5/5	
	Overall	8/12	66.7%	12/12	100%
Agonist sub-pocket	(+)	3/4		4/4	
	(-)	2/4		3/4	
	Overall	5/8	62.5%	7/8	87.5%
Vestibule pocket	(+)	4/9		8/9	
	(-)	1/2		1/2	
	Overall	5/11	45.5%	9/11	81.8%
Top pocket	(+)	4/6	66.7%	5/6	83.3%
Transmembrane intersubunit site	(+)	4/8		7/8	
	(-)	6/8		8/8	
	Overall	10/16	62.5%	15/16	93.8%
Transmembrane intrasubunit site	(+)	2/5	40.0%	5/5	100%

Figure S8. Comparison of residues in the orthosteric binding site and five allosteric binding sites between *Asu*-ACR-16 and human $\alpha 7$ nAChR.

CHAPTER 3

**STRUCTURE-BASED DRUG DISCOVERY: (S)-5-ETHYNYL-ANABASINE AND
OTHER NICOTINE ALKALOIDS AS ASU-ACR-16 AGONISTS**

A manuscript in preparation for *Journal of Molecular Pharmacology*

Fudan Zheng, Xiangwei Du, Alan P. Robertson, Edward W. Yu, Brett VanVeller* and
Richard J. Martin*

Department of Chemistry, College of Liberal Arts and Sciences (F.Z., X.D., E.W.Y.,
B.V.), Department of Biomedical Sciences, College of Veterinary Medicine (A.P.R.,
R.J.M.), Department of Physics and Astronomy, College of Liberal Arts and
Sciences (E.W.Y.) Iowa State University, Ames, IA, USA

Running title: synthesis and pharmacological activities of nicotine derivatives on
Asu-ACR-16

Number of text pages: 41

Number of tables: 2

Number of figures: 7

Number of references: 26

Number of words in the *Abstract*: 182

Number of words in the *Introduction*: 565

Number of words in the *Discussion*: 987

Supplemental figures: 6

Abbreviations: *Asu*-ACR-16, *Ascaris suum* nicotinic acetylcholine receptor subtype 16 ; (-) complementary side; ECD, extracellular domain; *Lst*-AChBP, *Lymnaea stagnalis* acetylcholine binding protein; nAChRs, nicotinic acetylcholine receptors; (+) principal side;

Abstract

The ACR-16 nicotinic acetylcholine receptor of *Ascaris suum* (*Asu*-ACR-16) is a homopentameric neurotransmitter-gated ion channel, which is widely distributed in *A. suum* tissues and plays an important role in the locomotion of worms. We chose *Asu*-ACR-16 as our pharmaceutical target and nicotine as our basic moiety to develop novel agonists of *Asu*-ACR-16. Our goal is to counteract the drug resistance which has occurred in the treatment of *Ascaris* infections. The structural models of the extracellular domains of *Asu*-ACR-16 was used to study the agonist-binding site and binding properties of potential agonists. We designed, synthesized and characterized the pharmacological profiles of several nicotine derivatives on *Asu*-ACR-16 using *Xenopus* oocytes expression system and two-electrode voltage clamp. (S)-SIB 1508Y (EC_{50} 0.37 ± 0.10 μ M, I_{max} 100.01 ± 4.36 %) is significantly more potent and efficient than (S)-nicotine (EC_{50} 6.21 ± 0.56 μ M, I_{max} 82.39 ± 2.52 %). 6-AN is a very potent non-competitive antagonist (IC_{50} 2.00 ± 0.41 μ M). These

data suggest that (S)-5-ethynyl-anabasine and several other nicotine alkaloids with high potencies and efficacies on *Asu*-ACR-16 may be promising leads for future anthelmintic drug development.

Keywords: *Asu*-ACR-16, agonist-binding site, nicotine alkaloids, *Xenopus* expression, *Ascaris suum*, anthelmintic

Introduction

The nicotinic acetylcholine receptors (nAChRs) are pentameric ligand-gated ion channels and involved in fast synaptic transmission in the central and peripheral nervous systems (Taly *et al.*, 2009). The nAChRs can be activated by the neurotransmitter acetylcholine (ach), nicotine or its structurally related derivatives, which then lead to the opening of channel and a flux of sodium, potassium ions and sometimes calcium ions.

The agonist-binding site of nAChRs was well studied by the combination of photolabeling, mutagenesis and electrophysiological approaches (Arias, 2000a). Our understanding of ligand-receptor interactions has improved via co-crystal structures of invertebrate acetylcholine binding proteins (AChBPs) with cholinergic ligands (Sixma *et al.*, 2003; Rucktooa *et al.*, 2009). AChBPs are homologs of the extracellular agonist-binding site domain of nAChRs and share 20–24 % sequence identity with the extracellular domain of AChRs (Blum *et al.*, 2010). The agonist-binding site of nAChRs is at the interface between principal subunit (with vicinal cysteines) and complementary subunit (without vicinal cysteines) in the extracellular

domain. Five aromatic amino acids in the agonist-binding site are highly conserved in nAChRs and contribute to the cation- π interaction with a characteristic cationic nitrogen in nAChR agonists (Dougherty, 2013). Another feature of nAChR agonists is the hydrogen bond acceptor, which is about 4-6 Å from the cationic nitrogen. Based on the high-resolution structures of AChBPs, the hydrogen bond acceptor in agonist is stabilized by a water molecule, which further interacts with carbonyl or amide backbones of two less conserved residues on loop E of the complementary subunit through three hydrogen bonding interactions (Van Arnam *et al.*, 2014).

Ascaris, a genus of clade III nematode parasites, are gastrointestinal roundworms that infect humans, pigs and other animals worldwide (Taylor *et al.*, 2016) and were estimated to cause more than 1.2 billion infections (de Silva *et al.*, 2003a). With no effective vaccines and inadequate sanitation in many countries, the control of *Ascaris* infection mainly relies on the limited number of available anthelmintic drugs. Unfortunately, drug resistances in various parasites have been reported due to the frequent use of anthelmintics (Garcia *et al.*, 2016), which demand more potent and efficacious drugs for treatment.

The ACR-16 nicotinic acetylcholine receptor of *Ascaris suum* (*Asu*-ACR-16) is a nematode homopentameric receptor, which closely resembles vertebrate $\alpha 7$ nAChRs (Mongan *et al.*, 2002). *Asu*-ACR-16 is widely distributed in *A. suum* tissues and may function in the motility of parasite. As one of the recently characterized nematode parasitic nAChRs, *Asu*-ACR-16 is pharmacologically different to its host $\alpha 7$ nAChR and has been exploited as an anthelmintic drug target to counter resistance (Holden-Dye *et al.*, 2013; Zheng *et al.*, 2016).

The agonist-binding site of the *Asu*-ACR-16 can be predicted by homology modeling using the human $\alpha 7$ nAChR chimera as structural template, which shares 38% identity and 73% similarity in sequence. Five conserved aromatic residues and two hydrogen-bond interacting residues are in the close orientations with their corresponding residues in nAChRs, which therefore facilitates our further investigation of drug-receptor interactions on *Asu*-ACR-16 (Zheng *et al.*, 2016).

The *Asu*-ACR-16 is sensitive to six nicotinic agonists: nicotine, ach, cytisine, 3-bromocytisine, epibatidine, dimethyl-4-phenylpiperazinium iodide (DMPP), whereas insensitive to other cholinergic anthelmintic agonists (Abongwa *et al.*, under review). All six *Asu*-ACR-16 agonists share the nicotinic pharmacophore: a cationic nitrogen separated certain distance from a hydrogen bond acceptor. Hence, we used a combination of structural modeling and synthetic strategy based on nicotinic pharmacophore to explore the pharmacological profiles of nicotine derivatives on *Asu*-ACR-16.

Materials and Methods

Materials

Table 1 lists the chemicals used in electrophysiological studies. Acetylcholine chloride (ach), (-)-nicotine hydrogen tartrate salt ((S)-nicotine), anabasine ((S, R)-anabasine), (\pm)-nornicotine (nornicotine), 5-(1-methyl-pyrrolidin-2-yl)-pyridin-2-ylamine dihydrochloride (6-AN) and (-)-cotinine ((S)-cotinine), which were purchased from Sigma-Aldrich (St Louis, MO, USA). SIB 1508Y maleate (SIB 1508Y) was obtained from Tocris Bioscience (Ellisville, MO, USA). (S)-anabasine, rac-5-

methylnicotine (5-methylnicotine), S-(-)-nicotine-5-carboxaldehyde ((S)-nicotine-5-carboxaldehyde), (±)-6-methylnicotine (6-methylnicotine), (S)-1-methylnicotinium iodide ((S)-1-methylnicotinium), (S)-1'-methylnicotinium iodide ((S)-1'-methylnicotinium), (R, S)-N-ethyl nornicotine (homonicotine), N-methyl anabasine were acquired from Toronto Research Chemicals (Toronto, ON, Canada).

The following chemicals were used for the synthesis of (S)-5-bromonicotine, (S)-5-bromoanabsine and (S)-5-ethynyl-anabsine: 4, 4'-di-tert-butyl-2, 2'-dipyridyl, copper(II) bromide and 2-methyl-3-butyn-2-ol obtained from Sigma-Aldrich (St Louis, MO, USA); di- μ -methoxobis(1,5-cyclooctadiene)diiridium(I) and methanesulfonato(2-di-t-butylphosphino-2',4',6'-tri-i-propyl-1,1'-biphenyl)(2'-amino-1,1'-biphenyl-2-yl)palladium(II) obtained from Strem Chemicals (Newburyport, MA, USA); S-(-)-nicotine and (-)-anabasine obtained from Alfa Aesar (Ward Hill, MA, USA); bis(pinacolato)diboron obtained from Matrix Scientific (Columbia, SC, USA); (trimethylsilyl)acetylene obtained from Oakwood Products (Estill, SC, USA).

Synthesis of nicotine derivatives

The reaction schemes for (S)-5-bromonicotine, (S)-5-bromoanabasine and (S)-5-ethynyl-anabasine were shown (Fig. 1) (Gros *et al.*, 2006; Liskey *et al.*, 2010). Given that this part of work was not contributed by me, and the synthetic and biological studies of (S)-5-ethynyl-anabasine have not been completed yet, all the work and result related to (S)-5-ethynyl-anabasine are to be added in this manuscript.

Homology modeling and docking

The *Asu-ACR-16* sequence is available in the UniProtKB with the accession number F1KYJ9 (Wang *et al.*, 2011). Three crystal structures of human $\alpha 7$ nAChR chimera co-crystallized with ligands of different modes of action were used as templates to build three different bound-form models of the ECD-*Asu-ACR-16* (Table 2) (Li *et al.*, 2011a; Huang *et al.*, 2013; Zheng *et al.*, 2016). The smiles strings of nicotine derivatives were obtained from the ZINC (<http://zinc.docking.org/search/structure>) and converted to PDBQT format. Docking of these ligands was performed in the orthosteric ligand-binding sites of agonist-bound and apo form ECD-*Asu-ACR-16* models using AutoDock Vina Software (Trott *et al.*, 2010; Zheng *et al.*, 2016).

Expression and electrophysiology of *Asu-ACR-16* in oocytes

Full length *Asu-acr-16* cRNA and ancillary gene *Asu-ric-3* cRNA (UniProtKB accession number: F1L1D9) were prepared using the previous method (Zheng *et al.*, 2016). The cRNA mixture of 25 ng *Asu-acr-16* and 5 ng *Asu-ric-3* cRNA in 50 nL RNase-free water was injected into the de-folliculated *Xenopus laevis* oocyte (Ecocyte Bioscience, Austin, TX, USA). The injected oocytes were incubated in the incubation solution (100 mM NaCl, 2 mM KCl, 1.8 mM CaCl₂·2H₂O, 1 mM MgCl₂·6H₂O, 5 mM HEPES, 2.5 mM Na pyruvate, 100 U/mL penicillin, 100 µg/mL streptomycin, pH 7.5) at 19 °C for 4 – 8 days and added with 100 µM BAPTA-AM 3 h before recording.

Two-electrode voltage-clamp was used to assay the electrophysiology of the *Asu-ACR-16* expressed in oocytes. The oocytes were kept in the recording solution

(100 mM NaCl, 2.5 mM KCl, 1 mM CaCl₂·2H₂O and 5 mM HEPES, pH 7.3) and clamped at -60 mV during recording. Inward current signal in oocytes was induced by the addition of testing chemical each in the recording solution and measured by the two-electrode voltage-clamp (Molecular Devices, CA, USA). The data was acquired in Clampex 9.2 (Molecular Devices, CA, USA) and analyzed by GraphPad Prism 5.0 (Graphpad Software Inc., CA, USA).

Pharmacological characterization of nicotinic derivatives and data analysis

With the exception of ach, (S)-nicotine, SIB 1508Y, (S)-1-methylnicotinium, (S)-1'-methylnicotinium, nornicotine, (S)-cotinine, (S)-anabasine, (S,R)-anabasine which were dissolved in the recording solution, the rest of chemicals for electrophysiological studies were dissolved in DMSO to make 100 mM stock solutions of each. Recording solution was used to dilute the stock solutions and prepare a series of working solutions.

100 μM ach was applied initially for 10 s as a control to check the *Asu*-ACR-16 expression in all recordings and was used to normalize other current peak sizes. Recording solution was then used to wash out the drug from the oocytes for 3 min prior to next application of drug perfusion.

To characterize the nicotine derivatives as agonists, increasing concentrations of the derivatives were applied for 10 s, with 3 min wash intervals to determine the dose-response relationship of each agonist. The dose-response relationships were described by the Hill equations to give estimates of the EC_{50} (μM), Hill slope (n_H), maximum response (I_{max} , %) and expressed as mean ± S.E.M.

($N = 5$) by using GraphPad Prism 5.0 (Graphpad Software Inc., CA, USA). The EC_{50} and I_{max} of each agonists were compared using the unpaired student t -test. $P < 0.05$ are used to evaluate the statistic difference.

To determine the rank order potency of the nicotine derivatives as antagonists, 100 μM ach was applied for 10 s, followed by a 10 s co-application of 100 μM nicotine derivative with 100 μM ach, and then a 10 s wash of 100 μM ach. The inhibition (%) of the 100 μM ach response was measured as described (Zheng *et al.*, 2016), expressed as mean \pm S.E.M. ($N = 5$) and compared using unpaired student t -test for the rank order of inhibition.

To characterize the antagonism of the selected nicotine derivative, increasing concentrations of the antagonist was applied using the previous procedure of 30 s co-application with 100 μM ach to determine the ach inhibitory dose-response relationship. The inhibitory dose-response relationship was fitted into the Hill equations to give estimates of the IC_{50} (μM), Hill slope (n_H), maximum inhibition ($Inhibition_{max}$, %) and expressed as mean \pm S.E.M. ($N = 5$).

To determine the effect of membrane potential on inhibition (%) of the selected antagonist, 3 μM antagonist was applied using the previous procedure of 30 s co-application with 100 μM ach while holding the membrane potential at three different values to. ($N = 5$).

To further study the antagonism, the selected antagonist was applied before and during 10 s application of increasing concentrations of ach. The ach dose-response relationships in the presence of antagonist was fitted into the Hill equations

to estimate the EC_{50} (μM), Hill slope (n_H), I_{max} (%) and expressed as mean \pm S.E.M. ($N = 5$).

Results

Ligand-binding sites

Lst-AChBP (PDB code: 1UW6) (Celie *et al.*, 2004) showing 23.33% sequence identity and 64.29% sequence similarity with ECD-*Asu*-ACR-16 (Fig. S1A), is the only crystal structure of *Asu*-ACR-16 homologous protein co-crystalized with nicotine to date. The ligand-binding site for agonist is at the interface between the principal side (+) and the complementary side (-) in two adjacent subunits of nAChRs (Li *et al.*, 2011a; Rucktooa *et al.*, 2012).

Nicotine adopted the same binding poses in all five ligand-binding sites in *Lst*-AChBP pentamer (Fig. 2A). The pyrrolidine ring of nicotine is oriented toward the basal side of the binding site on the principal subunit, whereas the pyridine ring faces the apical side on the complementary subunit. The protonated N2 in pyrrolidine ring is involved in cation- π interaction with five aromatic side chains of residues in the binding site (principal subunit: Y89, W143, Y185, Y192; complementary subunit: W53). N2 is also hydrogen-bonded to the hydroxyl moiety of Y89 and W143 carbonyl backbone. Hydrophobic interactions from disulfide-bonded C187 and C188 on loop C stabilize nicotine in the binding site. The pyridine ring N1 is hydrogen-bonded to a water molecule, which is stabilized by the carbonyl backbone of L102 and M114 amide backbone of the complementary subunit (Fig. 2B) (Celie *et al.*, 2004; Van Arnem *et al.*, 2014).

Fig. 2C shows the ligand-binding site of the agonist-bound *Asu*-ACR-16 dimer viewed from the same angle as Fig. 2B. The residues involved in the binding site were highlighted in Fig. 2C and indicated in Fig. S1A by arrows. The interacting residues in the binding site of the agonist-bound *Asu*-ACR-16 model share similar orientations with those in the binding site of *Lst*-AChBP. The hydrophobic, hydrogen-bond and van der Waals contacts between nicotine and AChBP were therefore predicted correspondingly in *Asu*-ACR-16. Y117, W173, Y214, Y221 from (+) and W79 from (-) constitute the aromatic cage which makes cation- π interaction with protonated tertiary amine or tetramethyl ammonium salt of nicotine or its derivatives. The hydroxyl moiety of Y117 and W173 carbonyl backbone are hydrogen-bonded to the protonated tertiary amine or ammonium of the ligand. The carbonyl backbone of N131 and I143 amide backbone from the complementary face have water-mediated hydrogen bond with the pyridine ring N1 of the ligand.

Structural superimposition of the binding-site residues among three different bound forms *Asu*-ACR-16 showed the close-in conformational changes of residues when agonist is in complex, especially the inward movement of vicinal cysteines toward pyrrolidine N2 of nicotine. The antagonist-bound model has less steric hindrance in the open-up binding site (Fig. 2D) (Huang *et al.*, 2013).

The human $\alpha 7$ nAChR chimera (PDB code: 3SQ6) (Li *et al.*, 2011a) shows 62.98% sequence identity and 80.29% sequence similarity with the extracellular domain of human $\alpha 7$ nAChR (UniProtKB accession number: P36544). The residues constituting the ligand-binding site are highly conserved between human $\alpha 7$ nAChR chimera and human $\alpha 7$ nAChR (Fig. S1B). The crystal structure of human $\alpha 7$

nAChR chimera co-crystalized with epibatidine could be used to study the binding site of agonist-bound human $\alpha 7$ nAChR. Comparison of the binding sites in *Lst*-AChBP (Fig. 3A), human $\alpha 7$ nAChR chimera (Fig. 3B), agonist-bound *Asu*-ACR-16 (Fig. 3C) and apo form *Asu*-ACR-16 (Fig. 3D) reveals that 5-substituted pyridine derivatives of nicotine may be favorable to the binding site in the ECD-*Asu*-ACR-16, while disfavored by the human $\alpha 7$ nAChR sterically.

Rank order of potency and efficiency for nicotine derivatives

The EC_{50} and I_{max} for (S)-nicotine are $6.21 \pm 0.56 \mu\text{M}$ and $82.39 \pm 2.52 \%$, $N = 5$ (Table 1). (S)-nicotine is a potent agonist of *Asu*-ACR-16, but can also activate mammalian nAChRs non-selectively and cause adverse side effects (Chavez-Noriega *et al.*, 1997). As a low-molecular-weight and water soluble molecule, (S)-nicotine was selected as our initial lead for the further lead optimization (Bleicher *et al.*, 2003). Using (S)-nicotine as a pharmacophore and the predicted three-dimensional structures of *Asu*-ACR-16 ligand-binding site, we studied the structure-activity relationship by characterizing the pharmacological properties of nicotine derivatives (Fig. 4) on *Asu*-ACR-16 (Fig. 5 & Fig. S2).

Among the tested fifteen nicotine alkaloids, except for pyridine N1 methylated substituent: (S)-1-methylnicotium, 5'-carbonylated pyrrolidine substituent: (S)-cotinine, and piperidine N2 methylated substituent: N-methyl anabasine do not show any intrinsic activities as agonists. The rest ten alkaloids act as agonists. The stimulatory dose-response relationships for ach and (S)-nicotine as controls (Fig.

6A), pyridine substituted nicotine derivatives (Fig. 6B) and the pyrrolidine substituted nicotine derivatives (Fig. 6C) were shown.

The rank order of potency based on the EC_{50} values is: (S)-5-bromoanabasine \approx (S)-SIB 1508Y < 5-methylnicotine \approx (S)-anabasine < (S)-5-bromonicotine < 6-methylnicotine \approx (S)-nicotine \approx ach < (S)-1'-methylnicotinium \approx (S)-nicotine-5-carboxaldehyde \approx 6-AN < homonicotine \approx nornicotine (Table 1). Two piperidine ring derivatives: (S)-5-bromoanabasine and (S)-anabasine, two 5-substituted pyridine derivatives: (S)-SIB 1508Y and 5-methylnicotine are more potent than ach and (S)-nicotine ($P < 0.5$, $N = 5$).

The rank order of efficiency based on I_{max} is: (S)-SIB 1508Y \approx ach \approx (S)-1'-methylnicotinium \approx (S)-anabasine \approx (S)-nicotine \approx (S)-5-bromoanabasine \approx 5-methylnicotine > 6-methylnicotine \approx (S)-5-bromonicotine \approx nornicotine \approx (S)-nicotine-5-carboxaldehyde > homonicotine > 6-AN (Table 1). (S)-SIB 1508Y is more efficacious than (S)-nicotine ($P < 0.5$, $N = 5$), whereas (S)-1'-methylnicotinium and (S)-anabasine are as efficacious as (S)-nicotine ($P > 0.5$, $N = 5$).

Inhibitory properties of nicotine derivatives

The selected nicotine derivatives at 100 μ M all illustrated the inhibitory effects on ach response for *Asu*-ACR-16 (Fig. S3). The rank order of inhibition based on the Inhibition (%) of 100 μ M ach response is: 6-AN > homonicotine \approx (S)-5-bromonicotine \approx 5-methylnicotine \approx 6-methylnicotine \approx (S)-nicotine-5-carboxaldehyde \approx (S)-SIB 1508Y \approx N-methyl anabasine > (S)-1-methylnicotinium \approx

(S)-nicotine \approx (S)-anabasine \approx nornicotine $>$ (S)-1'-methylnicotinium $>$ (S)-cotinine (Table 1).

6-AN is the most potent inhibitor at 100 μ M. Its IC_{50} is $2.00 \pm 0.41 \mu$ M, n_H is 1.02 ± 0.05 , $inhibition_{max}$ is $94.88 \pm 1.49 \%$ ($N = 5$) (Fig. 7A & S4A). The inhibition (%) of 6-AN on ach response is both concentration dependent and voltage dependent (Fig. 7B). The ach dose-response curves in the continual presence of 1 μ M 6-AN, showed the reduction in I_{max} with little shift of EC_{50} (Fig. 7C & 7D & S4B). Thus, 6-AN is a potent non-competitive antagonist of *Asu*-ACR-16.

Enantiomers comparison

We compared the pharmacological profiles of (S)-anabasine and its racemic mixture on *Asu*-ACR-16 (Fig. S5). The EC_{50} of (S)-anabasine is significantly lower than the EC_{50} of its racemic mixture ($P < 0.05$, $N = 5$). The I_{max} of (S)-anabasine is slightly higher than that of its racemic mixture ($P > 0.05$, $N = 5$). These results are consistent with other published results that illustrated the higher intrinsic activities on nAChRs in (S)-enantiomer nicotine alkaloids rather than their (R)-enantiomer (Cosford *et al.*, 2000). Therefore, (S)-enantiomers of anabasine derivatives: (S)-5-bromonicotine, (S)-5-bromoanabsine and (S)-5-ethynyl-anabsine were designed, synthesized and further tested in electrophysiology.

Correlation between affinity and potency among nicotine derivatives

The binding affinities of the selected nicotine derivatives were calculated by docking ligands into the agonist-binding site in the agonist-bound form, the apo form and the antagonist-bound form ECD-*Asu*-ACR-16 models respectively. We used

EC_{50} (μM) to evaluate the potency, I_{max} (%) to evaluate the efficacy, *Inhibition* (%) to evaluate the inhibitory effect of nicotine derivatives. The only correlation (positive) between the binding affinity and the potency toward the receptor was found in the apo form model ($P < 0.05$) (Fig. S6).

Discussion

Structure-activity relationships of nicotine derivatives

Pyridine ring substituted derivatives To study the effects of functional groups added to the different positions of pyridine moiety on nicotine, methyl group as substituent at the 5- or 6- or N-pyridine moiety on nicotine or amino group at the 6-pyridine moiety on nicotine are selected for the electrophysiology characterization. 5-methylnicotine is the most potent and efficacious agonist, while 6-methylnicotine comes the second. 6-AN barely shows stimulatory activity, whereas behaves as a potent antagonist. The electron-donating group of methyl or amino at the 5- or 6-pyridine increases the electronegativity and alkalinity of the pyridine N1, and so stabilizes the water-mediated hydrogen bond with the carbonyl backbone of N131 and I143 amide backbone from the complementary subunit of the receptor. Instead, the lone pair electrons on the pyridine N1 of (S)-1-methylnicotinium are replaced by the methyl group. Thus, N1 cannot make hydrogen-bond with the carbonyl backbone of N131 and I143 amide backbone from the receptor, which inhibits the intrinsic activity of N-pyridine substituted derivatives.

5-substituted pyridine derivatives Given that the electron-donating group substituting at the 5-pyridine of nicotine shows the highest activity as agonist, electron-withdrawing groups of acetylene, bromine or aldehyde at the 5-pyridine of

nicotine are then selected. (S)-SIB 1508 is the most potent and efficacious agonist, while (S)-5-bromonicotine and (S)-nicotine-5-carboxaldehyde come the second and third. Extra cavity is shown in the binding site of *Asu*-ACR-16 models for the linear acetylene substituent or globular bromine atom at the 5-pyridine moiety of nicotine to extend into. Instead, the bent structure of aldehyde may be less favored in the binding pocket.

Pyrrolidine ring substituted derivatives To study the effects of functional groups added to the different positions of pyrrolidine moiety on nicotine, methyl or ethyl group as substituent at the N-pyrrolidine moiety on nicotine or ketone at the 5'-pyrrolidine moiety on nicotine are selected for the electrophysiology characterization. The additional methyl group linked to the pyrrolidine N2 on (S)-1'-methylnicotinium makes it become quaternary ammonium, which increases its cation- π interaction with the five aromatic residues from the receptor, but also increases the steric hindrance around the pyrrolidine N2 and causes its stereochemically unfavorable. The increased steric hindrance due to the ethyl group at pyrrolidine N2 of homonicotine may be the reason of its reduced intrinsic activity. The secondary amine in nornicotine reduces its alkalinity and chance to make cation- π interaction with the receptor.

Due to the conjugative effect of the lone pair electrons on pyrrolidine N2 of (S)-cotinine to the π bond of carbonyl group, the pyrrolidine N2 is hardly protonated and therefore inhibits the cation- π interaction with the aromatic cage from the receptor and cause the inactivity.

Piperidine ring derivatives The N-methyl pyrrolidine moiety was replaced by the N-methyl piperidine ring in nicotine structure to study the effect of increasing the membrane ring on the stimulatory activity of *Asu*-ACR-16. Yet, given that N-methyl anabasine is inactive, the piperidine moiety without methyl group was then studied and showed high intrinsic activity. The substituent piperidine of (S)-anabasine could sterically and electrostatically stabilize the aromatic cage on the receptor better than the N-methylated pyrrolidine ring of nicotine.

Given that the electron-withdrawing substituent at the 5-pyridine of nicotine, such as (S)-SIB 1508Y, also shows high activity, we designed and synthesized the novel lead compound, (S)-5-ethynyl-anabasine, which is a combination of the 5-ethynyl pyridine moiety from (S)-SIB 1508Y and the piperidine moiety from (S)-anabasine structure.

Open-channel block properties of nicotine derivatives

The selected nicotine derivatives in high doses showed the tail current responses after the 10 s drug application (Fig. S2 & Fig. 5), which implied the ion channel switched from the open-blocked state to the open state. In addition, a voltage-sensitive inhibition (%) relationship was observed in a derivative with protonated N⁺. This property is consistent with the feature of open-channel blocker (Rossokhin *et al.*, 2014).

Both stimulatory effects and inhibitory effects were observed on several nicotine derivatives. 6-AN, a most potent *Asu*-ACR-16 inhibitor in our study, behaves as a non-competitive antagonist which bind to the site other than the orthosteric

ligand-binding site. Our electrophysiology results show 6-AN and other nicotine alkaloids are open-channel blockers of *Asu-ACR-16*. Since all these nicotine alkaloids have protonated tertiary amine or tetramethyl ammonium moiety, the cationic nitrogen of them not only makes cation- π interaction with the aromatic cage in the agonist-binding site of the receptor, but also acts as a cation that may interact with the channel pore and interfere with the channel gating. The ligands initially bind to the agonist-binding site and turn the channel from the rest state to the open state where the ions flow through the channel pore. As the channel is open, the extra ligands bind to the inside pore of channel and inhibit the current response, while preventing the dissociation of the initial ligand from the orthosteric site (Jackson, 2010).

Docking study as a probe for searching potent *Asu-ACR-16* agonist

The potency (EC_{50}) of the selected nicotinic alkaloids is correlated most with the binding affinity in the apo model of *Asu-ACR-16*. This might be due to the movement of vicinal cysteines or the open-up orientation of W79 in the agonist-bound and antagonist-bound form *Asu-ACR-16*, which reduces the cation- π interaction between W79 and nicotine N2 (Blum *et al.*, 2010; Van Arnam *et al.*, 2014). The statistical correlation between the predicted ligand binding affinities in the apo model of *Asu-ACR-16* and their corresponding potencies (EC_{50}), suggests that the apo model may be reliable as a probe to search potent agonists by docking.

Conclusion

We used the structural models of ECD-*Asu*-ACR-16 agonist-binding site and electrophysiology characterization of ion channel to study the structure-activity relationships of several nicotine alkaloids on *Asu*-ACR-16 receptor. We designed and synthesized (S)-5-etynyl-anabasine as our new lead compound, which was predicted to be more potent and efficacious than (S)-nicotine as a novel *Asu*-ACR-16 agonist. Our structure-based drug discovery of ACR-16 agonists also proposed several other nicotine alkaloids as promising leads for further physicochemical and pharmacokinetic optimizations.

Acknowledgements

We would like to express our gratitude to Tsung-Han Chou of Iowa State University for helpful suggestions. This research was supported by the Iowa State University startup to BV, NIH R21AI121831-01 to APR, NIH R01AI047194 to RJM.

Authorship Contributions

Participated in research design: Zheng, Du, Robertson, VanVeller, and Martin.

Conducted experiments: Zheng, and Du.

Contributed new reagents or analytic tools: VanVeller, Yu, Martin, and Robertson.

Performed data analysis: Zheng, and Du.

Wrote or contributed to the writing of the manuscript: Zheng, Du, Robertson, VanVeller, and Martin.

Statement of conflict of interest

The authors declare no competing interest in this work.

References

- Arias HR (2000) Localization of agonist and competitive antagonist binding sites on nicotinic acetylcholine receptors. *Neurochem Int* **36**(7): 595-645.
- Bleicher KH, Bohm H-J, Muller K and Alanine AI (2003) Hit and lead generation: beyond high-throughput screening. *Nat Rev Drug Discov* **2**(5): 369-378.
- Blum AP, Lester HA and Dougherty DA (2010) Nicotinic pharmacophore: the pyridine N of nicotine and carbonyl of acetylcholine hydrogen bond across a subunit interface to a backbone NH. *Proceedings of the National Academy of Sciences of the United States of America* **107**(30): 13206-13211.
- Celie PH, van Rossum-Fikkert SE, van Dijk WJ, Brejc K, Smit AB and Sixma TK (2004) Nicotine and carbamylcholine binding to nicotinic acetylcholine receptors as studied in AChBP crystal structures. *Neuron* **41**(6): 907-914.
- Chavez-Noriega LE, Crona JH, Washburn MS, Urrutia A, Elliott KJ and Johnson EC (1997) Pharmacological characterization of recombinant human neuronal nicotinic acetylcholine receptors h alpha 2 beta 2, h alpha 2 beta 4, h alpha 3 beta 2, h alpha 3 beta 4, h alpha 4 beta 2, h alpha 4 beta 4 and h alpha 7 expressed in *Xenopus* oocytes. *The Journal of pharmacology and experimental therapeutics* **280**(1): 346-356.
- Cosford NDP, Bleicher L, Vernier J-M, Chavez-Noriega L, Rao TS, Siegel RS, Suto C, Washburn M, Lloyd GK and McDonald IA (2000) Recombinant human receptors and functional assays in the discovery of altinicline (SIB-1508Y), a novel acetylcholine-gated ion channel (nAChR) agonist. *Pharmaceutica Acta Helveticae* **74**(2-3): 125-130.
- de Silva NR, Brooker S, Hotez PJ, Montresor A, Engels D and Savioli L (2003) Soil-transmitted helminth infections: updating the global picture. *Trends Parasitol* **19**(12): 547-551.
- Dougherty DA (2013) The cation-pi interaction. *Accounts of chemical research* **46**(4): 885-893.
- Garcia CM, Sprenger LK, Ortiz EB and Molento MB (2016) First report of multiple anthelmintic resistance in nematodes of sheep in Colombia. *Anais da Academia Brasileira de Ciencias* **88**(1): 397-402.
- Gros PC, Doudouh A and Woltermann C (2006) TMSCH₂Li-induced regioselective lithiation of (S)-nicotine. *Organic & Biomolecular Chemistry* **4**(23): 4331-4335.

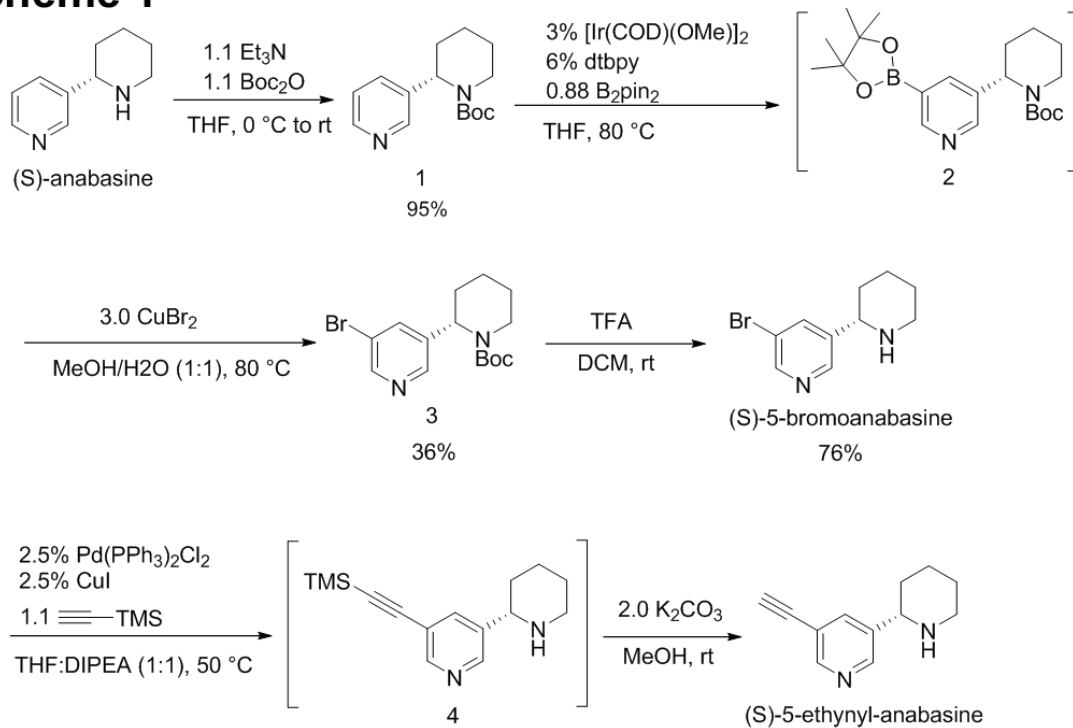
- Holden-Dye L, Joyner M, O'Connor V and Walker RJ (2013) Nicotinic acetylcholine receptors: A comparison of the nAChRs of *Caenorhabditis elegans* and parasitic nematodes. *Parasitology International* **62**(6): 606-615.
- Huang S, Li S-X, Bren N, Cheng K, Gomoto R, Chen L and Sine SM (2013) Complex between α -bungarotoxin and an $\alpha 7$ nicotinic receptor ligand-binding domain chimera. *The Biochemical journal* **454**(2): 303-310.
- Jackson MB (2010) Open channel block and beyond. *The Journal of Physiology* **588**(Pt 4): 553-554.
- Li S-X, Huang S, Bren N, Noridomi K, Dellisanti CD, Sine SM and Chen L (2011) Ligand-binding domain of an $[\alpha]7$ -nicotinic receptor chimera and its complex with agonist. *Nature neuroscience* **14**(10): 1253-1259.
- Liskey CW, Liao X and Hartwig JF (2010) Cyanation of Arenes via Iridium-Catalyzed Borylation. *Journal of the American Chemical Society* **132**(33): 11389-11391.
- Mongan NP, Jones AK, Smith GR, Sansom MS and Sattelle DB (2002) Novel $\alpha 7$ -like nicotinic acetylcholine receptor subunits in the nematode *Caenorhabditis elegans*. *Protein science : a publication of the Protein Society* **11**(5): 1162-1171.
- Rossokhin AV, Sharonova IN, Bukanova JV, Kolbaev SN and Skrebitsky VG (2014) Block of GABAA receptor ion channel by penicillin: Electrophysiological and modeling insights toward the mechanism. *Molecular and Cellular Neuroscience* **63**: 72-82.
- Rucktooa P, Haseler CA, van Elk R, Smit AB, Gallagher T and Sixma TK (2012) Structural characterization of binding mode of smoking cessation drugs to nicotinic acetylcholine receptors through study of ligand complexes with acetylcholine-binding protein. *The Journal of biological chemistry* **287**(28): 23283-23293.
- Rucktooa P, Smit AB and Sixma TK (2009) Insight in nAChR subtype selectivity from AChBP crystal structures. *Biochemical pharmacology* **78**(7): 777-787.
- Sixma TK and Smit AB (2003) Acetylcholine binding protein (AChBP): a secreted glial protein that provides a high-resolution model for the extracellular domain of pentameric ligand-gated ion channels. *Annual review of biophysics and biomolecular structure* **32**: 311-334.
- Taly A, Corringer P-J, Guedin D, Lestage P and Changeux J-P (2009) Nicotinic receptors: allosteric transitions and therapeutic targets in the nervous system. *Nat Rev Drug Discov* **8**(9): 733-750.
- Taylor HL, Spagnoli ST, Calcutt MJ and Kim DY (2016) Aberrant *Ascaris suum* Nematode Infection in Cattle, Missouri, USA. *Emerging infectious diseases* **22**(2): 339-340.

- Trott O and Olson AJ (2010) AutoDock Vina: improving the speed and accuracy of docking with a new scoring function, efficient optimization, and multithreading. *J Comput Chem* **31**(2): 455-461.
- Van Arnam EB and Dougherty DA (2014) Functional probes of drug-receptor interactions implicated by structural studies: Cys-loop receptors provide a fertile testing ground. *J Med Chem* **57**(15): 6289-6300.
- Wang J, Czech B, Crunk A, Wallace A, Mitreva M, Hannon GJ and Davis RE (2011) Deep small RNA sequencing from the nematode *Ascaris* reveals conservation, functional diversification, and novel developmental profiles. *Genome research* **21**(9): 1462-1477.
- Zheng F, Robertson AP, Abongwa M, Yu EW and Martin RJ (2016) The *Ascaris* suum nicotinic receptor, ACR-16, as a drug target: Four novel negative allosteric modulators from virtual screening. *International Journal for Parasitology: Drugs and Drug Resistance* **6**(1): 60-73.

Figures

Figure 1

Scheme 1



Scheme 2

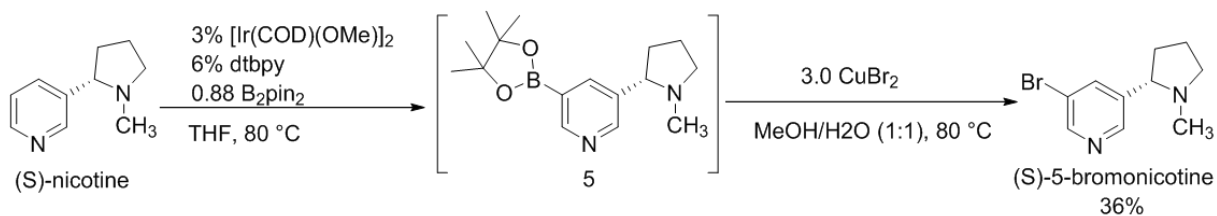


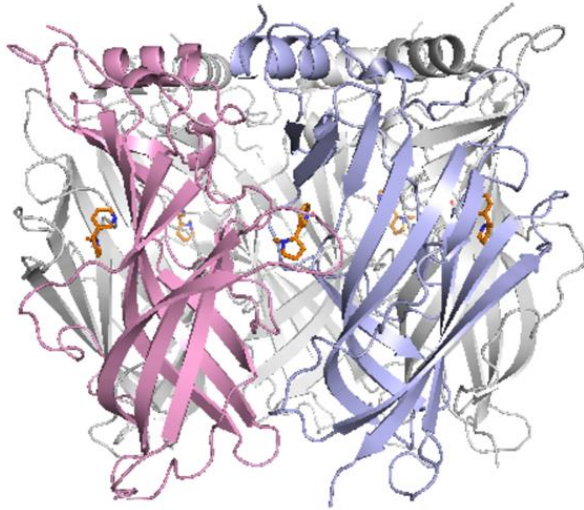
Figure 1 Reaction schemes.

Scheme 1 Reaction schemes of synthesizing (S)-5-bromoanabasine and (S)-5-ethynyl-anabasine from (S)-anabasine

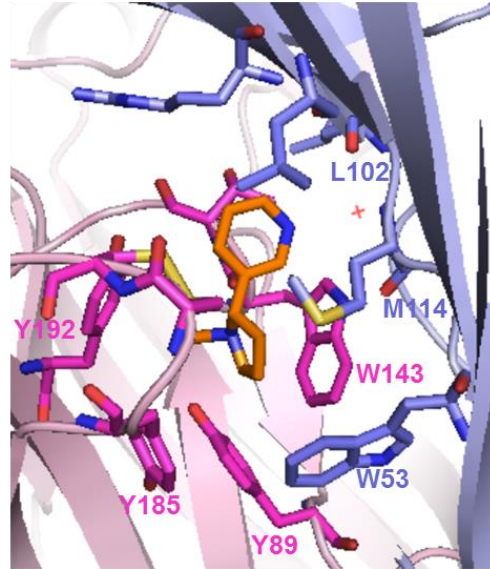
Scheme 2 Reaction schemes of synthesizing (S)-5-bromonicotine from (S)-nicotine

Figure 2

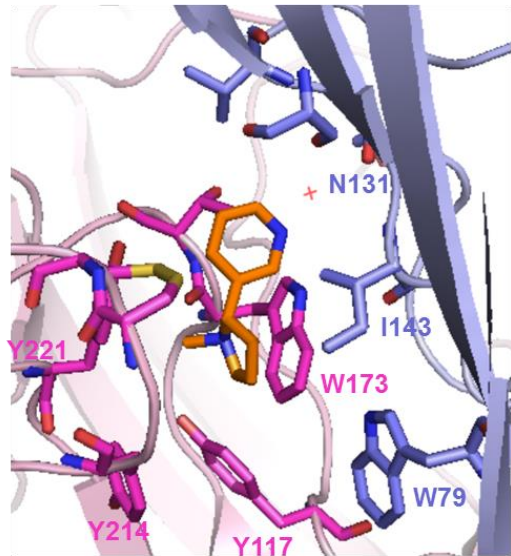
A



B



C



D

agonist-bound *Asu*-ACR-16
apo form *Asu*-ACR-16
antagonist-bound form *Asu*-ACR-16

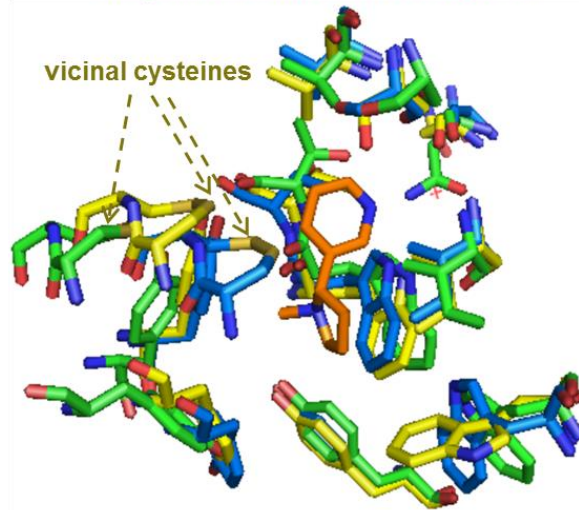


Figure 2. Crystal structure of *Lst*-AChBP bound with nicotine (PDB code: 1UW6) and the agonist-bound model of *Asu*-ACR-16

(A) Ribbon diagram of the AChBP co-crystalized with nicotine, as viewed with membrane at the bottom. The principal subunit is highlighted by light pink and the complement subunit is highlighted by light purple, for clarity. Nicotine (orange) is bound in the five ligand-binding sites in the extracellular domain of AChBP.

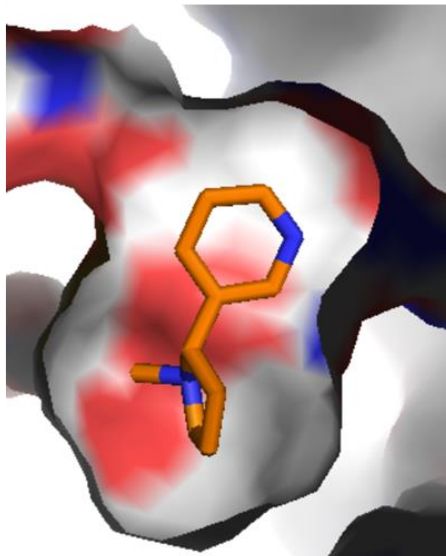
(B) Close view of the AChBP ligand-binding site. The principal subunit in light pink, the complementary subunit in light purple. Residues interacting with nicotine (orange) are represented as sticks ((+), pink; (-), purple), and water molecule is shown as red dot, view with membrane at the bottom.

(C) Close view of the agonist-bound model of *Asu*-ACR-16 ligand-binding site. The principal subunit in light pink, the complementary subunit in light purple. The interacting residues are represented as sticks ((+), pink; (-), purple), and water molecule is shown as red dot, view with membrane at the bottom.

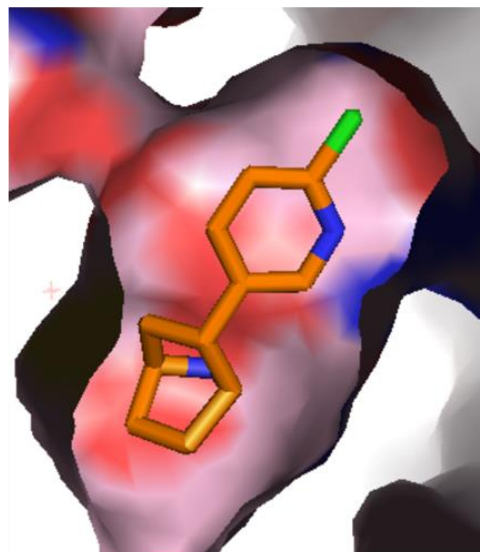
(D) Superposition of residues in agonist-binding site, among agonist-bound form (blue), apo form (yellow), antagonist-bound form (green) of *Asu*-ACR-16 models are shown.

Figure 3

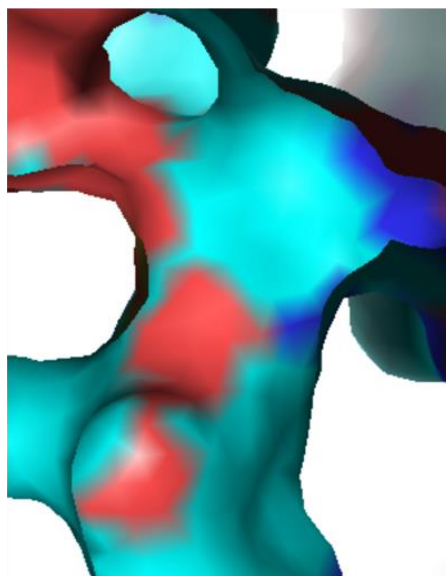
A

Lst-AChBP

B

human $\alpha 7$ AChR chimera

C

agonist-bound *Asu*-ACR-16

D

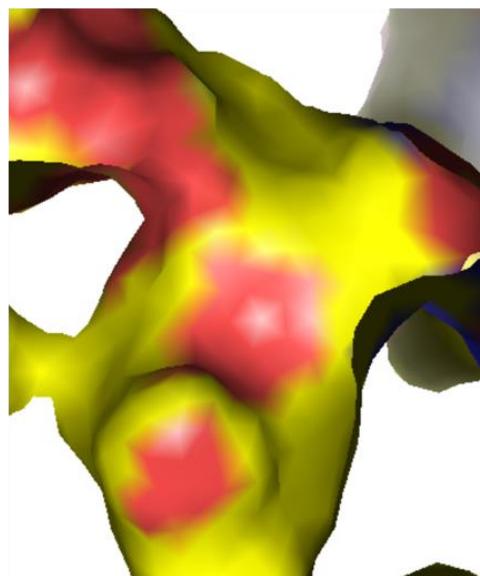
apo form of *Asu*-ACR-16

Figure 3. Ligand-binding sites of *Asu*-ACR-16 and its homologous proteins

(A) Surface representation in the open-up ligand-binding site of *Lst*-AChBP in complex with nicotine (PDB code: 1UW6). Oxygen-rich area (red), nitrogen-rich area (blue) and carbon-rich area (gray) are displayed. Empty space was observed around the 5-pyridine ring of nicotine, which suggests the ligand-binding site is in favor of the linear functional group linking toward the 5-pyridine ring of nicotine. Few space was found around the pyrrolidine ring of nicotine.

(B) Surface representation in the open-up ligand-binding site of human $\alpha 7$ AChR chimera in complex with epibatidine (PDB code: 3SQ6), viewed by the same angle as (A). Oxygen-rich area (red), nitrogen-rich area (blue), carbon-rich area (pink) and chloride (green) are displayed. The azabicyclic ring N1 of epibatidine was superimposed with the pyrrolidine ring N2 of nicotine, while the pyridine ring N2 of epibatidine was superimposed with the pyridine ring N1 of nicotine.

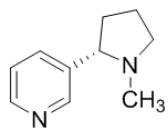
(C) Surface representation in the open-up ligand-binding site of agonist-bound *Asu*-ACR-16 model, viewed by the same angle as (A). Oxygen-rich area (red), nitrogen-rich area (blue) and carbon-rich area (cyan) are displayed. Assuming the nicotine has the same binding pose as in (A) within agonist-bound *Asu*-ACR-16, empty space is observed around the 5-pyridine ring and pyrrolidine ring of nicotine, which would make the nicotinic derivatives with modification in these positions favorable to the binding site.

(D) Surface representation in the open-up ligand-binding site of apo form *Asu*-ACR-16 model, viewed by the same angle as (A). Oxygen-rich area (red), nitrogen-rich area (blue) and carbon-rich area (yellow) are displayed. Assuming the nicotine has

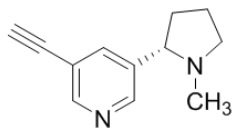
the same binding pose as in (A) within apo form *Asu-ACR-16*, empty space is observed around the 5-pyridine ring and pyrrolidine ring of nicotine, which would make the nicotinic derivatives with modification in these positions favorable to the binding site.

Figure 4

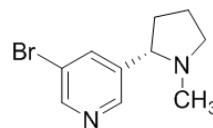
5-electron-withdrawing group substituted pyridine derivatives



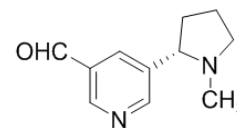
(S)-nicotine



(S)-SIB 1508Y

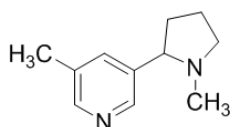


(S)-5-bromonicotine

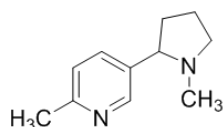


(S)-nicotine-5-carboxaldehyde

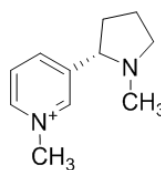
other pyridine ring substituted derivatives



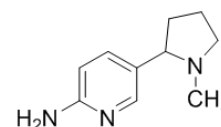
5-methylnicotine



6-methylnicotine

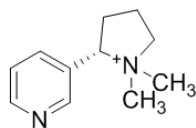


(S)-1-methylnicotinium

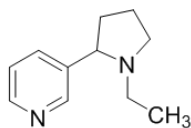


6-AN

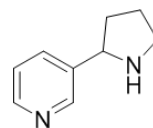
pyrrolidine ring substituted derivatives



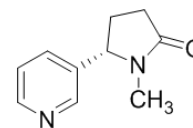
(S)-1'-methylnicotinium



homonicotine

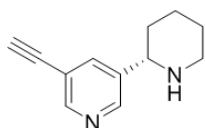


nornicotine

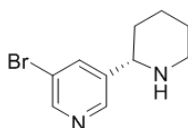


(S)-cotinine

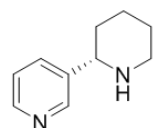
piperidine ring derivatives



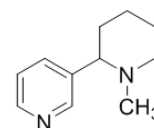
(S)-5-ethynyl-anabasine



(S)-5-bromoanabasine



(S)-anabasine



N-methyl anabasine

Figure 4. Chemical structures of (S)-nicotine and its fifteen derivatives. 5-substituted pyridine ring derivatives: (S)-SIB 1508Y, (S)-5-bromonicotine, (S)-nicotine-5-carboxaldehyde and 5-methylnicotine; other pyridine ring substituted derivatives: (S)-1-methylnicotinium, 6-methylnicotine and 5-(1-methyl-pyrrolidin-2-yl)-pyridin-2-ylamine (6-AN); pyrrolidine ring substituted derivatives: (S)-1'-methylnicotinium, homonicotine, nornicotine and (S)-cotinine; piperidine ring derivatives: (S)-5-ethynylanabasine, (S)-5-bromoanabasine, (S)-anabasine and N-methyl anabasine are shown.

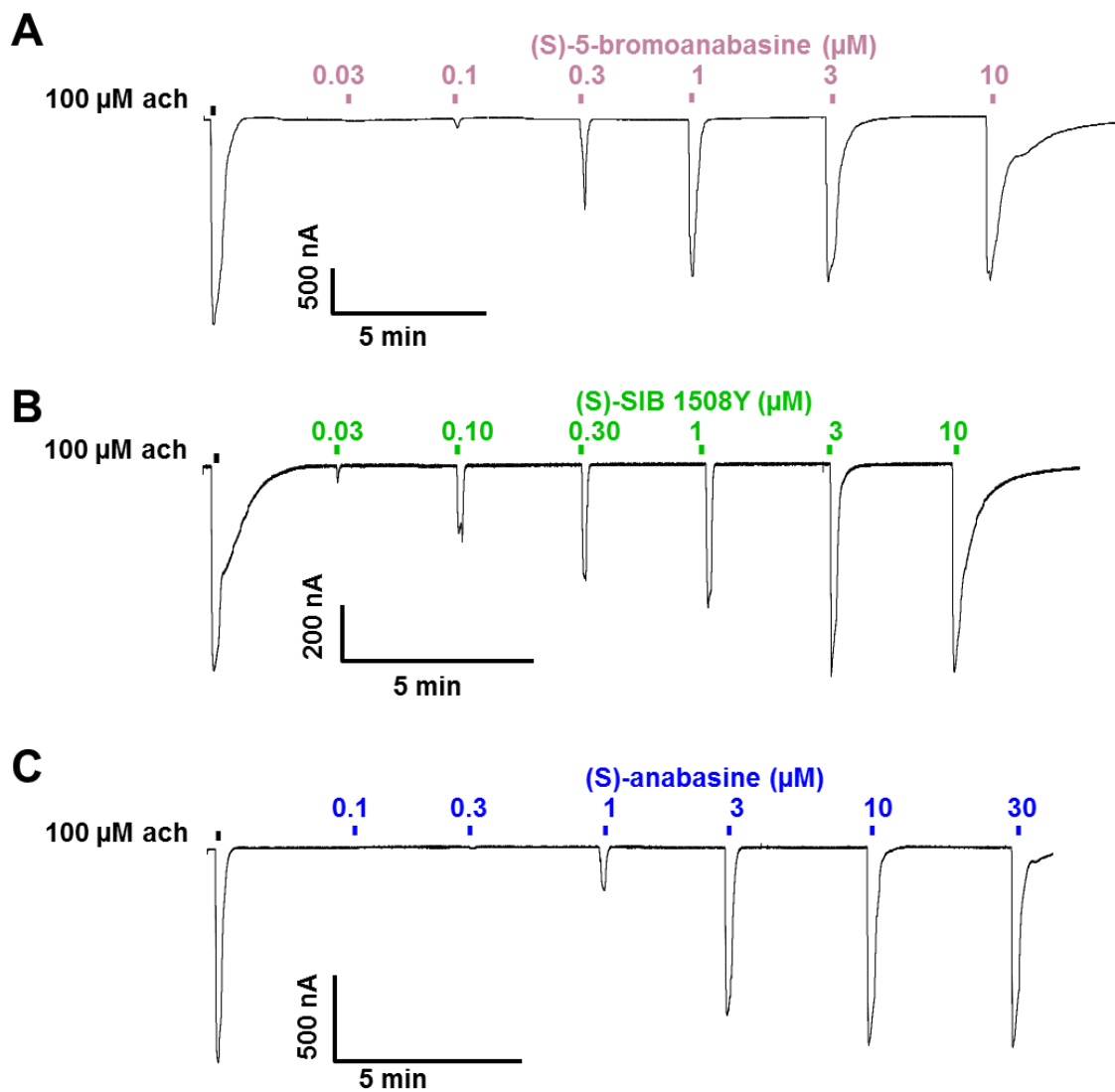
Figure 5

Figure 5. Sample traces for nicotine derivatives dose-response relationships of *Asu-ACR-16*. (S)-5-bromoanabasine (A), (S)-SIB 1508Y (B), (S)-anabasine (C) are depicted.

Figure 6

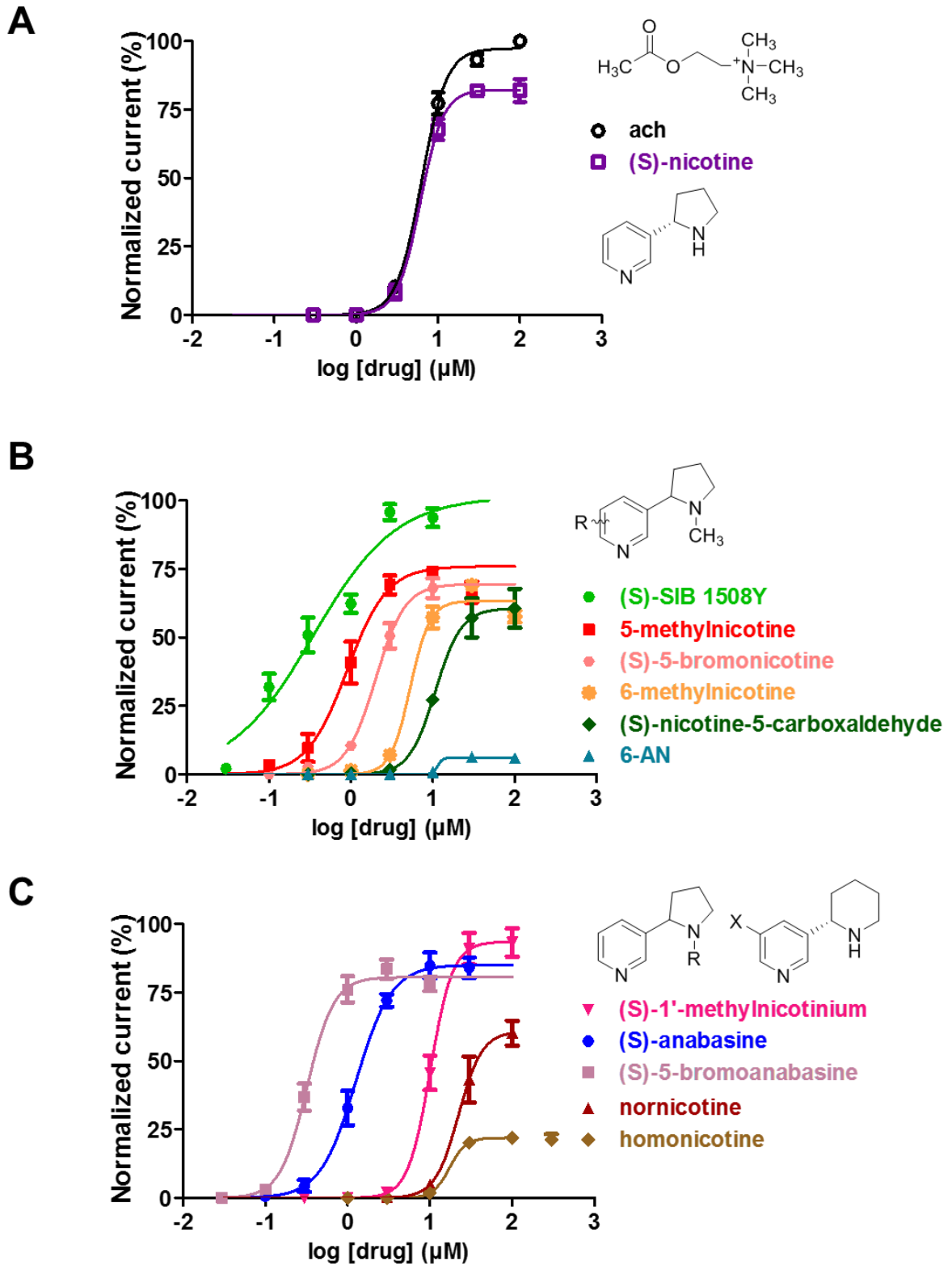


Figure 6. Dose-response curves of nicotine derivatives for *Asu*-ACR-16.

(A) Ach and (S)-nicotine as two controls.

(B) Pyridine ring substituted derivatives. Responses of 30 μ M 5-methylnicotine and 100 μ M 6-methylnicotine were shown but not fitted into their stimulatory dose-response plots correspondingly due to their inhibitory effects.

(C) Pyrrolidine ring substituted derivatives. Response of 300 μ M homonicotine was shown but not fitted into its stimulatory dose-response plot due to its inhibitory effect.

Figure 7

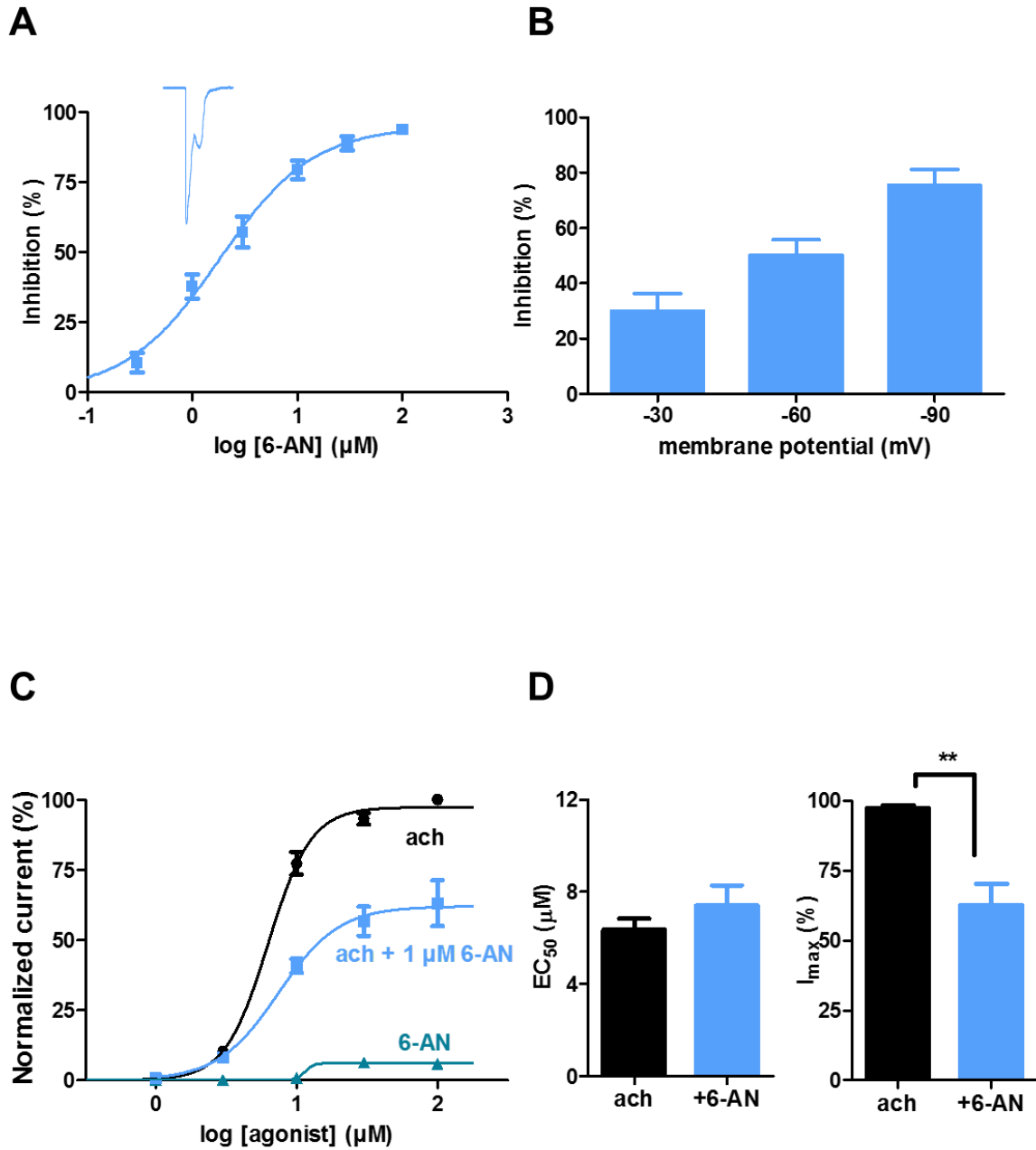


Figure 7 Inhibitory effect of 6-AN on ach response for *Asu*-ACR-16.

(A) 6-AN inhibitory dose-response relationship for *Asu*-ACR-16. One representative trace used to measure the inhibition (%) of 1 μM 6-AN on 100 μM ach response for *Asu*-ACR-16 was shown above the plot.

(B) Voltage dependent-inhibition (%) of 3 μM 6-AN on 100 μM ach response for *Asu*-ACR-16.

(C) Ach dose-response relationships for *Asu*-ACR-16 in the absence of (black) and in the continual presence of 6-AN (blue), compared with 6-AN dose-response relationship (teal).

(D) Bar chart comparing the EC_{50} (μM) and I_{max} (%) of ach dose-response relationships in the absence of (black) and in the presence of 6-AN (blue) by unpaired student-*t* test. ** $P < 0.01$.

Tables

Table 1. Pharmacological profiles of ach and sixteen nicotine derivatives. Results (mean \pm S.E.M.) were expressed as the EC_{50} (μ M), Hill slope (n_H) and maximum response (I_{max} , %), number of repeats of each agonist experiment ($N_{agonist}$), inhibition (%) and number of repeats of each inhibitor experiment ($N_{inhibitor}$).

	EC_{50} (μ M)	n_H	I_{max} (%)	$N_{agonist}$	Inhibition (%)	$N_{inhibitor}$
(S)-5-bromoanabasine	0.32 \pm 0.03	4.19 \pm 1.58	80.69 \pm 2.87	5		
(S)-SIB 1508Y	0.37 \pm 0.10	0.94 \pm 0.04	100.1 \pm 4.36	5	50.01 \pm 3.02	5
5-methylnicotine	0.99 \pm 0.17	2.09 \pm 0.14	76.05 \pm 1.22	5	77.71 \pm 5.70	5
(S)-anabasine	1.26 \pm 0.19	2.26 \pm 0.20	84.82 \pm 4.20	5	28.44 \pm 3.74	5
(S)-5-bromonicotine	2.04 \pm 0.12	2.46 \pm 0.21	69.66 \pm 3.28	5	83.03 \pm 4.22	5
6-methylnicotine	6.13 \pm 0.53	3.25 \pm 0.24	69.74 \pm 1.56	5	67.17 \pm 2.24	5
(S)-nicotine	6.21 \pm 0.56	3.39 \pm 0.36	82.39 \pm 2.52	5	31.08 \pm 3.45	5
ach	6.36 \pm 0.49	2.93 \pm 0.13	97.42 \pm 0.93	5		
(S)-1'-methylnicotinium	10.25 \pm 0.62	3.52 \pm 0.26	93.38 \pm 5.25	5	22.26 \pm 0.99	5
(S)-nicotine-5-carboxaldehyde	11.51 \pm 0.63	8.61 \pm 4.04	62.20 \pm 6.80	5	60.13 \pm 3.89	5
6-aminonicotine	12.18 \pm 0.29	10.10 \pm 0.15	6.29 \pm 0.62	5	98.20 \pm 0.26	5
homonicotine	16.62 \pm 1.44	6.78 \pm 2.50	22.01 \pm 1.39	5	84.55 \pm 2.02	5
nornicotine	25.73 \pm 4.71	3.25 \pm 0.49	62.64 \pm 3.42	5	26.17 \pm 0.96	5
N-methyl anabasine					41.43 \pm 2.96	5
(S)-1-methylnicotinium					31.44 \pm 2.93	5
(S)-cotinine					15.48 \pm 1.26	5

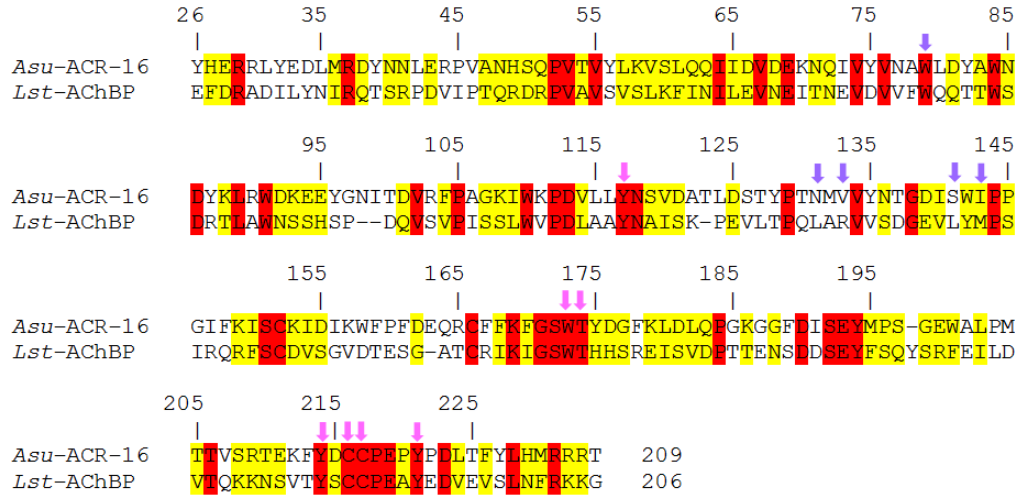
Table 2. Structural information for the ECD-*Asu*-ACR-16 and two of its homologous proteins (human $\alpha 7$ nAChR chimera and *Lst*-AChBP).

Protein	Organism	PDB code	Resolution (Å)	Ligand	Pharmacology
ECD-ACR-16	<i>Ascaris suum</i>				
$\alpha 7$ nAChR chimera	<i>Homo sapiens</i> &	3SQ6	2.8	epibatidine	agonist
	<i>Lymnaea stagnalis</i>	3SQ9	3.1	none	none
		4HQP	3.51	α -bungarotoxin	antagonist
AChBP	<i>Lymnaea stagnalis</i>	1UW6	2.2	nicotine	agonist

Supplemental Data

Figure S1

A



B

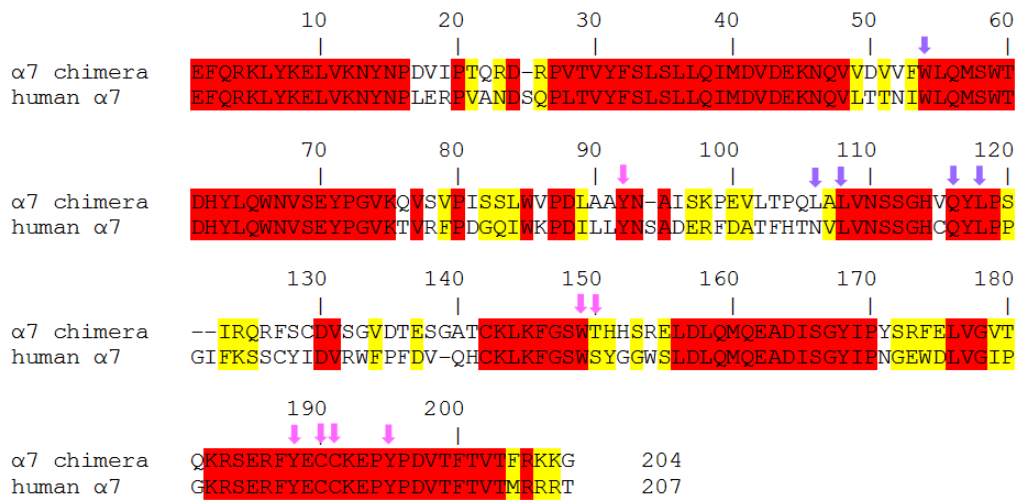


Figure S1. Sequence alignment between *Asu*-ACR-16 and its homologous proteins

(A) Sequence and numbering of the ECD-*Asu*-ACR-16 (SwissProt ID: F1KYJ9) and its alignment with the *Lst*-AChBP (SwissProt ID: P58154). Completely conserved residues (red) and partially conserved residues (yellow) were indicated. Residues in the ligand-binding site of the principal subunit (pink arrow) were highly conserved, while the residues in the ligand-binding site of the complementary subunit of (purple arrow) were variable between *Asu*-ACR-16 and *Lst*-AChBP subunit.

(B) Sequence and numbering of the ECD of human $\alpha 7$ nAChR chimera (PDB code: 3SQ6) and its alignment with the ECD of human $\alpha 7$ nAChR (SwissProt ID: P36544). Completely conserved residues (red) and partially conserved residues (yellow) were indicated. Residues in the ligand-binding site of the principal subunit (pink) and residues in the ligand-binding site of the complementary subunit (purple) were highlighted by arrows. Except T150 on (+) and L106 on (-) of human $\alpha 7$ nAChR chimera are different with S172 on (+) and N129 on (-) of human $\alpha 7$ nAChR, the rest of interacting residues in human $\alpha 7$ nAChR chimera and human $\alpha 7$ nAChR were identical.

Figure S2

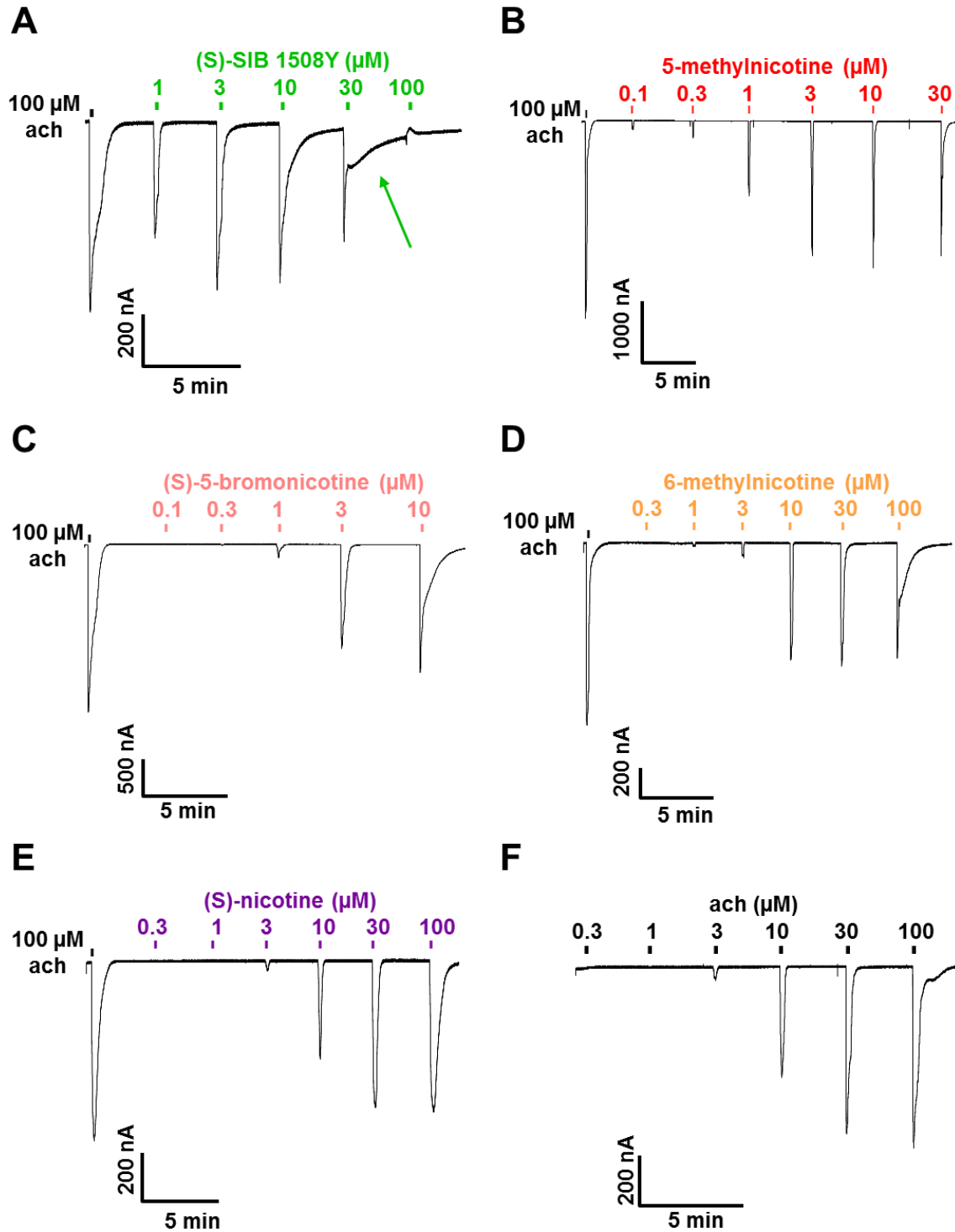


Figure S2

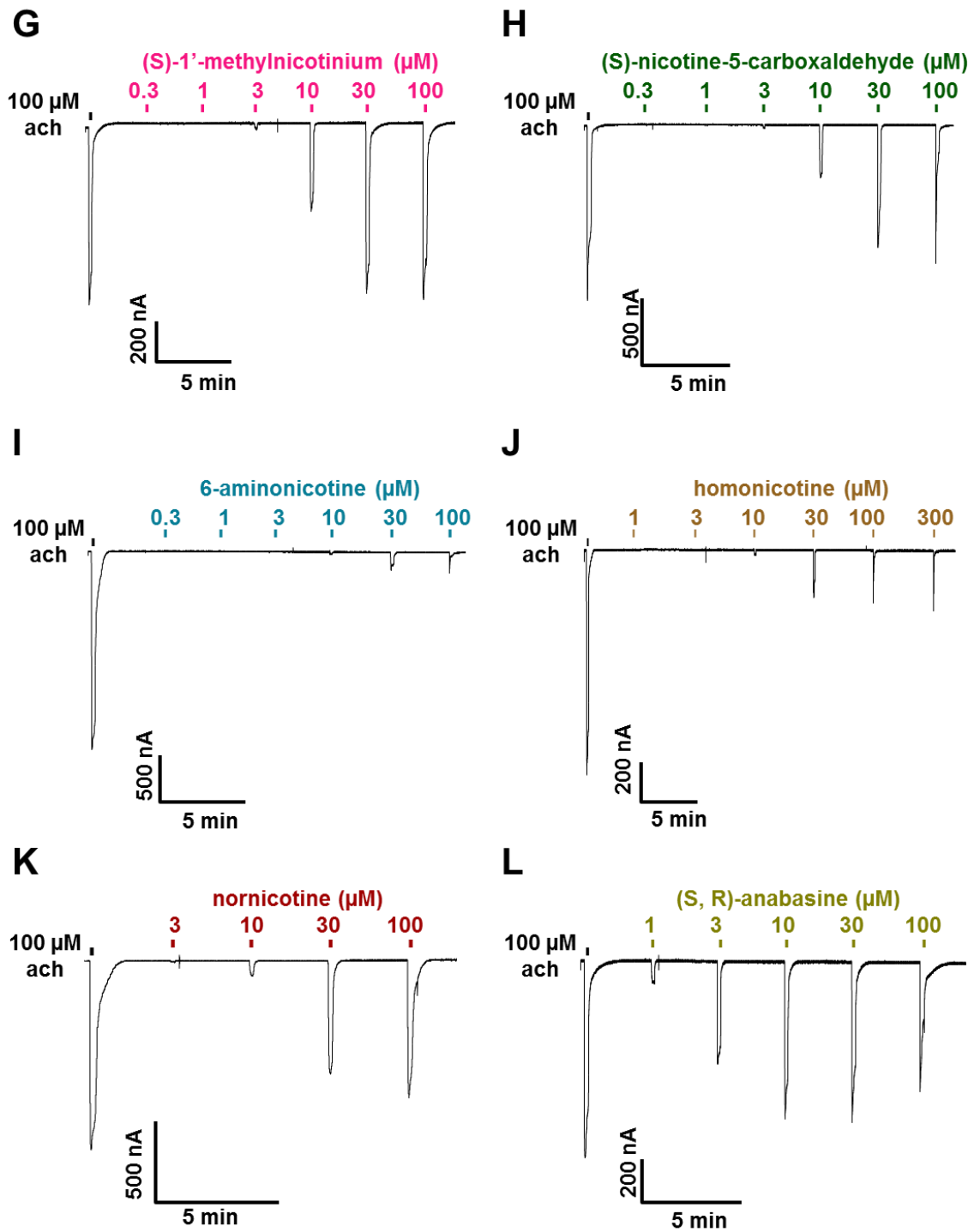
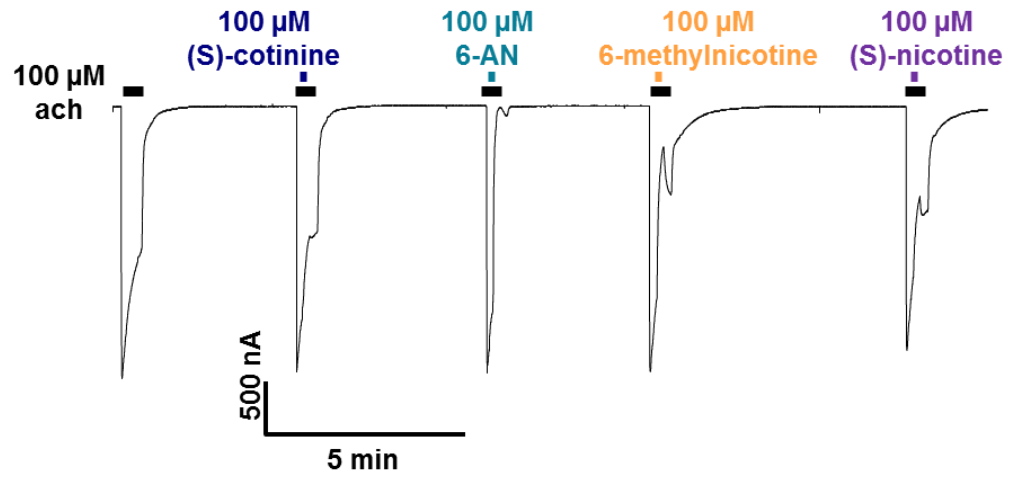


Figure S2. Sample traces for nicotine derivatives concentration-response relationships of *Asu*-ACR-16.

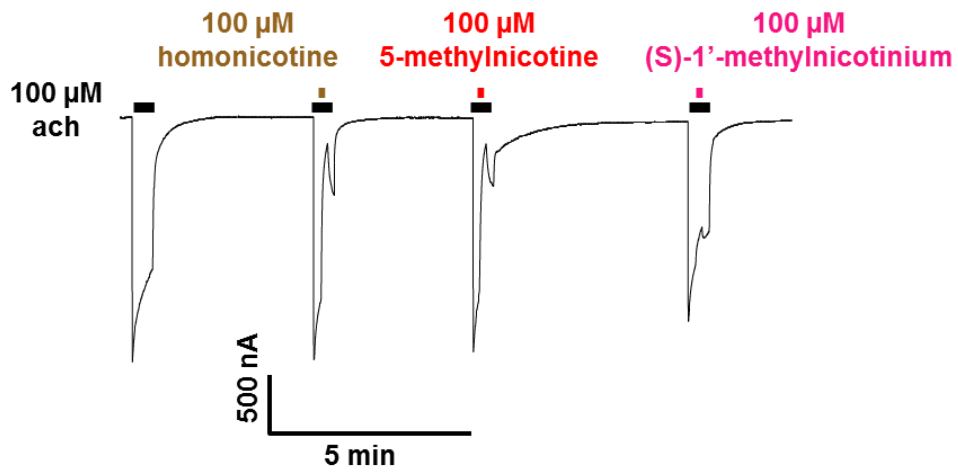
(S)-SIB 1508Y (A), 5-methylnicotine (B), (S)-5-bromonicotine (C), 6-methylnicotine (D), (S)-nicotine (E), ach (F), (S)-1'-methylnicotinium (G), (S)-nicotine-5-carboxaldehyde (H), 6-AN (I), homonicotine (J), nornicotine (K) and (S, R)-anabasine (L) are depicted. The characteristic tail current in (S)-SIB 1508 is labeled by green arrow in (A).

Figure S3

A



B



C

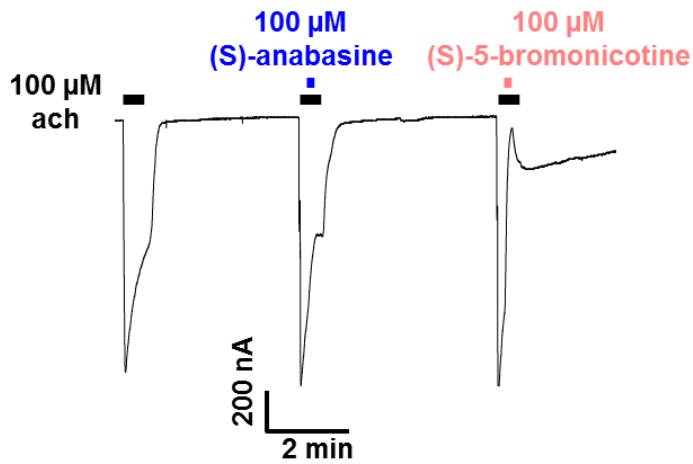


Figure S3

D

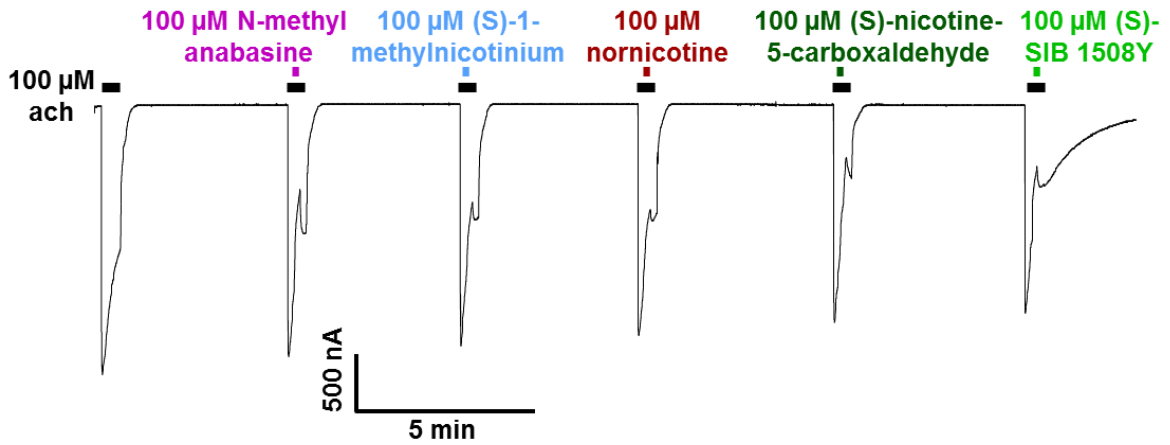
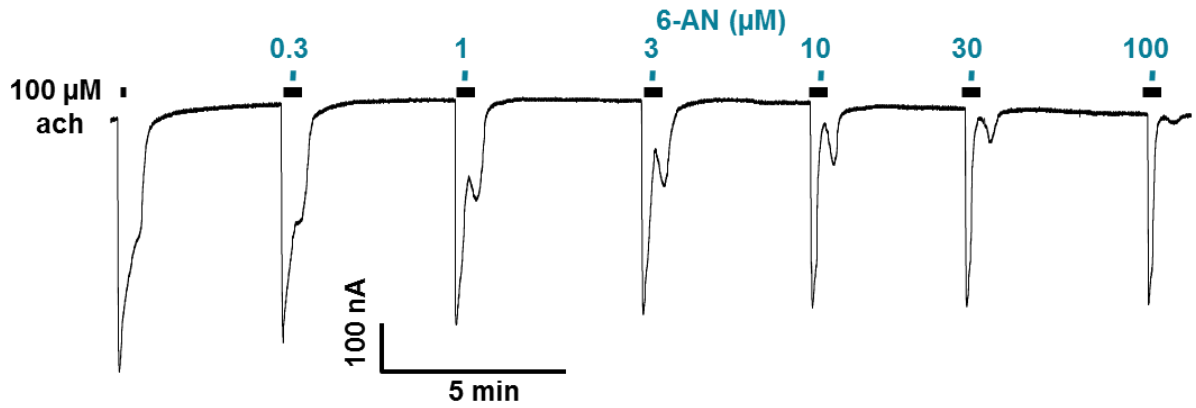


Figure S3 Sample traces showing the inhibitory effects of 100 μM nicotine derivatives on 100 μM ach response.

(S)-cotinine, 6-AN, 6-methylnicotine and (S)-nicotine (A); homonicotine, 5-methylnicotine and (S)-1'-methylnicotinium (B); (S)-anabasine and (S)-5-bromonicotine (C); N-methylanabasine, (S)-1-methylnicotinium, nornicotine, (S)-nicotine-5-carboxaldehyde and (S)-SIB 1508Y (D) and (S)-5-bromoanabasine and (S)-5-ethynyl-anabsine (E) inhibitory effects on ach response for *Asu*-ACR-16 are depicted.

Figure S4

A



B

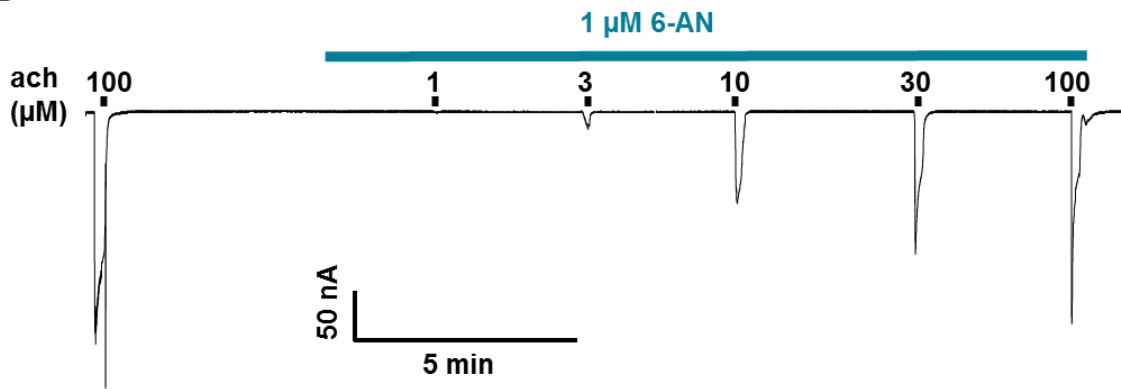


Figure S4 Sample traces evaluating the potency and mechanism of 6-AN as an antagonist.

(A) Sample trace showing the inhibitory dose-response relationship for *Asu-ACR-16*.

(B) Sample trace showing the effects of 1 μM 6-AN on ach dose-response relationship for *Asu-ACR-16*.

Figure S5

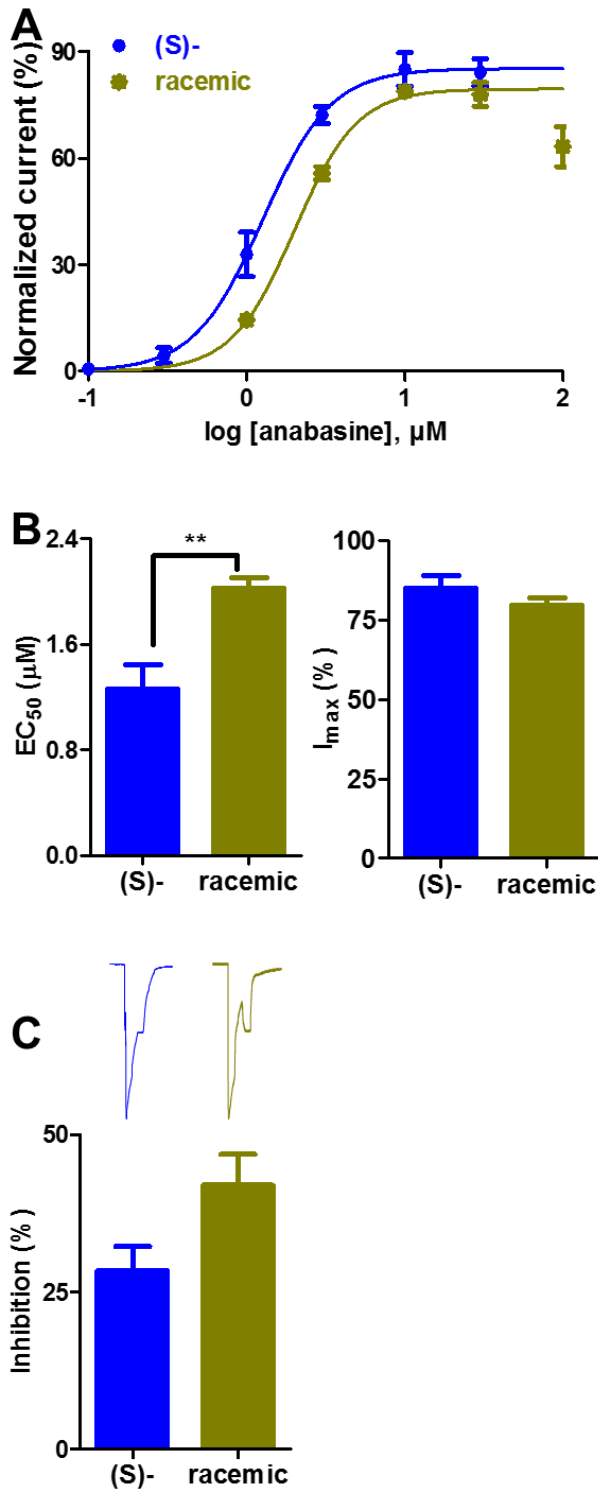


Figure S5. Pharmacological profiles of (S)-anabasine and its racemic mixture.

(A) Dose-response curves of (S)-anabasine (blue) and (S, R)-anabasine (dark yellow) for *Asu*-ACR-16. Response of 100 μ M (S, R)-anabasine was shown but not fitted into its stimulatory dose-response plot due to its inhibitory effect.

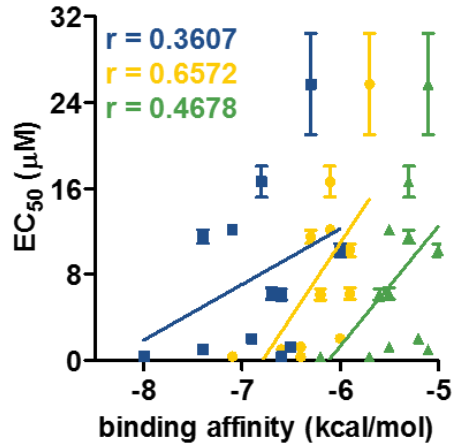
(B) Bar chart representing the EC_{50} and I_{max} (mean \pm S.E.M, μ M) of (S)-anabasine and its racemic mixture in (A). Significance was determined by un-paired student *t*-test. (S)-anabasine ($1.26 \pm 0.19 \mu$ M, $N = 5$) < (S, R)-anabasine ($2.03 \pm 0.08 \mu$ M, $N = 5$), ** $P < 0.01$. (S)-anabasine ($84.82 \pm 4.20 \%$, $N = 5$) \approx (S, R)-anabasine ($79.56 \pm 2.24 \%$, $N = 5$), $P > 0.05$.

(C) Bar chart representing the *Inhibition* (mean \pm S.E.M, %) of (S)-anabasine and its racemic mixture. Representative traces used to measure the inhibition (%) of 100 μ M (S)-anabasine or its racemic mixture on 100 μ M ach response for *Asu*-ACR-16 were shown above the chart. (S)-anabasine ($28.44 \pm 3.74 \%$, $N = 5$) \approx (S, R)-anabasine ($41.98 \pm 4.88 \%$, $N = 5$), $P > 0.05$.

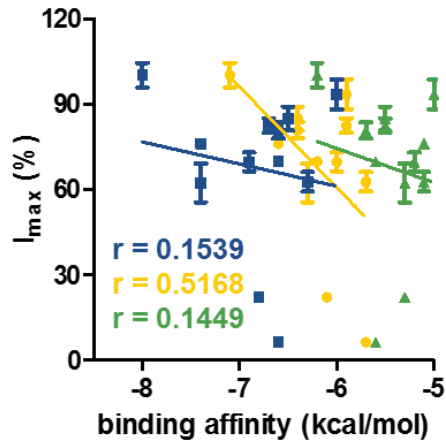
Figure S6

A

- agonist-bound *Asu*-ACR-16
- apo form *Asu*-ACR-16
- ▲ antagonist-bound *Asu*-ACR-16



B



C

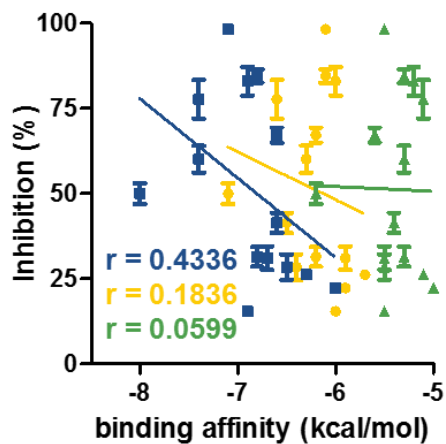


Figure S6. Correlations between binding affinities (kcal/mol) and EC_{50} (μ M) (A), binding affinities (kcal/mol) and I_{max} (%) (B), binding affinities (kcal/mol) and *Inhibition* (%) (C), for the selected nicotine derivatives. The binding affinity of each derivative in the agonist-bound *Asu-ACR-16* (blue), in the apo form *Asu-ACR-16* (yellow), in the antagonist-bound *Asu-ACr-16* (green) and their correlation coefficients (r) were shown.

CHAPTER 4

GENERAL CONCLUSION AND FUTURE OUTLOOK

The continual emergence of anthelmintic resistance in many animal species requires us to discover new lead compounds for anthelmintic drugs or to enhance the potency of existing anthelmintics. To achieve this goal, I used two different structure-based approaches: receptor-based drug design (Chapter 2) and ligand-based drug design (Chapter 3) (Tollenaere).

Receptor-based drug design relies on the structural and functional knowledge of a drug target. It is time-consuming and labor-intensive to resolve crystal structure of transmembrane receptor and to perform high-throughput drug screening. Advance in computational methods allows us to predict the receptor structure in atomic level and identify potential binding ligands from a large compound library, before investing in the experimental side.

In Chapter 2, we made three-dimensional model of *Asu*-ACR-16, our drug target, and defined the ligand-binding sites based on other homologous co-crystal structures. Ligands from ZINC database were docked into these sites on *Asu*-ACR-16 and each was output a binding affinity using the scoring functions. Those high-affinity ligands were selected for further electrophysiology studies. TEVC was applied to characterize the pharmacological activities of ligands on the *Asu*-ACR-16 receptor expressed in *Xenopus* oocytes. As an outcome, four out of nine ligands identified from virtual screening were validated to be negative allosteric modulators of *Asu*-ACR-16 and showed effects on worm locomotion.

The accuracy of virtual screening is mainly depended on the target structure and the scoring function that rank the interaction strengths between ligand and receptor. The predicted structure of receptor is based on the rigid crystal structure of homologous proteins, the conditions of which may not be the same as the protein *in vivo*. Thus, the conformation or folding of homologous proteins may be altered in the crystal structures *ex vivo*. In addition, it is insufficient to use static structures to mimic the dynamic nature of macromolecules, which as a result makes the predicted ligand-receptor interaction inaccurate (Sliwoski *et al.*, 2014). Molecular dynamics simulations take multiple conformations of target receptor and solvent interactions into account and may serve as a solution (Nair *et al.*, 2014). Another possible error may happen, when we use the ligand-binding site of homologous protein structure to predict ligand-binding site of target protein without site-direct mutagenesis. It largely limits our scopes to identify new binding sites on target receptor where potential ligands interact. Fragment-based lead discovery is an approach to link several weak-binding fragments in discrete binding sites together into a high-affinity ligand. This approach is not heavily relied on the precise binding site localization, and thus may be more worthwhile to apply for future drug discovery (Erlanson *et al.*, 2004).

Ligand-based drug design relies on the analysis of ligands known to interact with the target receptor. The objective is to maintain the physicochemical properties that are essential for ligand-receptor interactions, while discard those not relevant to the interactions. In contrast to the receptor-based drug design, ligand-based drug design can also be applied when the structure of target receptor is unknown or unclear. It is also found that active compounds identified by ligand-based screening

methods are usually more potent than those identified by receptor-based screening methods (Stumpfe *et al.*, 2012).

In Chapter 3, we used nicotine, a potent but non-selective agonist of nAChRs, as our basic moiety/pharmacophore. We investigated the pharmacological properties of different substituents on nicotinic pharmacophore on *Asu-ACR-16* receptor. As a result, we found several 5-substituted pyridine derivatives of nicotine that show significantly higher potency and efficacy than nicotine on *Asu-ACR-16* receptor.

Future work includes constructing quantitative structure-activity relationship (QSAR) models based on certain pharmacophore. The general idea of QSAR-based drug discovery is to develop mathematical descriptors that describe the physicochemical and structural properties of several structurally similar ligands. A QSAR model is developed to relate these descriptors with experimental/biological activity. QASR model can then be used to predict biological activity for a library of compounds using the same descriptors (Zhang, 2011).

REFERENCES

- Adams PD, Afonine PV, Bunkoczi G, Chen VB, Davis IW, Echols N, *et al.* (2010). PHENIX: a comprehensive Python-based system for macromolecular structure solution. *Acta crystallographica. Section D, Biological crystallography* **66**(Pt 2): 213-221.
- Altschul SF, Madden TL, Schaffer AA, Zhang J, Zhang Z, Miller W, *et al.* (1997). Gapped BLAST and PSI-BLAST: a new generation of protein database search programs. *Nucleic acids research* **25**(17): 3389-3402.
- Arias HR (2000a). Localization of agonist and competitive antagonist binding sites on nicotinic acetylcholine receptors. *Neurochem Int* **36**(7): 595-645.
- Arias HR (2000b). Localization of agonist and competitive antagonist binding sites on nicotinic acetylcholine receptors. *Neurochemistry International* **36**(7): 595-645.
- Ballivet M, Alliod C, Bertrand S, Bertrand D (1996). Nicotinic acetylcholine receptors in the nematode *Caenorhabditis elegans*. *Journal of molecular biology* **258**(2): 261-269.
- Berman HM, Westbrook J, Feng Z, Gilliland G, Bhat TN, Weissig H, *et al.* (2000). The Protein Data Bank. *Nucleic acids research* **28**(1): 235-242.
- Bertrand D, Bertrand S, Cassar S, Gubbins E, Li J, Gopalakrishnan M (2008). Positive allosteric modulation of the alpha7 nicotinic acetylcholine receptor: ligand interactions with distinct binding sites and evidence for a prominent role of the M2-M3 segment. *Molecular pharmacology* **74**(5): 1407-1416.
- Bethony J, Brooker S, Albonico M, Geiger SM, Loukas A, Diemert D, *et al.* (2006). Soil-transmitted helminth infections: ascariasis, trichuriasis, and hookworm. *The Lancet* **367**(9521): 1521-1532.
- Bleicher KH, Bohm H-J, Muller K, Alanine AI (2003). Hit and lead generation: beyond high-throughput screening. *Nat Rev Drug Discov* **2**(5): 369-378.
- Blum AP, Lester HA, Dougherty DA (2010). Nicotinic pharmacophore: the pyridine N of nicotine and carbonyl of acetylcholine hydrogen bond across a subunit interface to a backbone NH. *Proceedings of the National Academy of Sciences of the United States of America* **107**(30): 13206-13211.
- Boulin T, Fauvin A, Charvet CL, Cortet J, Cabaret J, Bessereau JL, *et al.* (2011). Functional reconstitution of *Haemonchus contortus* acetylcholine receptors in *Xenopus* oocytes provides mechanistic insights into levamisole resistance. *British journal of pharmacology* **164**(5): 1421-1432.

Boulin T, Gielen M, Richmond JE, Williams DC, Paoletti P, Bessereau JL (2008). Eight genes are required for functional reconstitution of the *Caenorhabditis elegans* levamisole-sensitive acetylcholine receptor. *Proceedings of the National Academy of Sciences of the United States of America* **105**(47): 18590-18595.

Brejč K, van Dijk WJ, Klaassen RV, Schuurmans M, van Der Oost J, Smit AB, *et al.* (2001). Crystal structure of an ACh-binding protein reveals the ligand-binding domain of nicotinic receptors. *Nature* **411**(6835): 269-276.

Brenner S (1974). The genetics of *Caenorhabditis elegans*. *Genetics* **77**(1): 71-94.

Brooker S, Bethony J, Hotez PJ (2004). Human hookworm infection in the 21st century. *Advances in parasitology* **58**: 197-288.

Buxton SK, Charvet CL, Neveu C, Cabaret J, Cortet J, Peineau N, *et al.* (2014). Investigation of acetylcholine receptor diversity in a nematode parasite leads to characterization of tribendimidine- and derquantel-sensitive nAChRs. *PLoS pathogens* **10**(1): e1003870.

Campbell WC, Benz GW (1984). Ivermectin: a review of efficacy and safety. *Journal of veterinary pharmacology and therapeutics* **7**(1): 1-16.

Cavasotto CN, Orry AJ (2007). Ligand docking and structure-based virtual screening in drug discovery. *Current topics in medicinal chemistry* **7**(10): 1006-1014.

Cavasotto CN, Phatak SS (2009). Homology modeling in drug discovery: current trends and applications. *Drug discovery today* **14**(13-14): 676-683.

Celie PH, van Rossum-Fikkert SE, van Dijk WJ, Brejč K, Smit AB, Sixma TK (2004). Nicotine and carbamylcholine binding to nicotinic acetylcholine receptors as studied in AChBP crystal structures. *Neuron* **41**(6): 907-914.

Changeux J-P, Edelstein SJ (1998). Allosteric Receptors after 30 Years. *Neuron* **21**(5): 959-980.

Chavez-Noriega LE, Crona JH, Washburn MS, Urrutia A, Elliott KJ, Johnson EC (1997). Pharmacological characterization of recombinant human neuronal nicotinic acetylcholine receptors h alpha 2 beta 2, h alpha 2 beta 4, h alpha 3 beta 2, h alpha 3 beta 4, h alpha 4 beta 2, h alpha 4 beta 4 and h alpha 7 expressed in *Xenopus* oocytes. *The Journal of pharmacology and experimental therapeutics* **280**(1): 346-356.

Cheng T, Zhao Y, Li X, Lin F, Xu Y, Zhang X, *et al.* (2007). Computation of octanol-water partition coefficients by guiding an additive model with knowledge. *Journal of chemical information and modeling* **47**(6): 2140-2148.

Chrzanowski FA, McGrogan BA, Maryanoff BE (1985). The pKa of butaclamol and the mode of butaclamol binding to central dopamine receptors. *Journal of Medicinal Chemistry* **28**(3): 399-400.

Coloquhoun L, Holden-dye L, Walker RJ (1991). The Pharmacology of Cholinoceptors on the Somatic Muscle Cells of the Parasitic Nematode *Ascaris Suum*. *Journal of Experimental Biology* **158**(1): 509-530.

Cosconati S, Forli S, Perryman AL, Harris R, Goodsell DS, Olson AJ (2010). Virtual Screening with AutoDock: Theory and Practice. *Expert opinion on drug discovery* **5**(6): 597-607.

Cosford NDP, Bleicher L, Vernier J-M, Chavez-Noriega L, Rao TS, Siegel RS, *et al.* (2000). Recombinant human receptors and functional assays in the discovery of altinicline (SIB-1508Y), a novel acetylcholine-gated ion channel (nAChR) agonist. *Pharmaceutica Acta Helveticae* **74**(2-3): 125-130.

Crompton DW (2000). The public health importance of hookworm disease. *Parasitology* **121** **Suppl**: S39-50.

de Silva NR, Brooker S, Hotez PJ, Montresor A, Engels D, Savioli L (2003a). Soil-transmitted helminth infections: updating the global picture. *Trends Parasitol* **19**(12): 547-551.

de Silva NR, Brooker S, Hotez PJ, Montresor A, Engels D, Savioli L (2003b). Soil-transmitted helminth infections: updating the global picture. *Trends in Parasitology* **19**(12): 547-551.

Devillers-Thiery A, Giraudat J, Bentaboulet M, Changeux JP (1983). Complete mRNA coding sequence of the acetylcholine binding alpha-subunit of *Torpedo marmorata* acetylcholine receptor: a model for the transmembrane organization of the polypeptide chain. *Proceedings of the National Academy of Sciences of the United States of America* **80**(7): 2067-2071.

Devillers-Thiery A, Giraudat J, Bentaboulet M, Klarsfeld A, Changeux JP (1984). Molecular genetics of *Torpedo marmorata* acetylcholine receptor. *Advances in experimental medicine and biology* **181**: 17-29.

Dold C, Holland CV (2011). *Ascaris* and ascariasis. *Microbes and Infection* **13**(7): 632-637.

Dougherty DA (2013). The cation-pi interaction. *Accounts of chemical research* **46**(4): 885-893.

Emsley P, Cowtan K (2004). Coot: model-building tools for molecular graphics. *Acta crystallographica. Section D, Biological crystallography* **60**(Pt 12 Pt 1): 2126-2132.

Erlanson DA, McDowell RS, O'Brien T (2004). Fragment-based drug discovery. *J Med Chem* **47**(14): 3463-3482.

Eswar N, Webb B, Marti-Renom MA, Madhusudhan MS, Eramian D, Shen MY, *et al.* (2007). Comparative protein structure modeling using MODELLER. *Current protocols in protein science / editorial board, John E. Coligan ... [et al.] Chapter 2*: Unit 2.9.

Finer-Moore J, Stroud RM (1984). Amphipathic analysis and possible formation of the ion channel in an acetylcholine receptor. *Proceedings of the National Academy of Sciences of the United States of America* **81**(1): 155-159.

Finkel AS, Gage PW (1985). Conventional Voltage Clamping With Two Intracellular Microelectrodes. In: Smith TG, Lecar H, Redman SJ, Gage PW (eds). *Voltage and Patch Clamping with Microelectrodes*, edn. New York, NY: Springer New York. p^{pp} 47-94.

Galzi J-L, Bertrand D, Devillers-Thiéry A, Revah F, Bertrand S, Changeux J-P (1991). Functional significance of aromatic amino acids from three peptide loops of the $\alpha 7$ neuronal nicotinic receptor site investigated by site-directed mutagenesis. *FEBS Letters* **294**(3): 198-202.

Garcia CM, Sprenger LK, Ortiz EB, Molento MB (2016). First report of multiple anthelmintic resistance in nematodes of sheep in Colombia. *Anais da Academia Brasileira de Ciencias* **88**(1): 397-402.

Gros PC, Doudouh A, Woltermann C (2006). TMSCH₂Li-induced regioselective lithiation of (S)-nicotine. *Organic & Biomolecular Chemistry* **4**(23): 4331-4335.

Halevi S, Yassin L, Eshel M, Sala F, Sala S, Criado M, *et al.* (2003). Conservation within the RIC-3 gene family. Effectors of mammalian nicotinic acetylcholine receptor expression. *The Journal of biological chemistry* **278**(36): 34411-34417.

Hassaine G, Deluz C, Grasso L, Wyss R, Tol MB, Hovius R, *et al.* (2014). X-ray structure of the mouse serotonin 5-HT₃ receptor. *Nature* **512**(7514): 276-281.

Hernando G, Berge I, Rayes D, Bouzat C (2012). Contribution of subunits to *Caenorhabditis elegans* levamisole-sensitive nicotinic receptor function. *Molecular pharmacology* **82**(3): 550-560.

Hewitson JP, Maizels RM (2014). Vaccination against helminth parasite infections. *Expert review of vaccines* **13**(4): 473-487.

Hibbs RE, Gouaux E (2011). Principles of activation and permeation in an anion-selective Cys-loop receptor. *Nature* **474**(7349): 54-60.

Hilf RJ, Dutzler R (2008). X-ray structure of a prokaryotic pentameric ligand-gated ion channel. *Nature* **452**(7185): 375-379.

Hilf RJ, Dutzler R (2009). Structure of a potentially open state of a proton-activated pentameric ligand-gated ion channel. *Nature* **457**(7225): 115-118.

Hillisch A, Pineda LF, Hilgenfeld R (2004). Utility of homology models in the drug discovery process. *Drug discovery today* **9**(15): 659-669.

Holden-Dye L, Joyner M, O'Connor V, Walker RJ (2013). Nicotinic acetylcholine receptors: A comparison of the nAChRs of *Caenorhabditis elegans* and parasitic nematodes. *Parasitology International* **62**(6): 606-615.

Hopkins AL, Groom CR, Alex A (2004). Ligand efficiency: a useful metric for lead selection. *Drug discovery today* **9**(10): 430-431.

Hotez PJ, Molyneux DH, Fenwick A, Kumaresan J, Sachs SE, Sachs JD, *et al.* (2007). Control of neglected tropical diseases. *New England Journal of Medicine* **357**(10): 1018-1027.

Huang S, Li S-X, Bren N, Cheng K, Gomoto R, Chen L, *et al.* (2013). Complex between α -bungarotoxin and an $\alpha 7$ nicotinic receptor ligand-binding domain chimera. *The Biochemical journal* **454**(2): 303-310.

Irwin JJ, Sterling T, Mysinger MM, Bolstad ES, Coleman RG (2012). ZINC: a free tool to discover chemistry for biology. *Journal of chemical information and modeling* **52**(7): 1757-1768.

Iturriaga-Vasquez P, Alzate-Morales J, Bermudez I, Varas R, Reyes-Parada M (2015). Multiple binding sites in the nicotinic acetylcholine receptors: An opportunity for polypharmacology. *Pharmacological research* **101**: 9-17.

Jackson MB (2010). Open channel block and beyond. *The Journal of Physiology* **588**(Pt 4): 553-554.

Johnson CD, Stretton AO (1985). Localization of choline acetyltransferase within identified motoneurons of the nematode *Ascaris*. *The Journal of neuroscience : the official journal of the Society for Neuroscience* **5**(8): 1984-1992.

Kaczanowski S, Zielenkiewicz P (2009). Why similar protein sequences encode similar three-dimensional structures? *Theoretical Chemistry Accounts* **125**(3): 643-650.

Kaplan RM (2004). Drug resistance in nematodes of veterinary importance: a status report. *Trends Parasitol* **20**(10): 477-481.

Keiser J, Utzinger J (2008). Efficacy of current drugs against soil-transmitted helminth infections: systematic review and meta-analysis. *Jama* **299**(16): 1937-1948.

Keiser J, Utzinger J (2010). Chapter 8 - The Drugs We Have and the Drugs We Need Against Major Helminth Infections. In: Xiao-Nong Zhou RBRO, Jürg U (eds). *Advances in parasitology*, edn, Vol. Volume 73: Academic Press. p^pp 197-230.

Kulke D, von Samson-Himmelstjerna G, Miltsch SM, Wolstenholme AJ, Jex AR, Gasser RB, *et al.* (2014). Characterization of the Ca²⁺-gated and voltage-dependent K⁺-channel Slo-1 of nematodes and its interaction with emodepside. *PLoS neglected tropical diseases* **8**(12): e3401.

Kuntz ID, Chen K, Sharp KA, Kollman PA (1999). The maximal affinity of ligands. *Proceedings of the National Academy of Sciences of the United States of America* **96**(18): 9997-10002.

Lacey E (1990). Mode of action of benzimidazoles. *Parasitology today (Personal ed.)* **6**(4): 112-115.

Lester HA, Dibas MI, Dahan DS, Leite JF, Dougherty DA (2004). Cys-loop receptors: new twists and turns. *Trends in neurosciences* **27**(6): 329-336.

Lewis JA, Wu CH, Levine JH, Berg H (1980). Levamisole-resistant mutants of the nematode *Caenorhabditis elegans* appear to lack pharmacological acetylcholine receptors. *Neuroscience* **5**(6): 967-989.

Li S-X, Huang S, Bren N, Noridomi K, Dellisanti CD, Sine SM, *et al.* (2011a). Ligand-binding domain of an [alpha]7-nicotinic receptor chimera and its complex with agonist. *Nature neuroscience* **14**(10): 1253-1259.

Li SX, Huang S, Bren N, Noridomi K, Dellisanti CD, Sine SM, *et al.* (2011b). Ligand-binding domain of an alpha7-nicotinic receptor chimera and its complex with agonist. *Nature neuroscience* **14**(10): 1253-1259.

Lipinski CA (2004). Lead- and drug-like compounds: the rule-of-five revolution. *Drug Discovery Today: Technologies* **1**(4): 337-341.

Lipinski CA, Lombardo F, Dominy BW, Feeney PJ (2001). Experimental and computational approaches to estimate solubility and permeability in drug discovery and development settings. *Advanced drug delivery reviews* **46**(1-3): 3-26.

Liskey CW, Liao X, Hartwig JF (2010). Cyanation of Arenes via Iridium-Catalyzed Borylation. *Journal of the American Chemical Society* **132**(33): 11389-11391.

Lubega GW, Prichard RK (1990). Specific interaction of benzimidazole anthelmintics with tubulin: high-affinity binding and benzimidazole resistance in *Haemonchus contortus*. *Mol Biochem Parasitol* **38**(2): 221-232.

Marti-Renom MA, Stuart AC, Fiser A, Sanchez R, Melo F, Sali A (2000). Comparative protein structure modeling of genes and genomes. *Annual review of biophysics and biomolecular structure* **29**: 291-325.

Martin R, Robertson A (2010). Control of Nematode Parasites with Agents Acting on Neuro-Musculature Systems: Lessons for Neuropeptide Ligand Discovery. In: Geary T, Maule A (eds). *Neuropeptide Systems as Targets for Parasite and Pest Control*, edn, Vol. 692: Springer US. pp 138-154.

Martin RJ (1982). Electrophysiological effects of piperazine and diethylcarbamazine on *Ascaris suum* somatic muscle. *British journal of pharmacology* **77**(2): 255-265.

Martin RJ (1997). Modes of action of anthelmintic drugs. *The Veterinary Journal* **154**(1): 11-34.

Martin RJ, Robertson AP, Buxton SK, Beech RN, Charvet CL, Neveu C (2012). Levamisole receptors: a second awakening. *Trends Parasitol* **28**(7): 289-296.

Mellanby H (1955). The identification and estimation of acetylcholine in three parasitic nematodes (*Ascaris lumbricoides*, *Litomosoides carinii*, and the microfilariae of *Dirofilaria repens*). *Parasitology* **45**(3-4): 287-294.

Miller PS, Aricescu AR (2014). Crystal structure of a human GABAA receptor. *Nature* **512**(7514): 270-275.

Miyazawa A, Fujiyoshi Y, Unwin N (2003). Structure and gating mechanism of the acetylcholine receptor pore. *Nature* **423**(6943): 949-955.

Mongan NP, Jones AK, Smith GR, Sansom MS, Sattelle DB (2002). Novel alpha7-like nicotinic acetylcholine receptor subunits in the nematode *Caenorhabditis elegans*. *Protein science : a publication of the Protein Society* **11**(5): 1162-1171.

Moriarty NW, Grosse-Kunstleve RW, Adams PD (2009). electronic Ligand Builder and Optimization Workbench (eLBOW): a tool for ligand coordinate and restraint generation. *Acta crystallographica. Section D, Biological crystallography* **65**(Pt 10): 1074-1080.

Morris GM, Goodsell DS, Halliday RS, Huey R, Hart WE, Belew RK, *et al.* (1998). Automated docking using a Lamarckian genetic algorithm and an empirical binding free energy function. *Journal of Computational Chemistry* **19**(14): 1639-1662.

Morris GM, Huey R, Lindstrom W, Sanner MF, Belew RK, Goodsell DS, *et al.* (2009a). AutoDock4 and AutoDockTools4: Automated Docking with Selective Receptor Flexibility. *Journal of computational chemistry* **30**(16): 2785-2791.

Morris GM, Huey R, Lindstrom W, Sanner MF, Belew RK, Goodsell DS, *et al.* (2009b). AutoDock4 and AutoDockTools4: Automated docking with selective receptor flexibility. *J Comput Chem* **30**(16): 2785-2791.

Nair PC, Miners JO (2014). Molecular dynamics simulations: from structure function relationships to drug discovery. *In Silico Pharmacology* **2**: 4.

Nussinov R, Tsai CJ (2013). Allostery in disease and in drug discovery. *Cell* **153**(2): 293-305.

Olsen JA, Balle T, Gajhede M, Ahring PK, Kastrup JS (2014a). Molecular recognition of the neurotransmitter acetylcholine by an acetylcholine binding protein reveals determinants of binding to nicotinic acetylcholine receptors. *PLoS one* **9**(3): e91232.

Olsen JA, Balle T, Gajhede M, Ahring PK, Kastrup JS (2014b). Molecular Recognition of the Neurotransmitter Acetylcholine by an Acetylcholine Binding Protein Reveals Determinants of Binding to Nicotinic Acetylcholine Receptors. *PLoS one* **9**(3).

Pan J, Chen Q, Willenbring D, Mowrey D, Kong XP, Cohen A, *et al.* (2012). Structure of the pentameric ligand-gated ion channel GLIC bound with anesthetic ketamine. *Structure* **20**(9): 1463-1469.

Park H, Lee J, Lee S (2006). Critical assessment of the automated AutoDock as a new docking tool for virtual screening. *Proteins* **65**(3): 549-554.

Peng X, Katz M, Gerzanich V, Anand R, Lindstrom J (1994). Human alpha 7 acetylcholine receptor: cloning of the alpha 7 subunit from the SH-SY5Y cell line and determination of pharmacological properties of native receptors and functional alpha 7 homomers expressed in *Xenopus oocytes*. *Molecular pharmacology* **45**(3): 546-554.

Polli JR, Dobbins DL, Kobet RA, Farwell MA, Zhang B, Lee MH, *et al.* (2015). Drug-dependent behaviors and nicotinic acetylcholine receptor expressions in *Caenorhabditis elegans* following chronic nicotine exposure. *Neurotoxicology* **47**: 27-36.

Prichard R (1994). Anthelmintic resistance. *Veterinary parasitology* **54**(1-3): 259-268.

Qian H, Martin RJ, Robertson AP (2006). Pharmacology of N-, L-, and B-subtypes of nematode nAChR resolved at the single-channel level in *Ascaris suum*. *FASEB journal : official publication of the Federation of American Societies for Experimental Biology* **20**(14): 2606-2608.

Raymond V, Mongan NP, Sattelle DB (2000). Anthelmintic actions on homomer-forming nicotinic acetylcholine receptor subunits: chicken $\alpha 7$ and ACR-16 from the nematode *Caenorhabditis elegans*. *Neuroscience* **101**(3): 785-791.

Rester U (2008). From virtuality to reality - Virtual screening in lead discovery and lead optimization: a medicinal chemistry perspective. *Current opinion in drug discovery & development* **11**(4): 559-568.

Robertson AP, Clark CL, Burns TA, Thompson DP, Geary TG, Trailovic SM, *et al.* (2002). Paraherquamide and 2-deoxy-paraherquamide distinguish cholinergic receptor subtypes in *Ascaris* muscle. *The Journal of pharmacology and experimental therapeutics* **302**(3): 853-860.

Robertson AP, Puttachary S, Buxton SK, Martin RJ (2008). Electrophysiological recording from parasitic nematode muscle. *Invertebrate neuroscience : IN* **8**(4): 167-175.

Robertson AP, Puttachary S, Buxton SK, Martin RJ (2015). Tribendimidine: mode of action and nAChR subtype selectivity in *Ascaris* and *Oesophagostomum*. *PLoS neglected tropical diseases* **9**(2): e0003495.

Rossokhin AV, Sharonova IN, Bukanova JV, Kolbaev SN, Skrebitsky VG (2014). Block of GABAA receptor ion channel by penicillin: Electrophysiological and modeling insights toward the mechanism. *Molecular and Cellular Neuroscience* **63**: 72-82.

Rucktooa P, Haseler CA, van Elk R, Smit AB, Gallagher T, Sixma TK (2012). Structural characterization of binding mode of smoking cessation drugs to nicotinic acetylcholine receptors through study of ligand complexes with acetylcholine-binding protein. *The Journal of biological chemistry* **287**(28): 23283-23293.

Rucktooa P, Smit AB, Sixma TK (2009). Insight in nAChR subtype selectivity from AChBP crystal structures. *Biochemical pharmacology* **78**(7): 777-787.

Rufener L, Baur R, Kaminsky R, Maser P, Sigel E (2010). Monepantel allosterically activates DEG-3/DES-2 channels of the gastrointestinal nematode *Haemonchus contortus*. *Molecular pharmacology* **78**(5): 895-902.

Rychlewski L, Jaroszewski L, Li W, Godzik A (2000). Comparison of sequence profiles. Strategies for structural predictions using sequence information. *Protein science : a publication of the Protein Society* **9**(2): 232-241.

Savioli L, Albonico M (2004). Focus: Soil-transmitted helminthiasis. *Nat Rev Micro* **2**(8): 618-619.

Shalaby HA (2013). Anthelmintics Resistance; How to Overcome it? *Iranian Journal of Parasitology* **8**(1): 18-32.

Shoichet BK, Leach AR, Kuntz ID (1999). Ligand solvation in molecular docking. *Proteins* **34**(1): 4-16.

Sixma TK, Smit AB (2003). Acetylcholine binding protein (AChBP): a secreted glial protein that provides a high-resolution model for the extracellular domain of pentameric ligand-gated ion channels. *Annual review of biophysics and biomolecular structure* **32**: 311-334.

Sliwoski G, Kothiwale S, Meiler J, Lowe EW, Jr. (2014). Computational methods in drug discovery. *Pharmacol Rev* **66**(1): 334-395.

Spurny R, Debaveye S, Farinha A, Veys K, Vos AM, Gossas T, *et al.* (2015). Molecular blueprint of allosteric binding sites in a homologue of the agonist-binding domain of the alpha7 nicotinic acetylcholine receptor. *Proceedings of the National Academy of Sciences of the United States of America* **112**(19): E2543-2552.

Spyrakakis F, BidonChanal A, Barril X, Luque FJ (2011). Protein flexibility and ligand recognition: challenges for molecular modeling. *Current topics in medicinal chemistry* **11**(2): 192-210.

Stemp G, Ashmeade T, Branch CL, Hadley MS, Hunter AJ, Johnson CN, *et al.* (2000). Design and Synthesis of trans-N-[4-[2-(6-Cyano-1,2,3,4-tetrahydroisoquinolin-2-yl)ethyl]cyclohexyl]-4-quinolinecarboxamide (SB-277011): A Potent and Selective Dopamine D3 Receptor Antagonist with High Oral Bioavailability and CNS Penetration in the Rat. *Journal of Medicinal Chemistry* **43**(9): 1878-1885.

Stewart TB, Hale OM (1988). Losses to internal parasites in swine production. *Journal of animal science* **66**(6): 1548-1554.

Stumpfe D, Ripphausen P, Bajorath J (2012). Virtual compound screening in drug discovery. *Future medicinal chemistry* **4**(5): 593-602.

Sun H (2008). Pharmacophore-based virtual screening. *Current medicinal chemistry* **15**(10): 1018-1024.

Taly A, Corringer P-J, Guedin D, Lestage P, Changeux J-P (2009). Nicotinic receptors: allosteric transitions and therapeutic targets in the nervous system. *Nat Rev Drug Discov* **8**(9): 733-750.

Taman A, Azab M (2014). Present-day anthelmintics and perspectives on future new targets. *Parasitology research* **113**(7): 2425-2433.

Taylor HL, Spagnoli ST, Calcutt MJ, Kim DY (2016). Aberrant *Ascaris suum* Nematode Infection in Cattle, Missouri, USA. *Emerging infectious diseases* **22**(2): 339-340.

Thompson JD, Higgins DG, Gibson TJ (1994). CLUSTAL W: improving the sensitivity of progressive multiple sequence alignment through sequence weighting, position-specific gap penalties and weight matrix choice. *Nucleic acids research* **22**(22): 4673-4680.

Tollenaere JP The role of structure-based ligand design and molecular modelling in drug discovery. *Pharmacy World and Science* **18**(2): 56-62.

Trott O, Olson AJ (2010). AutoDock Vina: improving the speed and accuracy of docking with a new scoring function, efficient optimization, and multithreading. *J Comput Chem* **31**(2): 455-461.

Unwin N (2005a). Refined Structure of the Nicotinic Acetylcholine Receptor at 4 Å Resolution. *Journal of molecular biology* **346**(4): 967-989.

Unwin N (2005b). Refined structure of the nicotinic acetylcholine receptor at 4Å resolution. *Journal of molecular biology* **346**(4): 967-989.

Van Arnam EB, Dougherty DA (2014). Functional probes of drug-receptor interactions implicated by structural studies: Cys-loop receptors provide a fertile testing ground. *J Med Chem* **57**(15): 6289-6300.

Wang J, Czech B, Crunk A, Wallace A, Mitreva M, Hannon GJ, *et al.* (2011). Deep small RNA sequencing from the nematode *Ascaris* reveals conservation, functional diversification, and novel developmental profiles. *Genome research* **21**(9): 1462-1477.

Wani I, Rather M, Naikoo G, Amin A, Mushtaq S, Nazir M (2010). Intestinal ascariasis in children. *World journal of surgery* **34**(5): 963-968.

Ward JD (2015). Rendering the Intractable More Tractable: Tools from *Caenorhabditis elegans* Ripe for Import into Parasitic Nematodes. *Genetics* **201**(4): 1279-1294.

Wolstenholme AJ, Fairweather I, Prichard R, von Samson-Himmelstjerna G, Sangster NC (2004). Drug resistance in veterinary helminths. *Trends Parasitol* **20**(10): 469-476.

Wu ZS, Cheng H, Jiang Y, Melcher K, Xu HE (2015). Ion channels gated by acetylcholine and serotonin: structures, biology, and drug discovery. *Acta pharmacologica Sinica* **36**(8): 895-907.

Xiu X, Puskar NL, Shanata JA, Lester HA, Dougherty DA (2009). Nicotine binding to brain receptors requires a strong cation- π interaction. *Nature* **458**(7237): 534-537.

Xu M, Molento M, Blackhall W, Ribeiro P, Beech R, Prichard R (1998). Ivermectin resistance in nematodes may be caused by alteration of P-glycoprotein homolog1. *Molecular and Biochemical Parasitology* **91**(2): 327-335.

Young GT, Zwart R, Walker AS, Sher E, Millar NS (2008). Potentiation of $\alpha 7$ nicotinic acetylcholine receptors via an allosteric transmembrane site. *Proceedings of the National Academy of Sciences of the United States of America* **105**(38): 14686-14691.

Zhang S (2011). Computer-Aided Drug Discovery and Development. In: Satyanarayanajois DS (ed). *Drug Design and Discovery: Methods and Protocols*, edn. Totowa, NJ: Humana Press. pp 23-38.

Zheng F, Robertson AP, Abongwa M, Yu EW, Martin RJ (2016). The *Ascaris suum* nicotinic receptor, ACR-16, as a drug target: Four novel negative allosteric modulators from virtual screening. *International Journal for Parasitology: Drugs and Drug Resistance* **6**(1): 60-73.